Propriétés optiques et structurales de boîtes quantiques GaN et InGaN dopées avec des ions terres rares

Thomas Andreev

Université Joseph Fourier – Grenoble I

Sciences & Géographie

THÈSE

Pour obtenir le grade de

DOCTEUR DE L'UNIVERSITÉ JOSEPH FOURIER

Physique

Présentée et soutenue publiquement par

Thomas Andreev

le 29 mars 2006

Growth and Optical Properties of GaN and InGaN Quantum Dots doped with Rare Earth ions

---

Composition du jury :

Benoît BOULANGER	Président
Daniel LE SI DANG	Examinateur
Pierre LEFÈBVRE	Rapporteur
Georges BOULON	Rapporteur
Bruno DAUDIN	Directeur de thèse

Cette thèse a été préparée au sein du CEA Grenoble

Département de Recherche Fondamentale sur la Matière Condensée

Service de Physique des Matériaux et des Microstructures

Offen auf alles Neue zuzugehen,
ohne das Detail aus dem Auge
zu verlieren, erlaubt so manche
unerwartete Entdeckung.

Remerciement

Pour commencer je voudrais remercier Prof. Pierre Lefèbvre et Prof. Georges Boulon d'avoir accepté de rapporter ce travail avec intérêt.

Ce travail a été effectué au sein de l'équipe mixte CEA-CNRS-UJF « Nano-physique et semi-conducteurs « du Sevice de Physique des Matériaux et Microstructures (DRFMC/ SP2M). A ce titre, je remercie Jean Michel Gérard et Noël Magnéa de m'avoir accueilli dans ce laboratoire.

Je voudrais remercier chaleureusement toutes les personnes qui m'ont aidé pendant ces trois ans de thèse.

Je remercie Bruno Daudin, mon directeur de thèse, pour la confiance qu'il m'a témoigne. Il m'a laissé une grande liberté pour donner des accents personnels à mon travail de thèse. En plus de cette liberté, il a toujours su être une oreille ouverte pour me donner des conseils et m'encourager. Il m'a aussi donné la possibilité d'apprendre plusieurs techniques expérimentales.

Un grand merci à Mitsuhiro Tanaka et Osamu Oda qui ont toujours témoigné beaucoup d'intérêt pour mon travail, ainsi qu'à tous les employés de l'entreprise NGK INSULATORS. Cette entreprise a généreusement financé beaucoup d'équipement pour le laboratoire comme la machine MBE et aussi mon travail de thèse.

Un merci particulier à mon collaborateur Yuji Hori de l'entreprise NGK INSULATORS. En début de thèse il m'a enseigné la méthode

MBE et m'a très bien introduit dans le projet. Je voudrais aussi le remercier pour la croissance de nombreux échantillons de très bonne qualité, que j'ai pu étudier en optique.

L'entreprise DOWA MINING est remerciée pour la participation au financement d'une partie de mon travail de dernière année. Personnellement je voudrais remercier Hiroyuki Togawa, Hideaki Kobayashi et Akira Otsuka pour les discussions qu'elles soient du domaine de la physique ou non.

Un grand merci aussi à Eva Monroy, Bruno Gayral et Frederic Fossard pour les nombreuses discussions physiques et non physiques. Au début de ma thèse ils m'ont donné beaucoup de conseils en optique, et par la suite, sur l'organisation du manuscrit et des publications toujours de façon très gentille.

Pendant ma thèse, j'ai eu la chance de travailler avec Daniel Le Si Dang, professeur, spécialiste de la caractérisation optique. Il m'a toujours encouragé et dispensé de très bons conseils, et ce, à chaque fois de façon très cordiale. Merci aussi pour les nombreuses discussions physique et non physique que j'ai pu avoir avec lui.

C'est avec plaisir que je voudrais remercier Nguyen Quang Liem, professeur de Vietnamese Academy of Science and Technology, pour le formidable travail qui a découlé de notre collaboration sur les caractérisations optiques. Nguyen Quang Liem m'a beaucoup appris, tant en optique que sur la culture de son pays. Il m'a donné

beaucoup des idées qui sont elles aussi responsables sur le succès de ce travail.

Un grand merci aussi à Denis Jalabert pour se explications sur la caractérisation structurelle par RBS, toujours avec humour et décontraction.

Xavier Biquard est remercié pour avoir très bien diriger l'expérience d'EXAFS à l'ESRF. Il est aussi remercié pour plusieurs analyses et discussions.

Je voudrais remercier aussi les étudiants du laboratoire du CEA pour la création d'une ambiance très sympathique. Le travail avec vous a été très agréable, ainsi que tous les week-ends que nous avons pu faire ensemble en montagne. De plus, un grand merci à tout les amis que j'ai rencontré à Grenoble et qui m'ont permis de passer des moments légers, amusants et intéressants ici en France.

Un gentil merci à Marlène Terrier, Yann Genuist, Gilbert Demoment et Yoann Curé, le personnel technique de laboratoire pour la rapidité de leurs réactions face aux divers problèmes posés pendant cette thèse.

Je voudrais remercier Fabrice Donatini pour l'installation de la Cathodoluminescence et pour sa pédagogie lors de ses explications.

Un très grand merci aussi à Virgine Charmard, qui m'a aidé à bien m'installer en France et pour les encouragements qu'elle m'a donnés.

Merci à Metin Tolan et Heinz Hövel, professeurs de l'Université de Dortmund pour leur intérêt porté à mon travail et pour plusieurs présentations invitées.

Je voudrais remercier aussi tous mes amis Allemands et non Allemands et mes parents, qui m'ont eux aussi très bien encouragé pendant les trois ans de thèse.

Résumé

Ce travail présente des résultats sur les propriétés optiques et structurales de boîtes quantiques III-nitrures dopées terres rares.

L'idée sous-jacente de ce travail est la fabrication d'une diode blanche à base de boîtes quantiques dopées terres rares en mélangeant les couleurs – Eu(rouge), Tm(bleu) et Tb(vert) – de leurs luminescences.

Deux choses importantes ont été étudiées. La première question porte sur la façon dont les terres rares modifient le régime de croissance lors de l'épitaxie par jets moléculaires et sur la localisation des atomes de terres rares dans les structures.

Le deuxième, quant à elle, a pour sujet les propriétés optiques des terres rares dans des boîtes (In)GaN. Il est important de comparer les propriétés optiques des terres rares dans les boîtes avec les propriétés d'une couche afin de comparer l'efficacité quantique de ces deux systèmes. A cette étude s'ajoute le problème du transfert d'énergie du matériau semi-conducteur vers les ions terre rare.

Croissance de structures à boîtes dopées terres rares à base de nitrures

Le premier chapitre répond à la première question : l'influence des terres rares durant la croissance et leur position dans les structures de boîtes GaN dopées terres rares dans l'AlN. Cette étude a principalement nécessité l'utilisation de méthodes structurales comme l'AFM, le RHEED, l'EXAFS et le RBS.

Pendant la croissance MBE, les atomes de terres rares ont tendance à ségréger à la surface. Cet effet est extrêmement visible dans le cas de l'Eu pour lequel la morphologie des boîtes GaN est drastiquement modifiée en fonction des concentrations. Au contraire, les boîtes GaN dopées Tm ne sont pas beaucoup affectées par la présence de Tm, ce qui prouve que le régime de croissance est totalement différent.

Il est aussi possible de réaliser des boîtes GaN dopées Tm avec des concentrations de l'ordre de 10%, contrairement aux boîtes Eu, pour lequel un dopage de plus de 3% supprime la formation des boîtes, ainsi que le révèle l'AFM.

Cette influence totalement différente du Tm et de l'Eu dans la formation des boîtes peut être expliquée par différentes localisations des terres rares dans les structures de boîtes GaN encapsulées dans l'AlN. Les résultats d'EXAFS et de RBS montrent que l'Eu est bien incorporé dans les boîtes alors que le Tm se trouve à l'interface des boîtes GaN/AlN et plutôt dans l'AlN.

Propriétés optiques d'une couche GaN dopée Eu

Ce chapitre développe une étude optique sur une couche GaN dopée Eu. Plusieurs nouvelles transitions intra 4f d'Eu partant des niveaux $^5D_2$, $^5D_1$ et $^5D_0$ ont été identifiées et montrent différentes diminution de l'intensité de la luminescence entre la température de l'hélium liquide et l'ambiante. La transition $^5D_0 \rightarrow {}^7F_2$, qui est la plus

intense des transitions d'Eu dans le rouge, a des raies bien séparées. Les différentes caractéristiques comme la structure fine des raies, la dépendance en température, la profondeur de pénétration des électrons par cathodoluminescence et la photoluminescence en fonction de la puissance, montrent qu'il y a deux types de sites différents : le premier proche de la surface, le deuxième à l'intérieur des échantillons.

Les transferts d'énergie, dont l'étude est basée sur des mesures par excitation de photoluminescence (PLE), nous montrent que les ions d'Eu sont excités par un mécanisme à l'energie du gap de GaN. L'excitation par les défauts est plus de cent fois plus faible que celle due au gap du GaN, elle n'a aussi été détectée que pour les ions à l'intérieur des échantillons. Les transitions fines (0.2 nm) permettent d'observer un décalage vers le bleu ce qui est dans la direction opposée aux décalages typiques des gaps avec la température croissante.

Propriétés optiques de boîtes quantiques GaN dopées avec Eu

Ce chapitre développe une étude optique sur les boîtes GaN dopées Eu. L'influence de la concentration d'Eu sur un spectre de photoluminescence est aussi discutée. Sur ce spectre, on peut observer une signature des boîtes à 300 nm ainsi que des raies fines à 622 nm. A faible concentration d'Eu, la signature des boîtes est plus prononcée et les raies d'Eu ont une intensité faible. En augmentant la

quantité d'Eu, la signature des boîtes baisse d'intensité et les émissions d'Eu dominent le spectre. Ce résultat montre qu'il existe un transfert énergétique entre les porteurs situés dans les boîtes quantiques et les ions d'Eu. Il est montré que le nombre d'atomes Eu mesuré par RBS est proportionnel à l'intensité de la luminescence. A partir de ce constat, un modèle simple permet de calculer le temps de vie radiatif des ions Eu.

La photoluminescence en fonction de la température des ions Eu dans les boîtes GaN est stable de la température de l'hélium liquide à l'ambiante. A l'opposé, une couche de GaN dopée Eu et des boîtes non dopées perdent 90% de leur luminescence ce qui montre la grande efficacité quantique des structures à boîtes dopées Eu. Le mécanisme déterminant est la localisation des porteurs dans les boîtes (sans défauts) parallèlement au piégeage rapide des porteurs par les terres rares.

L'émission d'Eu double entre 5 K et la température ambiante pour un échantillon à basse concentration d'Eu (0.4%). Cette dépendance de la photoluminescence de l'Eu avec les faibles concentrations d'Eu est difficile à interpréter.

Nous avons trouvé que la durée de vie d'Eu est plus longue dans les boîtes quantiques GaN que dans une couche GaN dopée Eu. Ceci pose la question de la localisation microscopique de l'Eu dans une boîte où les ions Eu voisins peuvent être excités mutuellement.

Les ions excités de cette façon ont typiquement des durées de vie plus longues.

Il est montré que l'influence de la taille des boîtes sur la luminescence d'Eu est négligeable.

Boîtes InGaN dopées Eu

Les structures à base de boîtes quantiques InGaN dopées terres rares sont intéressantes pour l'injection de courant, car il est possible, contrairement à l'AlN, de contrôler le dopage p- et n- du GaN.

Dans ce chapitre nous avons discuté les propriétés optiques des boîtes InGaN dopées Eu. La question de la localisation d'Eu dans des structures de boîtes InGaN encapsulées dans le GaN est abordée. Une étude de l'excitation de photoluminescences (PLE) montre que l'Eu peut être trouvé dans les boîtes et aussi dans la barrière de GaN. Ceci peut être expliqué par la forte ségrégation de l'Eu lors de la croissance des boîtes.

La signature de l'Eu dans la barrière montre une diminution de l'intensité de la photoluminescence en fonction de la température (de 5 K à 300 K). Par contre, les raies d'Eu dans les boîtes InGaN restent stables, ceci peut être comparé au comportement de l'Eu dans les boîtes GaN.

Boîtes GaN dopées Tm

Les boîtes quantiques dopées Tm sont intéressantes pour l'émission dans le bleu.

Dans un premier temps, ce chapitre traite de la position des terres rares dans des structures à boîtes GaN dopée Tm encapsulées dans l'AlN. En photoluminescence, seules les boites sont excitées, des raies larges dans le bleu sont visibles. En cathodoluminescence, toute la structure est excitée et les raies de Tm dans les boîtes sont encore visibles et on note, de plus, avec un décalage de 2 nm, la signature du Tm dans la barrière d'AlN. Ce résultat montre que les boîtes sont réellement dopées avec Tm mais que celui-ci peut être également trouvé dans la barrière d'AlN.

Aucune dépendance en température (5 K - 300 K) de la photo-luminescence n'est observée pour les transitions à partir du niveau $^1D_2$, ce qui est important pour l'émission dans le bleu. Dans le même temps, les transitions du niveau $^1I_6$ perdent deux ordres de grandeur dans leur photoluminescence. Les émissions des transitions des états excités $^1G_4$ et $^3H_4$ ont une dépendance intermédiaire et diminuent d'un ordre de grandeur. Ces différents comportements thermiques permettent d'identifier de nouvelles raies et de construire un diagramme d'énergies.

L'excitation de photoluminescences (PLE) montre que les ions de Tm sont excités par un transfert d'énergie provenant des boîtes.

Pour préciser le mécanisme d'excitation du Tm, des mesures de temps de vie ont été analysées. Il est observé que le temps de vie du Tm chute d'un facteur 2 entre 5 K et 300 K pour la transition $^1D_2 \rightarrow {}^3F_4$. Par contre, l'émission de cette transition est stable dans cette plage

de température. On peut ainsi conclure qu'il existe un deuxième canal de transfert d'énergie d'excitation dans le niveau $^1D_2$. Ce canal est actif pour des températures élevées probablement depuis les niveaux $^1I_6$, par un mécanisme de relaxation ou de transfert retour depuis un niveau de piège, et excite ensuite la terre rare.

Nous avons observé que les temps de vie des transitions du niveau 1I6 sont en général plus courts que les transitions du $^1D_2$ ceci étant en concordance avec la littérature.

Une étude a été effectuée sur des structures AlGaN dopées Tm. Elle montre des raies similaires aux boîtes GaN dopées Tm dans le bleu. Un effet de clusterisation doit probablement se produire pendant la croissance, ainsi l'environnement des atomes d'Eu consiste en des atomes de Ga (pas d'Al) et la structure a des similarités avec des boîtes.

Propriétés optiques des boîtes GaN dopées Tb

Nous nous sommes intéressé dans cette partie à la position des terres rares dans les structures à boîtes GaN dopées Tb encapsulées dans l'AlN. Les boîtes dopées Tb montrent une forte luminescence dans le vert.

Une étude optique de la photoluminescence en fonction de la température de structures à boîte GaN dopée Tb et d'un échantillon de référence d'AlN dopé Tb nous a permis de mettre en évidence le dopage au Tb dans les boîtes et dans l'AlN. Le comportement en

température de la photoluminescence des boîtes GaN dopées Tb permet d'identifier plusieurs transitions.

Une couche de GaN dopée Tb a une luminescence de très faible intensité. Ceci est reporté dans la littérature et est expliqué par les symétries des ions Tb dans le GaN.

Luminescence blanche des boîtes GaN dopées terres rares

Des structures à boîtes quantiques de GaN dopées avec des concentrations ajustées de Eu(rouge), Tm(bleue) et Tb(vert) ont montré de la luminescence blanche, ceci est particulièrement intéressant pour des applications dans l'éclairage. La couleur et l'intensité sont stables de l'ambiante jusqu'à des températures élevés, de l'ordre de 450 K.

La première étape d'injection de porteurs est réalisée par un contact Schottky pour les boîtes GaN dopées Eu (rouge). La couleur trouvée est plus jaune en électroluminescence qu'en photoluminescence, ceci montre qu'il existe différents mécanismes d'excitation des terres rares.

Content

1. Introduction

Rare earth (RE) ions with 3+ charge state have partly filled $4f^n$-shells, shielded from full filled outer orbitals ($5s^2$ and $5p^6$). By contrast, RE ions with other charge states like RE^{2+} ions exhibit partly filled outer shells. This difference in the electronic structure has consequences on the optical properties of RE^{3+} and RE^{2+} ions in host materials. Emission from RE^{2+} ions is found to be broad due to a strong influence from the environment [Owe81, Par03] while emission from RE^{3+} ions is typically very sharp as a result of shielding from outer shells. These sharp emissions are extending from the ultraviolet (UV) up to the infrared (IR) spectral region, depending on the RE atom and of course the inner shell transition itself. The energy levels of the RE^{3+} ions have been extensively investigated in the 1960es and tabulated by Dieke and co-workers [Die68]. In the so called Dieke diagram (Appendix B) ground state and excited states from free RE^{3+} are listed so that the emission wavelength from each transition can be deduced. As the host material influence on the transition is typically weak, the Dieke diagram can be used to predict which emission can be expected from each rare earth ion.

Nevertheless, all inner RE^{3+} transitions are intrinsically forbidden. Only interactions, for example with other atoms (free REs) or symmetry breaking by the host material, can make them “less” forbidden. The consequences are long decay times, typically between 1 μs to 10 ms. In spite of these long decay times the advantage of the sharp and clear defined inner RE^{3+} transitions resulted in numerous applications. RE^{3+} ions are used as a phosphor for color lamps and displays [Lum05], in optical fiber telecommunication (Er and Pr) and last but not least in Laser applications like the Nd:YAG Laser or Nd:glass Laser.

The idea of combining the RE luminescence with a semiconductor host came out by using Er and Yb (infrared) in GaAs, GaP, Si and SiC. Especially Er doped Si structures have been well investigated since the research was driven by the appeal of integration with Si microelectronics. In Ref. [Fav89] a systematic reduction of thermal quenching of infrared Er luminescence has been found by increasing the band width of the host semiconductor.

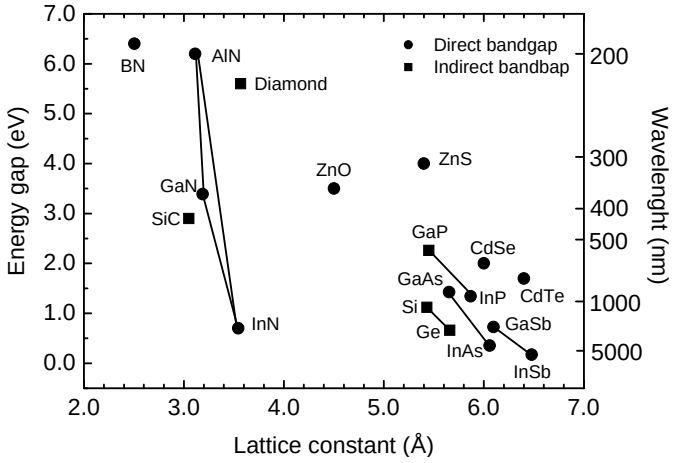

Figure 1.1: *Band-gap and lattice constants of common semiconductors. Data from www.ioffe.rssi.ru.*

For intense and thermally stable visible light emission from electroluminescence devices, wide band-gap semiconductors are required since efficient energy transfers can only occur if the band-gap of the host is wider than the energy difference between RE^{3+} ground states and excited state (Figure 1.1). Based on this idea, Steckl and his co-workers combined the RE^{3+} luminescent with the wide band-gap of GaN and realised electroluminescence from the blue to the red spectral range [Ste99, Hei99]. Furthermore the combination of different colors from RE^{3+} ions – red (Eu, Pr), green (Tb, Er, Ho) and blue (Tm, Dy, Ce) – would yield to white light emission. This idea is not new, as the combination of well defined RE-colors is used for example in mercury lamps where $LaPO_4$:RE is used as a phosphor to obtain white light.

The choice of GaN as a semiconductor host can be further explained since it exhibits first a direct band-gap, required for a good semiconductor host - RE^{3+} ion energy transfer probability and since it is a III-V semiconductor so that RE ions are supposed to occupy metal sites with 3+ charge, which was later experimentally established [Ban02, Hor04].

However, the RE radiative quantum efficiency strongly depends on the carrier-mediated energy transfer process, which has to compete with fast non-radiative recombination channels. Non-radiative processes can occur for example at defects, which are found with a density of about 10^{10} /cm^2 for GaN, which is a rather high number compared to other semiconductors. The result is a thermal quenching of the RE luminescence between one and two orders of magnitude from liquid helium to room temperature for REs in GaN films [Nye03, And05].

One way to overcome this problem can be the doping of nitride quantum dots (QDs) with RE ions. Then the carrier-mediated energy transfer to RE ions should

improve significantly since QDs are defect free regions and act as carrier confinement centers so that the thermal stability of the observed RE luminescence should be enhanced drastically. In other words the energy transfer to RE ions will be dominant over other possible non-radiative processes in the semiconductor host material.

It has to be noticed that GaN and AlN nitride exists in hexagonal and cubic phase and in different orientations (0001), (11-20), (-1100) and polarities (N-polar or metal-polar). The material of choice for the proposed device is a Ga-polar hexagonal 2H-GaN (0001), as the structural quality and reproducibility of cubic nitrides is significantly worse than in the case of hexagonal material, mostly due to the non-availability of suitable substrates for lattice-matched growth. Therefore, when growing cubic nitrides, overgrowth of QDs can lead to the appearance of stacking-faults and hexagonal inclusions.

Different possible types of nitride QDs can be grown by MBE starting from AlGaN QDs on AlN, GaN QDs on AlN, InGaN QDs on GaN to InN QDs on GaN and also InGaAlN QDs on AlN and GaN with well defined values of metal concentrations for ternary and quaternary QDs systems. For realizing these QDs systems the used growth mode is the Stranski Krastanow (SK) growth mode, which appears when two semiconductor materials are grown onto each other with the formation of QDs as a result. One possible driving force is the strain induced by the different lattice parameters of the two materials.

RE doping of QDs can be performed in situ, this means during growth of QDs, or ex-situ, by rare earth implantation. One advantage of RE implantation is that the total number of RE atoms implanted is well known, however the structural quality of the samples is getting worse as during implantation of RE a high number of defects is induced. Annealing in N-atmosphere can enhance the sample quality but in-situ doping is the method of choice for high quality samples.

A p-n junction light emitting diode (LED) emits light when an electric current is passed through it. It consists of a sandwich of a p-typed and a n-typed layer with an active region in the middle. The band-gap of the semiconductor corresponds to the required minimum energy of an electron from the valence band to be raised into the conduction band. If a constant current is passed through the LED, electrons flow from the n-doped side and holes from the p-doped side resulting in a high number of

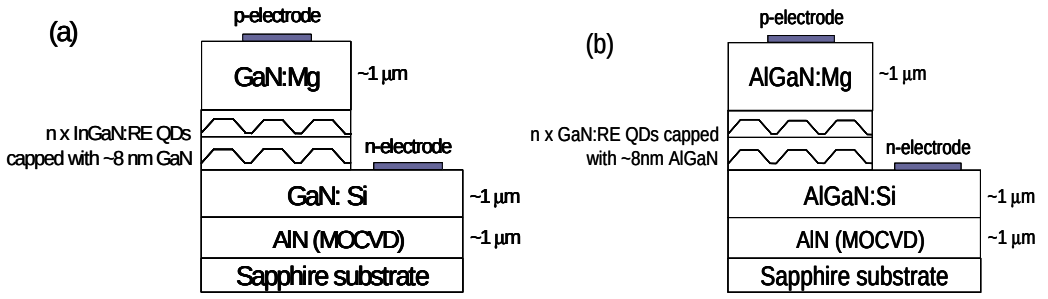

Figure 1.2: *Possible white LEDs with a superlattice of* **a)** *InGaN:RE QDs and* **b)** *GaN:RE QDs in the active region.*

observed radiative recombinations. In presence of a RE-doped active region, the high number of electron hole pairs can excite after recombination the RE atoms, followed by an inner shell transition inside the RE atoms resulting in visible light.

The injection of carriers into AlN is hindered by the difficulties in p-type and n-type doping of AlN, so that one solution could be the use of rare earth doped InGaN QDs grown on GaN for current injection devices, since -p and -n doping of GaN are well controlled by MBE (Figure 1.2a). Another way for realizing full color devices is the -n and -p doping of AlGaN and to use GaN:RE QDs in the active region (Figure 1.2b).

During this work we will study also the GaN:RE QDs grown on AlN in details. We will answer the question, if QDs are really doped with RE ions, which is not obvious, since during MBE growth the RE atoms are mobile. The issue of the quantum efficiency of RE doped nitride QDs and thin layers will be also adressed to clarify its potential for further devices.

References

[And05] T. Andreev, Y. Hori, X. Biquard, E. Monroy, D. Jalabert, A. Farchi, M. Tanaka, O. Oda, Le Si Dang, and B. Daudin, *Optical and morphological properties of GaN quantum dots doped with Tm*, Phys. Rev. B **71**, 115310 (2005).

[Ban02] H. Bang, S. Morishima, Z. Li, K. Akimoto, M. Nomura, and E. Yagi, *MBE growth of Eu- or Tb-doped GaN and its optical properties*, J. Cryst. Growth **237-239**, 1027 (2002).

[Die68] G. H. Dieke, *Spectra and Energy levels of Rare Earth Ions in Crystals* (Wiley, New York, 1968).

[Fav89] P. N. Favennec, H. L'Haridon, M. Salvi, D. Moutonnet, Y. Le Guillou, *Luminescence of Erbium implanted in various semiconductors: IV, III-V and II-VI materials*, Electron. Lett. **25**, 718 (1989).

[Hei99] J. Heikenfeld, M. Garter, D. S. Lee, R. Birkhahn, and A. J. Steckl, *Red light emission by photoluminescence and electroluminescence from Eu-doped GaN*, Appl. Phys. Lett. **75**, 1189 (1999).

[Hor04] Y. Hori, X. Biquard, E. Monroy, D. Jalabert, F. Enjalbert, Le Si Dang, M. Tanaka, O. Oda, and B. Daudin, *GaN quantum dots doped with Eu*, Appl. Phys. Lett. **84**, 206 (2004).

[Lum05] Invited article from lumileds lighting (In German), *Aus blau mach weiss*, Physik Journal **8/9**, 18 (2005).

[Nye03] Ei Ei Nyein, U. Hömmerich, J. Heikenfeld, D. S. Lee, A. J. Steckl, and J. M. Zavada, *Spectral and time-resolved photoluminescence studies of Eu-doped GaN*, Appl. Phys. Lett. **82**, 1655 (2003).

[Owe81] J. F. Owen, P. B. Dorain, and Takao Kobayasi, *Excited-state absorption in Eu^{2+}:CaF_2 and Ce^{3+}:YAG single crystals at 298 and 77K*, J. Appl. Phys. **52**(3), 1216 (1981).

[Par03] J. K. Park, M. A. Lim, C. H. Kim, H. D. Park, and S. Y. Choi, *Effect of Composition on Luminescence Properties of Eu^{2+} - Activated Mullite*, J. of the Electrochemical Society, **150**(10) H246-H249 (2003).

[Ste99] A. J. Steckl, M. Garter, D. S. Lee, J. Heikenfeld, and R. Birkhahn, *Blue emission from Tm doped GaN electroluminescent devices*, Appl. Phys. Lett. **75**, 2184 (1999).

2. Kinetics of rare earth luminescence in semiconductors

Knowledge about the kinetics of the rare earth luminescence in host materials is important for optimizing device structures [Sch91, Loz93]. A considerable effort has been made in the case of infrared emission of InP:Yb [Kli02, Tak89, Tag96, Loz94, Tag92], GaAs:Er [Cul98], Si:Er [Tsi98, Nee93, Küh99, Fuh97, Cof93]. Comparatively, the literature concerning RE-doped GaN thin films is rather scarce [Lee04]. Moreover, the energy transfer mechanism in rare earth doped GaN QDs has not been studied yet.

In this chapter a summary of results in literature is presented, which are important for understanding the further chapters, especially those where optical properties are discussed and where the energy transfer mechanism from the GaN QDs to the RE ions will be tackled.

2.1 Rare earth related trap levels in semiconductors

Isoelectronic impurities can produce bond states in the band-gap where carriers can be bound. Mechanisms governing the intensity of binding energy potential are the size difference between impurity and host and the electronegativity of the guest [Tho65]. Also spin orbit coupling and strain field, induced by size differences between guest and the host atoms can play an important role for creating trap levels [Bal72]. The covalent radius and the electronegativity of RE^{3+} ions are shown in Table 2.1 with respect to that of Ga and In, so that according to this statement it is getting understandable that RE^{3+} ions can act as traps in doped III-nitrides since the electronegativity is remarkably lower for RE^{3+} ion and the covalent radius bigger than for Ga and In ions.

Generally, most trap levels are attractive for electrons, but they can also bind in few cases a hole (GaAs:Er [Whi88, Ben91]) or excitons.

More complicate is the situation for n-type and p-type semiconductors. In the former case isoelectronic traps are electron occupied at higher temperature and empty in the latter, whereas at low temperature all traps will be empty for p-type, n-type and neutral semiconductor materials [Dap74, Bac72].

Element	**Electron configuration**	**Electron configuration RE^{3+} ion**	**Ionic radius (Å)**	**Covalent radius (Å)**	**Electronegativity**
Europium	$4f^7 5s^2 5p^6 6s^2$	$4f^6 5s^2 5p^6$	0.97	1.85	1.20
Terbium	$4f^9 5s^2 5p^6 6s^2$	$4f^8 5s^2 5p^6$	1.00	1.59	1.20
Holmium	$4f^{11} 5s^2 5p^6 6s^2$	$4f^{10} 5s^2 5p^6$	0.97	1.58	1.23
Erbium	$4f^{12} 5s^2 5p^6 6s^2$	$4f^{11} 5s^2 5p^6$	0.96	1.57	1.24
Thulium	$4f^{13} 5s^2 5p^6 6s^2$	$4f^{12} 5s^2 5p^6$	0.95	1.56	1.25
Ytterbium	$4f^{14} 5s^2 5p^6 6s^2$	$4f^{13} 5s^2 5p^6$	0.94	1.74	1.10
Gallium	$3d^{10} 4s^2 4p$		**0.62**	**1.26**	**1.81**
Indium	$4d^{10} 5s^2 5p$		0.81	1.44	1.78

Table 2.1: *Electron configuration of selected RE atoms, RE^{3+} ions (and some elements), ionic, covalent radii, and electronegativity. The complete table can be found in [Loz93].*

Experimentally trap levels can be demonstrated by measuring the lifetime of carriers, which is of course much longer when bond to an isoelectronic trap level. If after recombination of carriers the guest atom can be excited, like in the case of RE^{3+} ions, other methods have to be used to identify trap levels. These methods are for example: PLE, transmission experiments, and thermally activated PL measurements. In the present case, PLE was used and will be presented in details in chapter 4.2.

However in the case of RE^{3+} ions it has to be noted that the ions can occupy different sites in the lattice, like interstitial sites, which make the correct interpretation of results difficult. Other problems are the formation of native defects during sample growth, which are likely due to the large covalent radius of RE impurities. RE atoms can also interact with unwanted impurities like oxygen which can have detrimental effects on the excitation mechanisms.

2.2 Energy transfer mechanism from the semiconductor host to the RE^{3+} ions

The most extensively studied III-V semiconductor RE system is InP:Yb [Kli02, Tak89, Tag96, Loz94, Tag92]. The choice of this system is comprehensible as Yb^{3+} ions have only one excited state and they replace In atoms with only one optical

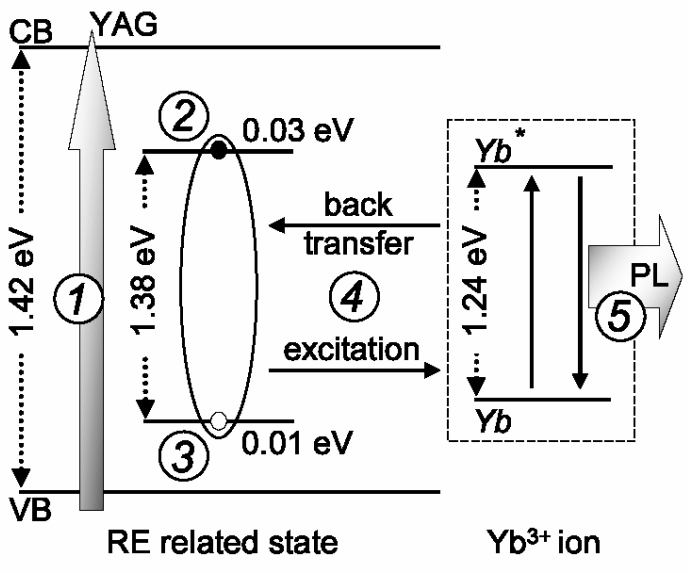

Figure 2.1: *Model of excitation of Yb^{3+} ions in InP host. After band to band excitation* ***(1)*** *the generated free electrons can be captured by a Yb related trap* ***(2)****. Binding of the hole* ***(3)*** *forms an electron hole pair on the trap. Nonradiative recombinations of the pair leads to excitation of the Yb^{3+} ion* ***(4)****, producing the observed PL* ***(5)****. An energy backtransfer can lead in a deexcitation of the Yb^{3+} ion. From [Kli02].*

active site [Wag84]. Kinetic models from other semiconductor RE systems like Si:Er [Tsi98, Nee93, Küh99, Fuh97, Cof93] show similar characteristics.

Figure 2.1 shows a schematic model of Yb^{3+} excitation in InP host. It is proposed that after band to band excitation of the semiconductor (1) the generated free electron can be captured by a RE related trap (2). Then a hole from the valence-band is bound due to the resulting Coulomb interaction (3).

The recombination energy is then used to excite the Yb^{3+} ion from the ground state to the excited state in a so called Auger process involving electrons from the 4f-shell of the Yb atom (4). It is understandable that the energy between excited state and ground state has to be well defined. Too low recombination energy from the recombining electron hole pair would not yield to any excitation of the RE^{3+} ion. On the other side, the use of too wide band-gap would yield to complex processes, the excess energy being released by the generations of phonons, which have been experimentally established in [Tag94].

Coming back to the end of the described energy transfer process shown in Figure 2.1, the excited electron in the Yb^{3+} atom can relax to the ground state which is associated with the light emission (5). However, an energy backtransfer process can also occur leading to deexcitation of the Yb^{3+} ion. In such a case the free energy can be used to excite again an Yb^{3+} ion, either the same or for samples with higher

content a neighbor ion. Another possibility is that an electron from the valence band can be generated with band edge related luminescence as the result. For matching the energy difference between trap level and conduction band a multiphonon process is proposed [Tag96].

The discussed processes occur in different time scales. The rise time of the Yb^{3+} atoms has been measured to be between 1 μs and 10 μs depending on the generation rate [Loz93, Loz94], whereas the decay is between 7 μs and 12 μs. Note that for other RE atoms the decay time can be much longer as it is depending strongly on the transition itself. Along the above discussion the rise time is including the process (1) to (3). For the decay time, only process (5) has to be considered. However an energy backtransfer with following rare earth ion excitation would yield to much longer decay times, which is discussed in more detail in chapter 5.3 for of Eu doped GaN QDs.

All RE^{3+} ions other than Yb^{3+} have more than one excited states so that the energy transfer mechanism is more complicate. At first the electron from the excited RE^{3+} ion can relax radiatively or with phonon emission to lower lying excited states.

Also cross relaxation processes can occur, which means that energy from an excited RE^{3+} ion is transferred, after radiative relaxation of the electron to a ground state, to another RE^{3+} ion, which is typically located close to the first ion in the lattice. This has of course detrimental effects on the optical output of the observed emission line as the cross excited luminescence is at the same (or lower) emission energy. Cross relaxation processes are typically yielding to long decay times of the emission lines which we will discuss in more detail for the example of Eu doping in chapter 5. This phenomenon has been experimentally established for Eu^{3+} ions in insulators [Dej95].

References

[Bac72] R. Z. Bachrach and O. G. Lorimor, *Measurement of the Extrinsic Room-Temperature Minority Carrier Lifetime in GaP*, J. of Appl. Phys. **43**, 500 (1972).

[Bal72] A. Baldereschi and J. J. Hopfield, *Binding to Isoelectronic Impurities in Semiconductors*, Phys. Rev. Lett. **28**, 171 (1972).

[Ben91] T. Benyattou, D. Seghier, G. Guillot, R. Moncorge, P. Galtier, and M. N. Charasse, *Time-resolved photoluminescence spectroscopy from erbium-doped $Ga_{0.55}Al_{0.45}As$*, Appl. Phys. Lett. **58**, 2132 (1991).

[Cof93] S. Coffa, F. Priolo, G. Franzò, V. Bellani, A. Carnera, and C. Spinella, *Optical activation and excitation mechanisms of Er implanted in Si*, Phys. Rev. B **48**, 11782 (1993).

[Cul98] T. D. Culp, J. G. Cederberg, B. Bieg, T. F. Kuech, K. L. Bray, D. Pfeiffer and C. H. Winter, *Photoluminescence and free carrier interactions in erbium-doped GaAs,* J. of Appl Phys. **83**, 4918, (1998).

[Dap74] P. D. Dapkus, W. H. Hackett, Jr., O. G. Lorimor, and R. Z. Bachrach, *Kinetics of recombination in nitrogen-doped GaP*, J. of Appl. Phys. **45**, 4920 (1974).

[Dej95] M. Dejneka, E. Snitzer, and R. E. Riman, *Blue, green and red fluorescence and energy transfer of Eu^{3+} in fluoride glasses*, J. of Luminescence **65**, 227 (1995).

[Fuh97] W. Fuhs, I. Ulber, G. Weiser, M. S. Bresler, O. B. Gusev, A. N. Kuznetsov, V. Kh. Kudoyarova, E. I. Terukov, and I. N. Yassievich, *Excitation and temperature quenching of Er-induced luminescence in a-Si:H(Er)*, Phys. Rev. B **56**, 9545 (1997).

[Kli02] M. A. J. Klik, T. Gregorkiewicz, I. V. Bradley, and J-P. R. Wells, *Optically Induced Deexcitation of Rare-Earth Ions in a Semiconductor Matrix*, Phys. Rev. Lett. **89**, 227401 (2002).

[Küh99] H. Kühne, G. Weiser, E. I. Terukov, A. N. Kusnetsov, and V. Kh. Kudoyarova, *Resonant nonradiative energy transfer to erbium ions in amorphous hydrogenated silicon*, J. of Appl. Phys. **86**, 896 (1999).

[Lee04] C. W. Lee, H. O. Everitt, D. S. Lee, A. J. Steckl, and J. M. Zavada, *Temperature dependence of energy transfer mechanisms in Eu-doped GaN*, J. of Appl. Phys. **95**, 7717 (2004).

[Loz93] H. J. Lozykowski, *Kinetics of luminescence of isoelectronic rare-earth ions in III-V semiconductors,* Phys. Rev. B **48**, 17758 (1993).

[Loz94] H. J. Lozykowski, A. K. Alshawa, and I. Brown, *Kinetics and quenching mechanisms of photoluminescence in Yb-doped InP*, J. Appl. Phys. **76**, 4836 (1994).

[Nee93] M. Needels, M. Schlüter, and M. Lannoo, *Erbium point defects in silicon*, Phys. Rev B **47**, 15533 (1993).

[Nuk97] J. Nukeaw, J. Yanagisawa, N. Matsubara, Y. Fujiwara, and Y. Takeda, *Observation of trap states in Er-doped InP by photoreflectance*, Appl. Phys. Lett. **70**, 84 (1997).

[Sch91] S. Schmitt-Rink, C. M. Varma, and A. F. J. Levi, *Excitation Mechanisms and Optical Properties of Rare-Earth Ions in Semiconductors*, Phys. Rev. Lett. **66**, 2782 (1991).

[Tag92] A. Taguchi, M. Taniguchi, and K. Takahei, *Direct verification of energy back transfer from Yb 4f-shell to InP host*, Appl. Phys. Lett. **60**, 965 (1992).

[Tag94] A. Taguchi, K. Takahei, and Y. Horikoshi, *Multiphonon-assisted energy transfer between Yb 4f shell and InP host*, J. of Appl. Phys. **76**, 7288 (1994).

[Tag96] A. Taguchi and K. Takahei, *Band-edge-related luminescence due to the energy backtransfer in Yb-doped InP*, J. of Appl. Phys. **79**, 3261 (1996).

[Tak89] K. Takahei, A. Taguchi, H. Nakagome, K. Uwai, and P. S. Whitney, *Intra-4f-shell luminescence excitation and quenching mechanism of Yb in In*, J. of Appl. Phys. **66**, 4941 (1989).

[Tho65] D. G. Thomas, J. J. Hopfield, and C. J. Frosch, *Isoelectronic Traps Due to Nitrogen in Gallium Phosphide*, Phys. Rev. Lett. **15**, 857 (1965).

[Tsi98] I. Tsimperidis, T. Gregorkiewicz, H. H. P. Bekman, and C. J. G. M. Langerak. *Direct Observation of the Two-Stage Excitation Mechanism of Er in Si*, Phys. Rev. Lett. **81**, 4748 (1998).

[Wag84] J. Wagner, J. Windscheif, and H. Ennen, *Photoluminescence excitation spectroscopy on InP: Yb*, Phys. Rev. B **30**, 6230 (1984).

[Whi88] P. S. Whitney, K. Uwai, H. Nakagome, and K. Takahei, *Electrical properties of ytterbium-doped InP grown by metalorganic chemical vapor deposition*, Appl. Phys. Lett. **53**, 2074, (1988).

[Yon02] Yong-Hoon Cho, B. J. Kwon, J. Barjon, J. Brault, B. Daudin, H. Mariette, and Le Si Dang, *Optical characteristics of hexagonal GaN self-assembled quantum dots: Strong influence of built-in electric field and carrier localization,* Appl. Phys. Lett. **81**, 4934 (2002).

3. Growth of undoped and rare earth doped nitride homo- and heterostructures

The aim of this chapter is to provide first a short summary of MBE growth of GaN, AlN and GaN QDs (Sections 3.1 and 3.2). The impact of RE doping on the growth regime of these structures will be considered in sections 3.3 and 3.4. The growth of more complicate heterostructures like GaN QDs on AlGaN (Section 3.2.2) and InGaN:Eu QDs on GaN (Section 3.5) will also be discussed. To learn more about the growth mechanisms, in-situ RHEED has been used as well as ex-situ experiments, e. g. RBS, AFM and EXAFS. A basic introduction to these techniques is given in Appendix A.

3.1 Growth of GaN and AlN layers

The growth of GaN layers has to be well controlled since the quality of the films depends strongly on the chosen growth conditions. Two growth parameters can be changed in MBE: the substrate temperature and the metal to N ratio.

It is not easy to measure the substrate temperature, as the templates are fixed with an In bonding onto a molyblock or are clipped onto a square shaped hole. That means the substrate temperature cannot be just measured by the current of the electric heating system. To solve this problem, and to ensure of the reproducibility of the experiments, one possibility could be to use a pyrometer, which allows one to measure the substrate temperature by black body radiation. A second possibility is to in-situ measure the desorption time of Ga-metal on substrate from the variation of the RHEED intensity [Ade03]. The idea is to expose the substrate to a Ga flux and measure the desorption time after closing the Ga shutter. This desorption time is a function of the substrate temperature, so that the substrate temperature can be calibrated.

However the desorption time is also depending onto the orientation of the substrate. Reference [Lau04] treats the case of a (11-20) gallium nitride surface.

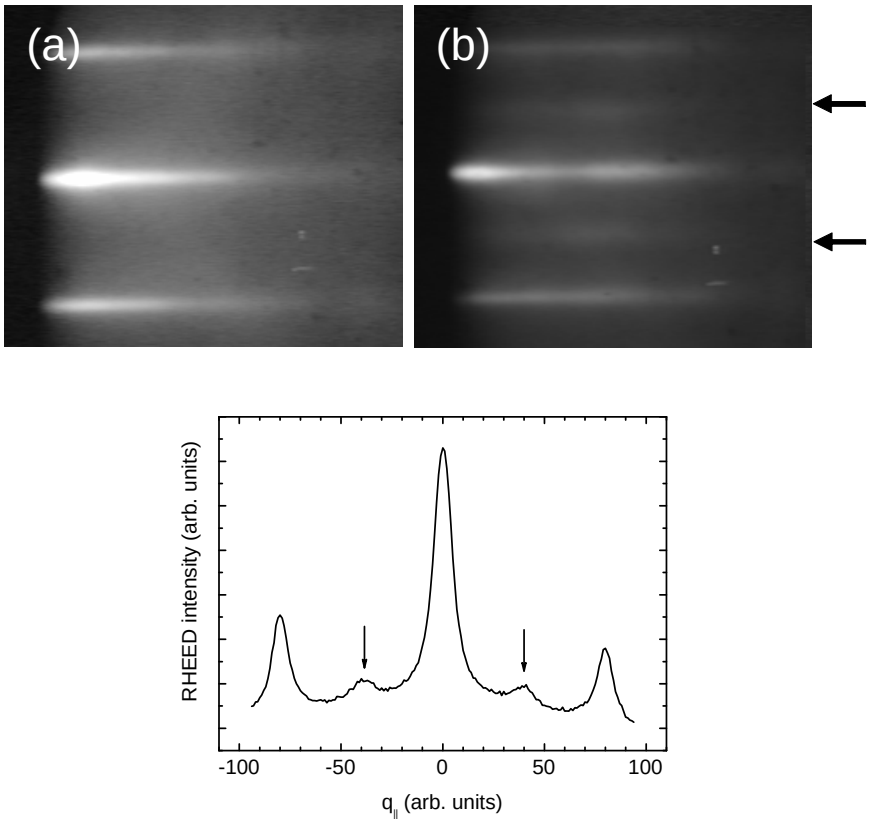

Figure 3.1 a) *RHEED image of a GaN layer during growth in slightly Ga-rich growth conditions at a substrate temperature of 720°C* **b)** *RHEED image of a GaN:Eu layer during growth in slightly Ga-rich growth conditions at a substrate temperature of 720°C. Azimuth direction for both images <10-10>. The arrows mark the position of the 2 reconstruction for clarity.* **c)** *Intensity profile along the <10-10> direction for GaN:Eu. The arrow marks the reconstruction for clarity.*

One can wonder, whether Ga adsorption followed by desorption could reduce the quality of the template, which would be the case for oxygen adsorbtion onto ZnO, where oxygen would stick onto the surface even for high substrate temperatures. Actually for hexagonal AlN and GaN substrate desorbed Ga atoms can remove some unwanted surface impurities, like oxygen, which enhances the cleanliness of the surface. Then, before growth two or three cycles of Ga metal adsorption - desorbtion were typically performed.

Suitable growth temperatures for GaN layers are between 700°C and 750°C. Higher temperatures are preferred for AlN, because the atomic mobility of Al atoms is low at this temperature.

Growth of GaN layers depends crucially on the Ga- to N-ratio. Ga-rich growth conditions result typically in smooth surfaces, yielding to streaky RHEED patterns (Figure 3.1). GaN films grown in N-rich growth conditions show typically spotty RHEED and rough surfaces, detrimental to electronic and optical properties [Tar97,

Hey00a, Hey00b]. The reasons are different diffusion barriers for Ga adatoms, which have been found in Ga-rich condition to be about 0.3 eV and in N-rich conditions 1.3 eV according to density functional calculations in literature [Zyw98, Neu03]. Therefore, GaN growth is commonly carried out in Ga-rich growth conditions. Nevertheless, too high Ga-fluxes or too low substrate temperatures can lead to the formation of Ga-droplets, which diminish the quality of GaN [Kru01]. Studies in literature have also shown that a "growth window" exists, where the Ga surface coverage is independent from fluctuation of the substrate temperature and Ga-flux [Ade02], the Ga-surface coverage being typically 2MLs as predicted by theoretical calculations [Nor00].

For high quality AlN nitride layers, metal-rich growth conditions are also required. During Al-rich growth, Al-excess lines can be observed near the RHEED pattern (not shown). By contrast, N-rich conditions lead also to spotty RHEED images as in case of GaN growth indicating three dimensional growth.

3.2 The Stranski Krastanow growth mode

SK growth mode can occur if two materials are grown on each other with the formation of islands as a result. Around this island a coherent strain distribution is acting as an additional diffusion barrier for adatoms. Thus, the growth rate decreases rapidly after island formation. From the theoretical point of view SK growth mode is not fully understood for complex systems. The first study in the year 1938 takes only the charges of the ions into account but not the difference in lattice constants [Str37][1]. In more recent studies also the lattice mismatch between the two materials is included [Che96, Jes98]. Common semiconductor QDs systems are: $In_xGa_{1-x}As/GaAs$ [Gol85], Si_xGe_{1-x}/Si [Eag90], CdSe/ZnSe [Xin96] and the here studied nitride systems like GaN/AlN [Dau97], $In_xGa_{x-1}N/GaN$ [Ade00] and $GaN/Al_xGa_{x-1}N$ [Hor05].

[1] Stranski and Krastanow simulated crystal growth of singel charged ions onto a double charged ion crystal in a solution.

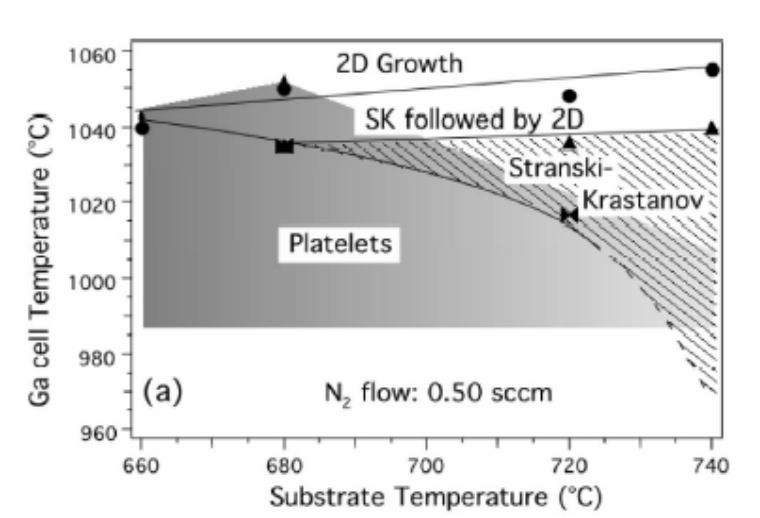

Figure 3.2: *Phase diagram indicating growth-modes in GaN heteroepitaxy on AlN. From [Mul01].*

3.2.1 Growth of GaN QDs on AlN

Figure 3.2 shows a phase diagram indicating the possible growth modes of GaN heteroepitaxy on AlN for a fixed N-flux. In the diagram different growth regimes can be found depending crucially onto the Ga-flux, associated here with the Ga-cell temperature.

For Ga-cell temperatures higher than 1040°C, Ga-rich growth conditions occur, which means that the growth is 2D, due to the above discussed surfactant effect of Ga.

For a lower Ga-flux and substrate temperatures higher than 680°C (Figure 3.2) SK growth mode occurs. During this a two ML thick substrate coherent GaN wetting-layer is deposed. Driven by lattice mismatch, GaN growth continues in QD formation.

For low substrate temperatures and a particular low Ga to N ratio, no clear 2D/3D transition can be observed. In these conditions GaN forms platelets that locally relax strain.

Most of the QDs studied in this work have been grown at 720°C by opening Ga and N sources until the RHEED shows spots with facets (Figure 3.3) resulting from QDs (10-20 sec). Next the Ga-flux was stopped to let the QDs ripen for 5-40 sec under N and after that for 5-20 sec under vacuum. Finally the QDs can be capped with about 10 nm AlN and the process can be repeated to achieve superlattices.

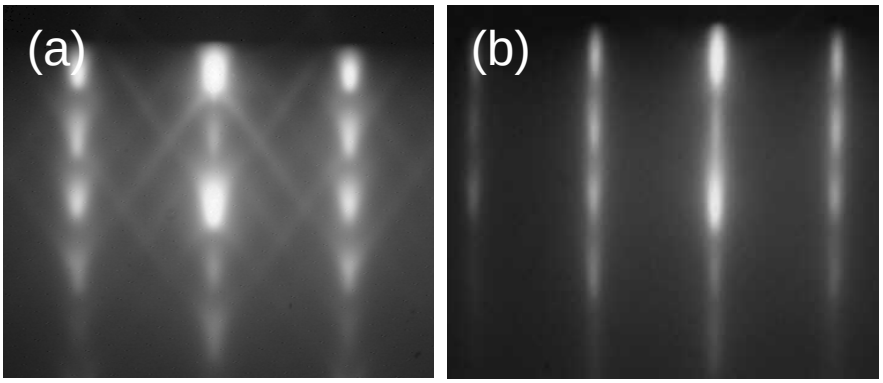

Figure 3.3 a) *RHEED image during growth of GaN QDs at a substrate temperature of 720°C* **b)** *RHEED image of a GaN:Eu QDs at a substrate temperature of 720°C. Azimuth direction for both images <10-10>. For the undoped sample clear facets can be found in RHEED after QD formation.*

The growth parameters influence the nucleation kinetics of QDs and structural property such as density, height and diameter. Typically an enhancement of the GaN amount deposited during QD growth yields to an increase of the QD density, which can be well controlled between $1 \cdot 10^{10}$ cm^{-2}-$2 \cdot 10^{11}$ cm^{-2}. Together with the density also the island height increases from typically 0.5 nm up to more than 4 nm. The substrate temperature has also an influence onto the morphological parameters of dots which can be in detail complicate. For more information see reference [Ade04].

Longer ripening times under N or under vacuum increase the sizes of GaN QDs which has been experimentally established in [Wid98].

In addition to the influence of the growth parameters also the used substrate can have an influence on the nucleation kinetics of QDs, so that reproducibility is only assured by use of similar substrates.

3.2.2 Growth of GaN QDs on AlGaN

In current injection devices the use of AlN has to be avoided since p- and n-doping is hardly achievable. To overcome this problem one possibility could be to grow GaN QDs on AlGaN, as n- and p- doping of AlGaN has been already demonstrated [Nak03, Zhu04]. However the key parameter to achieve SK growth mode on nitride systems is the lattice mismatch which is smaller for relaxed AlGaN than for AlN (Figure 1.1). We will see below, that GaN QD can be grown on AlGaN if the lattice parameter of AlGaN is similar to that of AlN.

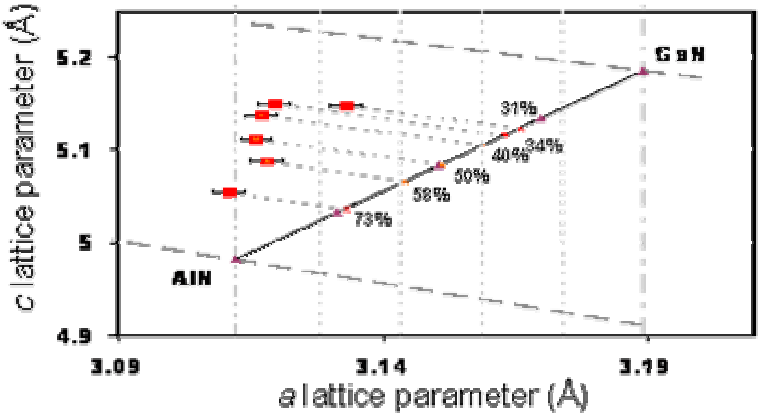

Figure 3.4: *c versus a lattice parameter variation of $Al_xGa_{1-x}N$ layers with x varying between 0.73 and 0.31. The thickness of layers is about 150 nm. The line between AlN and GaN corresponds to the expected behavior of fully relaxed $Al_xGa_{1-x}N$ layers.*

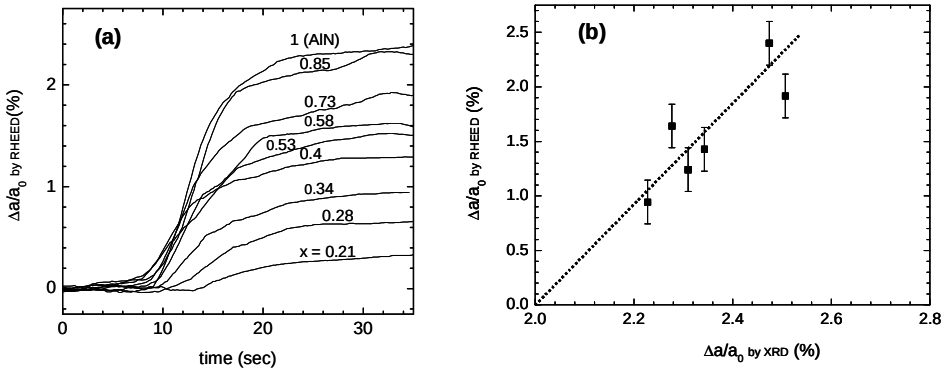

Figure 3.5: a) *In-plane lattice parameter variation as a function of time for GaN deposited on $Al_xGa_{1-x}N$ with x varying between 0.21 and 1.* **b)** *In-plane lattice parameter variation as a function of GaN/$Al_xGa_{1-x}N$ lattice mismatch. Dotted line is a guide.*

To address this possibility, a set of $Al_xGa_{1-x}N$ samples has been grown containing different Al concentrations. Then X-ray diffraction experiments, as shown in Figure 3.4, have been performed. The full line joining AlN and GaN illustrates the expected behavior of fully relaxed $Al_xGa_{1-x}N$ layers. By contrast, the experimental points strongly deviate from this behavior, as an evidence that $Al_xGa_{1-x}N$ layers, about 150 nm thick, are partially strained by the underlying AlN layer.

GaN QDs were then grown on this AlGaN buffers with concentrations shown in Figure 3.4 according to the SK growth mode. The growth was in-situ monitored by RHEED and by measuring the variation in the streaks spacing as a function of GaN deposition time on $Al_xGa_{1-x}N$ with various Al content. The result is displayed in Figure

3.5a. It shows that GaN elastic relaxation decreases for decreasing Al-content in $Al_xGa_{1-x}N$, consistent with the decreasing $GaN/Al_xGa_{1-x}N$ lattice mismatch. Furthermore, it shows that the critical thickness is unchanged as evidenced by the unchanged onset of GaN elastic relaxation, except for the lowest Al contents (28% and 21%) for which no GaN QDs could be identified by AFM. In Figure 3.5b, GaN relaxation yield as extracted from RHEED data was plotted as a function of the GaN/AlGaN lattice mismatch as extracted from X-rays diffraction results in Figure 3.4. Extrapolating the experimental values down to $\Delta a / a_0^{GaN}$ leads to suggest that the minimal lattice mismatch compatible with the occurrence of SK growth mode is 2 ± 0.1 %, of the same order as found for InGaAs/GaAs (~ 2%) [Leo93], GeSi/Si (1.4 %) [Eag90], PbSeTe/PbTe (1.6 %) [Pin98], and InGaN/GaN (1.4 - 1.8 %) [Ade00]. In conclusion the results show that it is possible to grow GaN QDs on AlGaN even with a Ga content of about 50 % due to the fact that the AlGaN layer is strained by the underlying Al substrate.

During this experiment great care was taken to grow AlGaN layers with suitable quality. For this the substrate temperature has been chosen higher than 730°C to enhance the mobility of Al-adatoms. As in case of GaN and AlN layers, metal-rich growth conditions are required, we took advantage of the surfactant properties of In which are discussed in more detail in reference [Mon03].

3.3 Rare earth doped GaN and AlN layers

MBE growth of RE doped GaN and AlN layers is a particularly new field. It is not clear, what is the incorporation rate of RE atoms into GaN in slightly Ga-rich and AlN in Al-rich growth conditions required for high quality layer growth.

Another problem of RE doping of nitride layers can be the creation of RE related defects, which reduces crystalline quality [Fil04]. These imperfections are expected to play an important role in RE excitation, which has to be avoided since they might result in non-radiative recombination channels, detrimental to the optical output.

This work is mainly focused on the growth of Eu, Tb and Tm doped GaN and AlN layers, following the pioneering work on Er and Eu doping of GaN, where the influence of the substrate temperature and the Ga to N-ratio has been studied in wide range [Lee02a, Lee02b, Liu04].

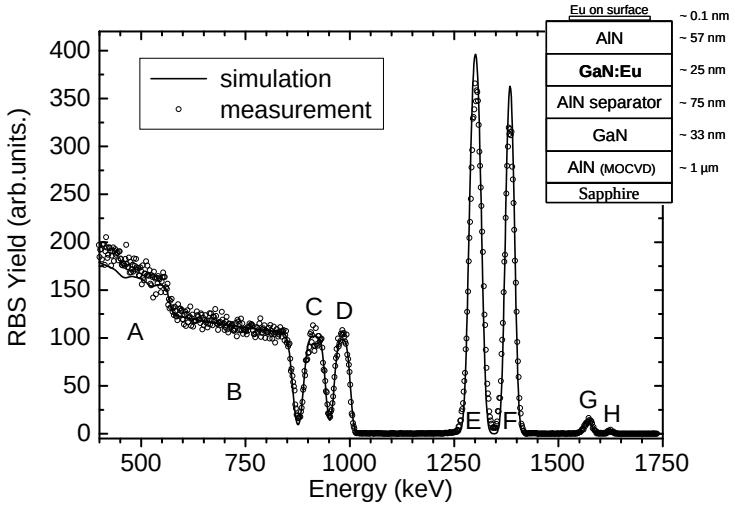

Figure 3.6: *RBS spectrum of an undoped and Eu doped GaN layer (both N-rich) caped with AlN. The sample structure found by analysis is also indicated in the Figure. Acceleration voltage of the He Ions: 1.8 MeV. Eu content inside GaN: 0.9%. The letters are used to label to the position of elements:* ***A*** *is N in AlN, GaN GaN:Eu;* ***B*** *is Al in AlN of the substrate;* ***C*** *is Al form AlN separator;* ***D*** *is Al from AlN capping;* ***E*** *is Ga in GaN,* ***F*** *is Ga in GaN:Eu,* ***G*** *is Eu in GaN:Eu and* ***H*** *is Eu on the sample surface.*

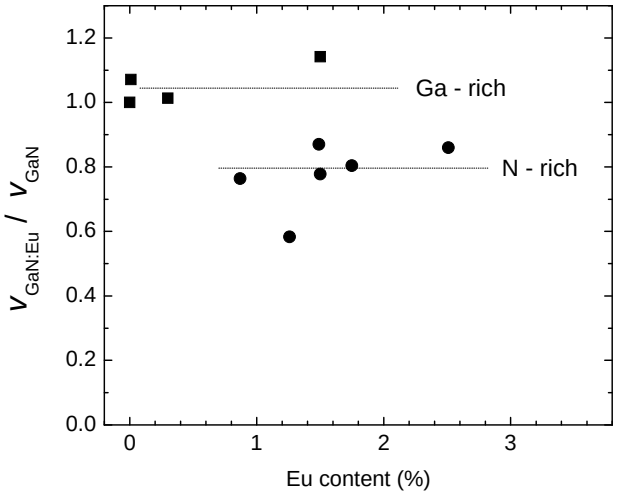

Figure 3.7: *Normalized growth rate of Eu-doped GaN layers as a function of Eu content. Circles correspond to growth in N-rich growth conditions and squares to Ga-rich conditions. The values are deduced from sample structures analyzed by RBS as shown in Figure 3.6.*

3.3.1 Growth of GaN:Eu layers

For studying the growth of GaN:Eu films, structures as given in Figure 3.6 have been grown. They consist of an undoped GaN layer and a GaN:Eu layer, both grown under identical conditions, for substrate temperature, Ga to N-flux ratio and growth time. The undoped and the doped GaN layer are capped with AlN to enable RBS analysis of the layer thicknesses.

One example of RBS spectrum and its analysis is shown in Figure 3.6. In the shown example growth conditions have been N-rich, mimic to those required for SK mode. From the quantitative analysis of the two peaks at about 1300 and 1400 keV, corresponding to Ga in GaN layer (E) and Ga in GaN:Eu layer (F) it can be concluded that the growth rate is significantly lower for the Eu doped GaN layer. Results for identical structures grown with different Eu content are shown in Figure 3.7. It is visible that Eu decreases the growth rate up to 20 % in N-rich regime for Eu concentrations between 1% and 3%. In N-rich growth conditions the growth rate is limited by impinging Ga flux, which suggests that the presence of Eu is associated with a change in the kinetics of Ga adatoms.

In order to study further the growth of Eu doped GaN layers, samples with the same structure have been grown also in Ga-rich conditions e. g. in N-limited regime. In Ga-rich regime no significant changes of the growth rate can be observed (Figure 3.7). This is further suggesting that Eu modifies the kinetics of Ga adatoms, but does not affect the kinetics of N adatoms. These results can be explained by a Eu tendency to segregate on the surface during growth. In the N-rich regime the mean free path of Ga adatoms is enhanced by the segregated Eu atoms. The enhancement of the mean free path is yielding to a reduction of the growth rate as the possibility is significantly higher that Ga atoms will be finally desorbed.

By contrast in Ga-rich growth conditions an excess of Ga-atoms covers the growing surface so that the growth rate is not significantly influenced. The presence of Eu at the surface is found in the RHEED pattern, where Eu induces a 2 x 4 reconstruction (Figure 3.1).

3.3.2 Remarks on the growth of Eu doped AlN

Eu segregation effect is especially visible during growth of AlN. This is also demonstrated in the RBS measurement in Figure 3.6, where Eu atoms are found at the surface of the undoped capping layer. This means that the Eu atoms are not

incorporated during growth of the last AlN layer so that they remain on the surface at the end of growth. It strongly suggests that Eu atoms have a higher tendency to incorporate into GaN than into AlN which is understandable since the substrate temperature has been the same for the growth of the Eu doped GaN and AlN layer, but the sticking coefficient of Al is much higher. Another reason could be that the lattice parameters of GaN are higher than of AlN, so that the rather large Eu atoms are preferably incorporated into GaN.

It is remarkable that Eu-doped AlN thin films grown in Al-rich growth conditions show no Eu related luminescence, which is in agreement with the above discussed RBS results. Samples grown in N-rich conditions show only very weak Eu luminescence and a broad tail at around 350 nm possibly related to defect related energy levels inside AlN. A solution for this discrepancy and a way to achieve high Eu emission in AlN host is to grow an AlN layer in suitable growth conditions (Al-rich) and to dope the material ex-situ by implantation, which has been done in reference [Jad01].

3.3.3 Rare earth incorporation in GaN versus AlN for the example of Tm

We compare now the incorporation rate of Tm atoms into GaN and AlN layers grown in metal-rich growth condition. For this purpose, a sample consisting of a 104 nm thick GaN:Tm layer capped by a 180 nm thick AlN:Tm film was grown on an AlN template. During the growth of both layers the Tm-flux and the substrate temperature (720°C) remained constant. Figure 3.8 shows the RBS spectrum measured for this sample. The RBS signal labeled by the letter “D” is corresponding to Ga in GaN:Tm with corresponding Tm content labeled by “E”. The signal corresponding to region C is Al in Tm-doped AlN. The expected position of the Tm signal in the AlN layer is marked by the two arrows.

Quantitative analysis demonstrated that Tm concentration in the GaN layer was 1.2%, contrary to the AlN layer where incorporated Tm is below the RBS detection limit of our system (~0.025%), as an evidence that Tm incorporation in AlN is much lower than its incorporation in GaN, for a fixed Tm flux. During growth of the Tm doped GaN layer also a 2 x 4 reconstructions has been found.

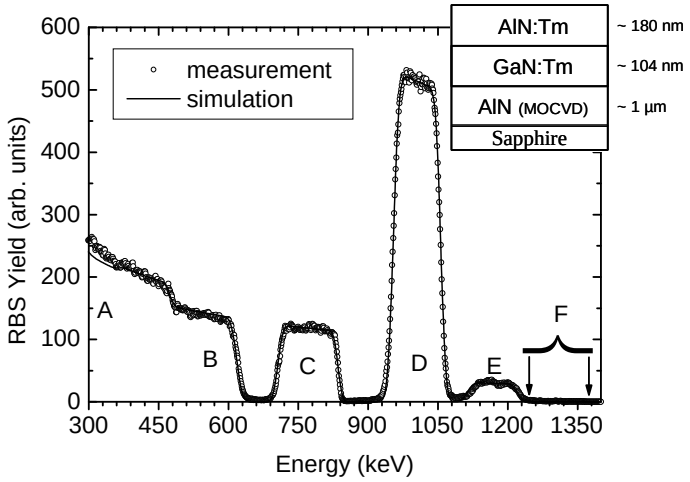

Figure 3.8: *RBS spectrum of a sample containing a 104 nm GaN:Tm layer with a 180 nm thick AlN:Tm on top. Acceleration voltage of the He Ions: 1.5 MeV. Tm content inside GaN: 1.2%. The letters are used to label to the position of elements:* ***A*** *is N in AlN, GaN:Tm and AlN:Tm;* ***B*** *is Al in AlN of the substrate;* ***C*** *is Al in AlN:Tm;* ***D*** *is Ga in GaN:Tm;* ***E*** *Tm in GaN:Tm. The arrows at the letter* ***F*** *indicate the calculated position of Tm in AlN.*

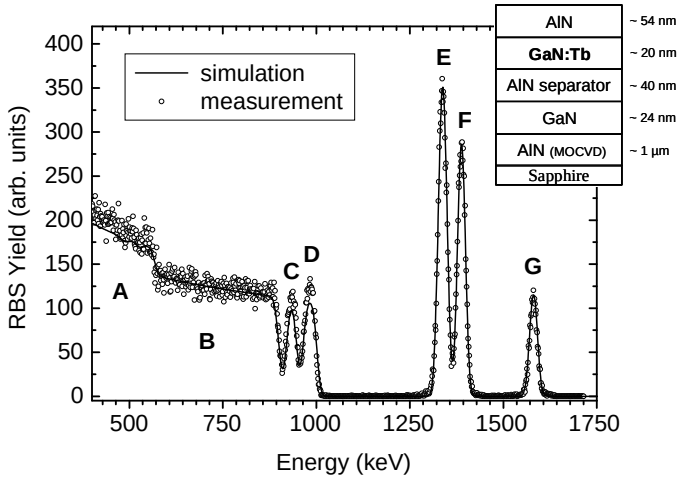

Figure 3.9: *RBS spectrum of an undoped and Tb doped GaN layer (both N-rich) caped with AlN. The sample structure found by analysis is also indicated in the Figure. Acceleration voltage of the He Ions: 1.8 MeV. Tb content inside GaN: 8.5%. The letters are used to label to the position of elements:* ***A*** *is N in AlN, GaN GaN:Tb;* ***B*** *is Al in AlN of the substrate;* ***C*** *is Al in AlN (separator);* ***D*** *is Al in AlN (AlN on top of sample);* ***E*** *is Ga in GaN,* ***F*** *is Ga in GaN:Tb and* ***G*** *is Tb in GaN:Tb.*

3.3.4 Growth of Tb doped GaN layers

In case of Tb doped layers, we have performed an analysis similar to that of Eu doped GaN shown in Figure 3.6. The result is that Tb doped GaN layers also show a reduction of the growth rate in N-rich conditions of about 17 % for high Tb content, as visible in the RBS spectrum in Figure 3.9. The result is similar to those shown in Figure 3.7 for Eu doping, as a clue that Tb also tends also to segregate during growth.

Nevertheless, properties of Tb doped GaN layers have been only preliminary studied as the samples show very low Tb luminescence and are therefore not interesting for device applications [Ban02]. A remarkable difference with Eu case is that Tb atoms have not been found on the sample surface. This could be either due to Tb incorportation into AlN but also due to Tb desorption during AlN growth.

3.4 Rare earth doped GaN quantum dots

Growth of RE-doped QDs is a rather complex process, because the RE atoms can change the mobility with Ga adatoms as we have seen in the last section. This means that the growth window for QD formation can change, combined with drastical influences on the diameters, height and densities of QDs. In the following study RE-doping has been performed in-situ by exposing the sample simultaneously to Ga, N, and RE-flux.

3.4.1 Growth of GaN QDs doped with Eu

Figure 3.10 shows the diameter, the height and the density of QDs containing different Eu contents. The data have been analyzed from AFM images as shown for three different contents of Eu in Figure 3.10a. The samples consist of ten layers of GaN QDs, grown at 720°C with an Ga to active N flux ration of 0.65%. Each plane of dots corresponds to an amount of 2.4 MLs of GaN nominally deposited.

A drastic influence of Eu on QD nucleation is illustrated in Figure 3.10. An AFM image of undoped GaN QDs is shown in Figure 3.10a. The effect of 1% Eu doping is also shown in Figure 3.10a, e. g. a lower density of bigger dots, while a further increase of Eu content up to 2.2% results in a larger density of smaller dots. A decrease in the density (Figure 3.10c) of QDs is correlated with an increase of their size (Figure 3.10b), which can be found for Eu concentrations up to 1.5 %. For higher Eu contents an increase can be observed while the dimensions decrease. For about 3% Eu, no more QDs have been observed, e.g. the spontaneous 3D islanding of GaN was completely inhibited.

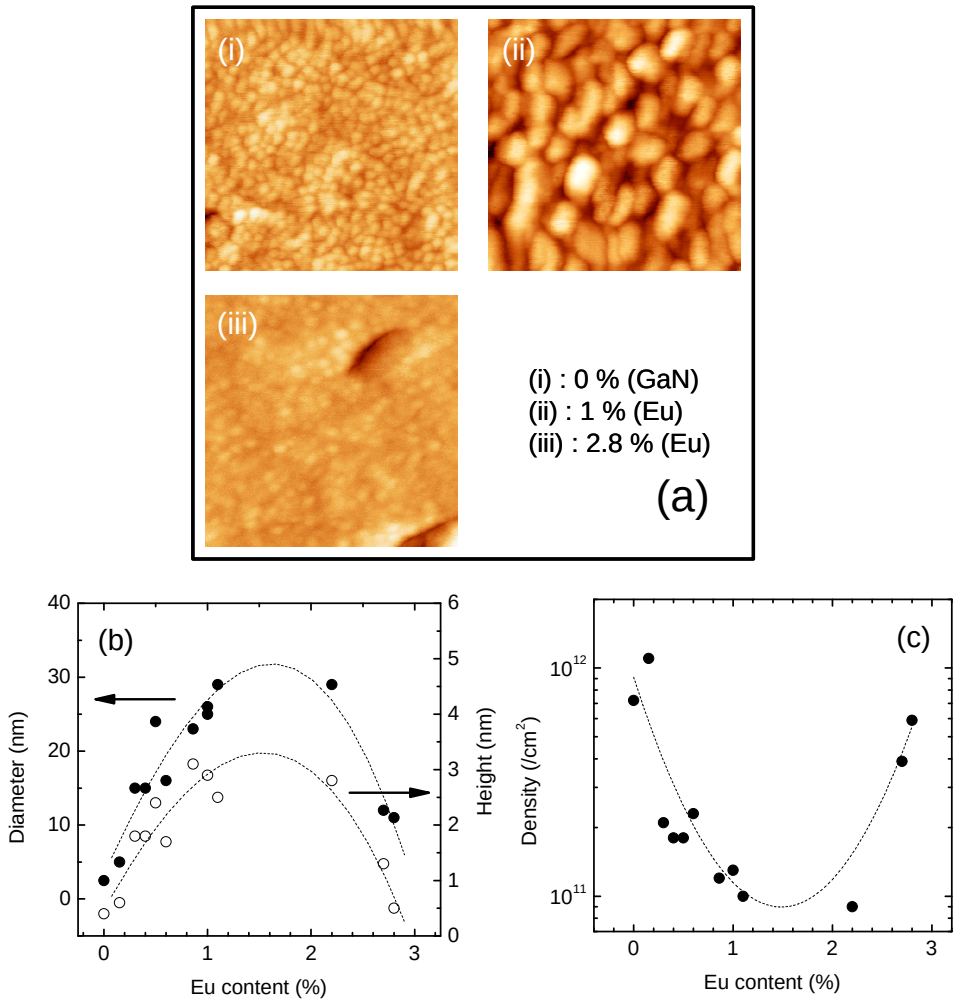

Figure 3.10: a) *AFM images of i) undoped GaN QDs, ii) GaN doped with Eu QDs containing 1% Eu and iii) 2.8 % Eu. The areas of images are 150 nm x 150 nm.* **b)** *diameter and height and* **c)** *density of GaN QDs measured by AFM for samples containing different Eu concentrations. The dashed lines are guides to the eye. The Eu content has been measured by RBS.*

To identify the mechanism that governs the variation morphology, we must take into account the height versus diameter plot shown in Figure 3.11, which reveals that the aspect ratio of QD is independent of the Eu content and equal to 0.1. This result strongly suggest that the dimensions of Eu-doped GaN QDs are kinetically limited, as the aspect ratio remains constant.

Having thus established for low Eu concentrations (between 0 and 1.6 %) the Ga diffusion length is increasing, as the GaN surface is occupied by more and more Eu atoms as a result of a high tendency of Eu atoms to segregate (see section 3.3 for the case of GaN:Eu layers). Therefore the reduction in the density and the increase in size of Eu-doped QDs result from an increased Ga kinetics leading to a larger capture radius of impinging material around nucleating islands.

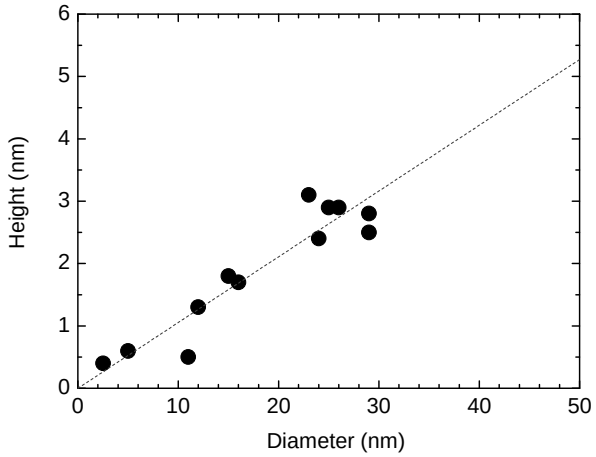

Figure 3.11: *Height versus diameter of Eu doped GaN QDs. The aspect ration (height/diameter) is constant and equal to 0.1 (dashed line).*

Then, what is the nature of regime change observed for a Eu concentration higher than 1.6%? It can be proposed that the kinetical limitation in this range results from the progressive saturation of the growing GaN surface with Eu.

As a consequence, the increasing probability that Eu atoms occupying Ga sites have Eu as a second neighbor would result in Eu-Eu interaction and would likely reduce the mobility of Ga adatoms, eventually leading to the formation of a continuous Eu film acting as a surfactant, which completely inhabits QD formation for Eu concentrations higher that 3%. Such a scheme is consistent with a dot size reduction and an increased density for high Eu flux while the volume of GaN material contributing to dot formation is constant.

Eu doped GaN QDs with a content of about 1.5% show no facets in RHEED and under the spots from QDs typically weak stripes are observed (Figure 3.3).

3.4.2 EXAFS on GaN QDs doped with Eu

We have seen above that Eu doping yields to a strong perturbation of structural parameters of GaN QDs. Now, in this section, EXAFS results on GaN:Eu QDs will be discussed to get more information about doping of dots. A more detailed description of EXAFS results can be found in Ref. [Hor04].

The EXAFS method provides information on nearest atomic neighbors, the bonding length, and the charge of ions. In case of GaN QDs the 4 first next neighbors from Eu have been found to be nitrogen atoms. All 12 second next neighbors have

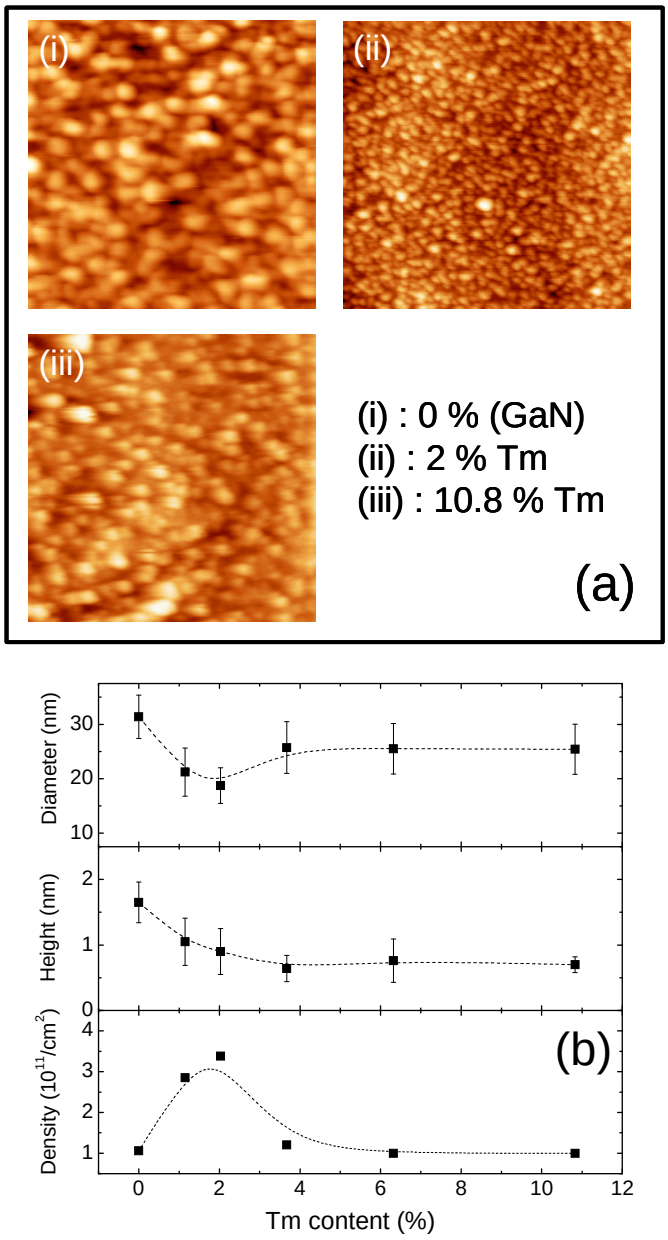

Figure 3.12: a) *AFM images from Tm doped GaN QDs with different concentrations.* **b)** *Diameter, height and density of QDs measured for samples containing different Tm concentrations. The dashed lines are guides to the eye. The error bars are calculated from Gaussian fits.*

been found to be Ga-atoms, which confirms that, Eu is well incorporated inside QDs. A Eu-N bond length distortion of about 1.7% is resulting from strain inside GaN QDs.

An additional question is that of Eu microscopic location in dots. For this, shells with higher coordination numbers have to be analyzed. However no model including these higher coordination shells has been found, which fits experimental EXAFS data so that the Eu location in a GaN QDs is up to now unclear. This means that Eu ions are not homogeneously distributed in a QD. Possible Eu location could be for example the near GaN-AlN interface layer, so that in the model Eu and Al fourth next

neighbors should be considered. In chapter 5.3 we will see that optical results are consistent with the suggestion.

3.4.3 Growth of GaN QDs doped with Tm

Figure 3.12a shows AFM images from Tm doped GaN QDs with different Tm contents. From these images the height, diameter and density of Tm doped QDs is analyzed and shown in Figure 3.12b. It was found that the most significant feature is a decrease of the QD height by a factor of two for Tm concentrations higher than 4%. Also the diameter is reduced by a factor of about 2, combined with an enhancement of the density of QDs for a Tm content of around 2%. However, these variations in the QD morphology are minimal when compared with those observed in Eu doped QDs, which indicates a much weaker perturbation of the growth kinetics. We have seen above that Eu, when incorporated in GaN at a concentration higher than 3%, inhibits the nucleation of GaN QDs on AlN. By contrast, in the case of Tm doping, GaN QDs are observed with Tm contents higher than 10% (Figure 3.12a and Figure 3.12.b).

It is important to mention, that in our case RBS leads to the determination of a RE content normalized to the GaN content but does not provide information to determine the location of incorporated RE. Figure 3.13 shows a RBS spectrum of a superlattice with 20 planes of Tm doped GaN, from which the Tm content has been deduced (2% in the example). The different planes of GaN QDs cannot be resolved so that only the total amount of Ga and Al (in capping layer) from the sample can be measured. However, the RBS spectra in Figure 3.13 provides information about the homogeneity of doping which can be seen by variations in the intensity of the Tm signal (E). In the shown example RE incorporation has been found homogeneous in agreement with other RBS data obtained for samples with rather low Tm content. A high Tm content, however, yields inhomogeneous Tm incorporation together with a decrease in the total amount of GaN material. This can be seen for example in the RBS spectrum in Figure 3.14, where the Tm incorporation has changed significantly during growth combined with a reduction of the amount of deposited GaN. It is interesting to compare the total amount of GaN material deduced from analysis of AFM images to that extracted from RBS spectra which has been done in Figure 3.15. More precisely, the total amount of material can be calculated from AFM pictures assuming that GaN QDs are truncated pyramids. Also a possible influence of the tip

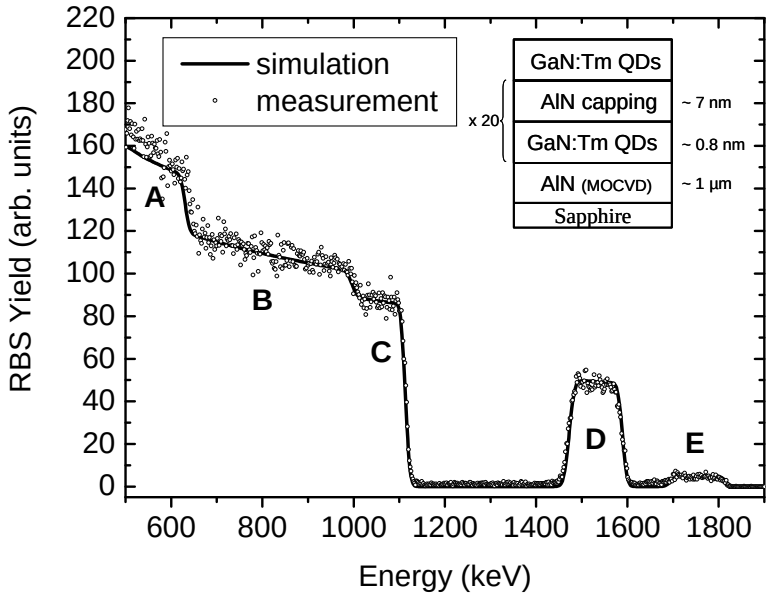

Figure 3.13: *RBS spectrum of a sample containing 20 stacks of Tm doped GaN QDs capped with AlN as indicated in the figure. GaN:Tm QDs have been also grown at the top for AFM analysis. Acceleration voltage of the He Ions: 2 MeV. Tm content inside GaN QDs: 2 %. The letters are used to label to the position of elements:* ***A*** *is N in AlN, GaN:Tm QDs and AlN:Tm;* ***B*** *is Al in AlN of the substrate;* ***C*** *is Al in AlN from the capping;* ***D*** *is Ga in GaN:Tm QDs;* ***E*** *Tm in GaN:Tm QDs and AlN:Tm capping.*

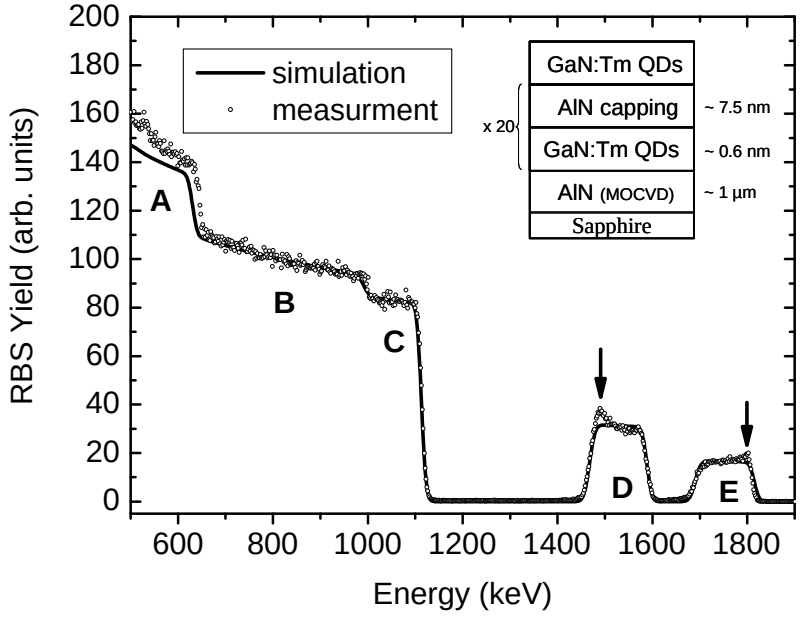

Figure 3.14: *RBS spectrum of a sample containing 20 stacks of Tm doped GaN QDs capped with AlN as indicated in the figure. GaN:Tm QDs have been also grown at the top for AFM analysis. Acceleration voltage of the He Ions: 2 MeV. Tm content inside GaN QDs: averaged 10.8 %. The letters are used to label to the position of elements:* ***A*** *is N in AlN, GaN:Tm QDs and AlN:Tm;* ***B*** *is Al in AlN of the substrate;* ***C*** *is Al in AlN from the capping;* ***D*** *is Ga in GaN:Tm QDs;* ***E*** *Tm in GaN:Tm QDs and AlN:Tm capping. The arrows show positions with the inhomogeneous Tm incorporation for clarity.*

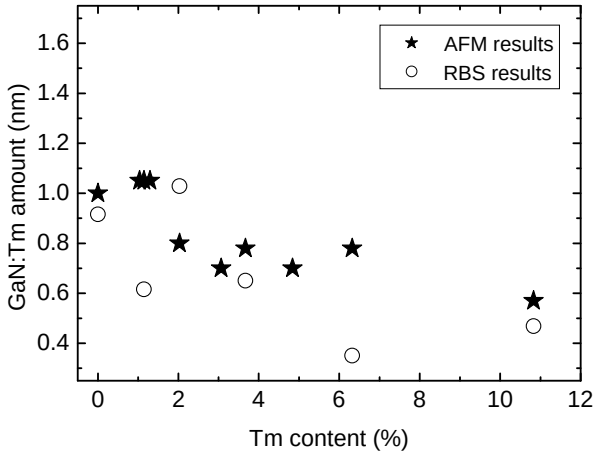

Figure 3.15: *Total amount of GaN material as measured by RBS (filled stars) and deduced from AFM images (circles).*

(Appendix A), which could yield to an overestimation of the GaN amount has been taken into account. This result has been compared with RBS results which provides direct measurement of the amount of GaN material (Signal D in Figure 3.13 and Figure 3.14). The AFM results in Figure 3.15 show a slightly higher GaN content than the RBS measurements which is difficult to understand since in AFM the GaN amount from the wetting layer cannot be measured. It might be possible that during the capping process of dots their dimensions are reduced, which has been recently reported in ref. [Gog04]. However, even taking this small difference into account, both methods show a tendency to a reduction of the total amount of material by a factor of 2, with increasing Tm content. This result indicates that Tm can modify the kinetics of Ga, yielding to a reduction of the total amount of GaN:Tm material.

3.4.4 Tm location in the GaN QDs grown in an AlN matrix

The possibility of growing QDs with a Tm content higher that 10 % suggests that not all Tm atoms are inside QDs, but mostly at the interface since we have seen in chapter 3.3.3 that it is difficult to dope Al with Tm content in the order of more than 0.1%. EXAFS experiments (not discussed here in detail, for more information see Ref [And05]) on Tm doped GaN QDs have shown that Tm atoms occupy metal site with atomic distribution of 1/4 Ga second neighbors and 3/4 Al second neighbors. This atomic distribution is in agreement with the above prediction that a high Tm content can be found at the interface. Compare the structure model of the interface shown in Figure 3.16.

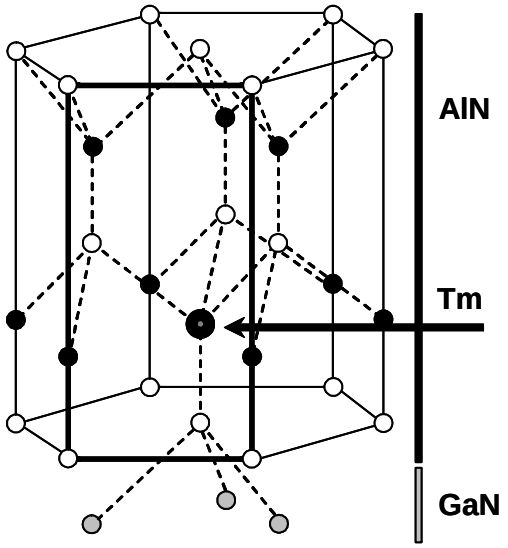

Figure 3.16: *Simplified structural model of the interface of a GaN QDs and the AlN capping in case of Tm doping. The color of the atoms is related to the elements (N white, Al black, Ga grey, and Tm black circle). 3 Ga and 9 Al second next neighbors are seen.*

Although contents as large as 10 %, normalized to GaN content are meaningless, the evidence for Tm segregation at the interface makes them understandable: the nominal GaN coverage rate being 5 MLs, the segregation of a full monolayer of Tm at the GaN/AlN interface would lead to a Tm content of about 20 %, normalized to GaN content, in qualitative agreement with EXAFS and RBS results. The reduction of the total amount of GaN material by a factor 2 can be explained with the presence of Tm atoms at the QD surface during growth. For this reason, places for adatoms are drastically limited, which is especially important in N-rich regime used for QD growth. The issue of effective Tm incorporation in GaN QDs will be addressed by optical studies in section 7.1.

3.4.5 Growth of GaN QDs doped with Tb and the influence of the substrate temperature

In the case of Tb doped GaN QDs the change of QD morphology is rather similar to Tm doping when QDs are grown at 700°C as shown in Figure 3.17. The QDs density and diameter are rather unaffected and the height shows as in case of Tm a reduction of a factor 2 which might indicate a similar growth mechanism. Another parallel to Tm doping is that QDs can be nucleated with a RE concentration higher

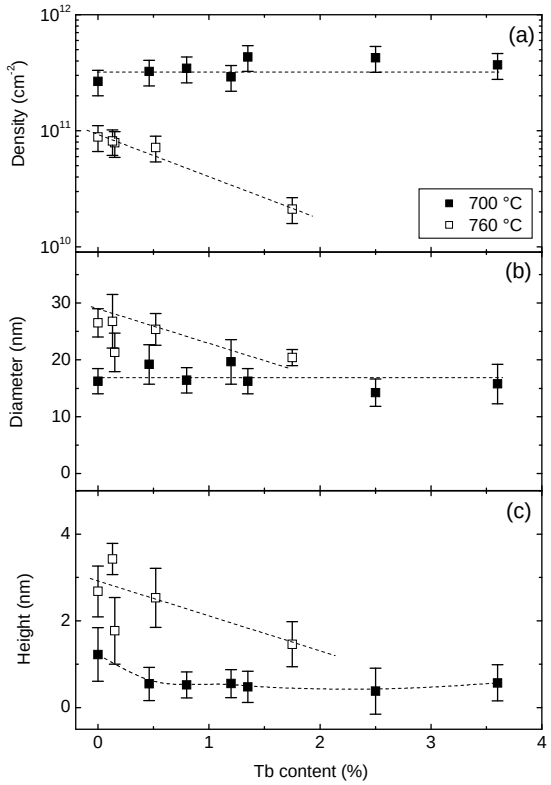

Figure 3.17: a) *Diameter* **b)** *height and* **c)** *density of GaN QDs measured by AFM for samples containing different Tb concentrations. Black filled squares correspond to higher growth temperature (760°C), unfilled squares to lower growth temperature (700°C). For the higher growth temperature no QDs have been found in AFM for a Tb content higher than 2%. The error bars are calculated from Gauss fits. The dashed lines are guides to the eye.*

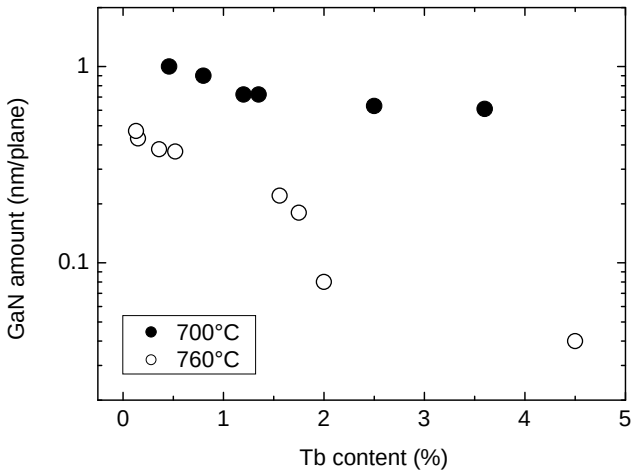

Figure 3.18: *Total amount of GaN material in one QD plane as a function of Tb content. Black circles correspond to a substrate temperature of 700°C, white ones to 760°C respectively.*

than 3%. A series of samples with GaN QDs different Tb contents has been grown at a rather high substrate temperature of 760°C. For increasing Tb content morphological parameter of QDs are starting to change significantly. The height and diameter are reduced by a factor 2 and the density by about 1 order of magnitude as visible in Figure 3.17. Also, for Tb contents higher than 2%, no nucleated QDs have been found in AFM. In agreement with AFM results, RBS has also shown a strong reduction of the total amount of GaN material for higher Tb contents (Figure 3.18). This is also in agreement with results shown in Figure 3.9, where we found a reduction of the growth rate of GaN:Tb layers, in N-rich conditions, compared to un-doped GaN layers. This strongly suggests that the incorporation rate of Ga adatoms is decreased in presence of Tb. This effect is drastically enhanced at higher substrate temperature, as the sticking coefficient of Ga adatoms is already lower, whereas Tb sticking coefficients seems to be fewly influenced.

During growth of GaN QDs with high Tb contents also a loss of the RHEED contrast has been found associated with accumulation of Tb at the surface.

This has been more drastically observed for the higher growth temperature (760°C), where the 2D/3D transition of QDs is inhibited. This result is in agreement with AFM results where no QDs have been found with Tb concentrations higher than 2%.

It might be interesting to try growth of RE-nitride structures at lower substrate temperature, as the presence of the here studied RE atoms is already enhancing the mean free path of Ga-adatoms.

3.4.6 Closing remarks to growth of GaN:RE QDs on AlN

We have seen for the example of Eu-doping that QDs dimensions are strongly perturbed. Structural parameters of Tm doped QDs have been rather unaffected which can be explained with a high Tm content at the GaN/AlN interface. A strong reduction of the amount of GaN material is found in case of Tb doping especially at higher substrate temperature which is also explained by RE segregation and concomitant increase of Ga desorption rate.

For achieving efficient devices the growth conditions have to be optimized to get maximal optical output. We will see in the next sections that the total number of RE atoms is proportional to the intensity of luminescence, if all RE atoms are excited

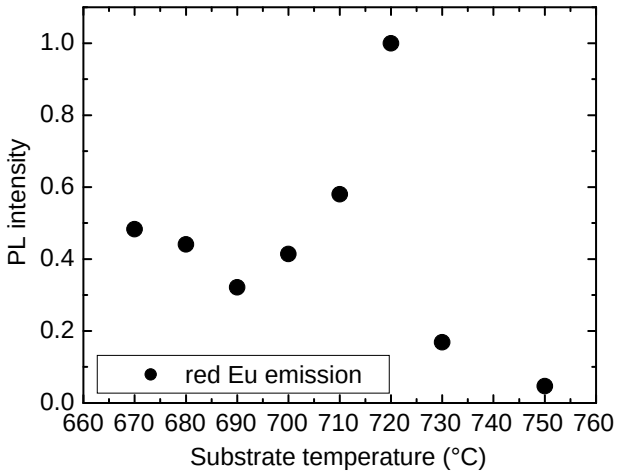

Figure 3.19: *Comparative PL study for a series of samples containing 10 stacks of GaN:Eu QDs grown at different substrate temperatures (other growth parameters like Eu flux constant). The black circles correspond to the integrated red Eu emission.*

through a near band edge related excitation mechanism. The number of inactive RE emission centers has to be therefore reduced since too high RE doping yields to the formation of native defects. A high quality GaN:Eu layer with intense Eu luminescence and no near band edge emission was grown for example with an Eu content of only 0.2% (Sec. 4). This is a rather low value compared to results in literarture which propose an optimum Eu content of 2%, established by a systematic study of the Eu^{3+} emission as a function of the Eu content [Ban04].

A comparative optical study is given in Figure 3.19 for the red Eu emission GaN:Eu QDs. The Ga- to N-ratio and the Eu-flux has been kept constant, but the substrate temperature has been changed between 670°C and 750°C. Highest Eu emission has been found at 720°C, for lower substrate temperature Eu emission decreased by a factor of two. For substrate temperatures higher than 720°C a rapid decrease of the red Eu emission of about one order of magnitude was found.

This result can be explained as following: For the substrate temperatures higher than 720° no QDs have been grown, but a thin GaN layer, which is in agreement with AFM results (not shown), where no dots have been found. The maximal emission at 720°C can be explained by higher quality of the grown material, since low substrate temperatures have typically detrimental effects onto the growth.

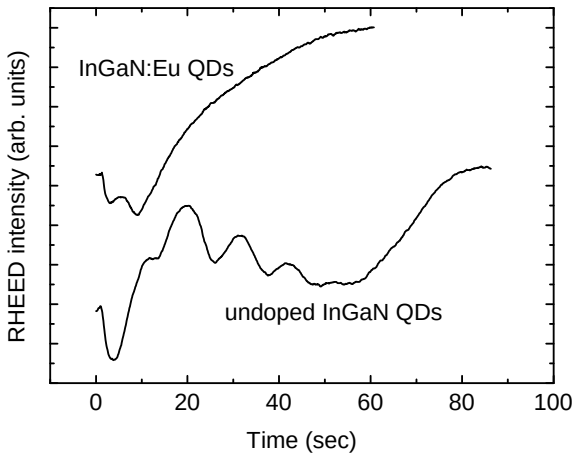

Figure 3.20: *Variation of the specular RHEED intensity during growth of undoped InGaN QDs and InGaN:Eu QDs.*

According to the shown example the best growth regimes for Tm and Tb doped QDs have been found by systematic changes of the growth parameters in series of samples which have been analyzed by comparative optical studies. For the optical studies in the following chapters, samples have been grown with already optimized growth parameters, or in other words maximal optical output.

3.5 Growth and morphological properties of InGaN:Eu QDs

Since S. Nakamura demonstrated blue light emission from LEDs containing InGaN in the active region [Nak98], big interest came out to understand InGaN based heterostructures.

Up to now a controversy exists over the possibility that luminescence could originate from InGaN QDs like structures [Don99, Nar99, Rib99]. Along this view MOCVD growth of InGaN QDs on GaN has been demonstrated using Si as an antisurfactant [Hir98]. Later on InGaN QDs were also grown by MOCVD without surfactant [Tac99]. Then growth of self assembled InGaN QDs has been demonstrated by MBE following SK growth mode [Ade00]. Nevertheless MBE growth of InGaN:RE QDs on GaN is not simple and requires good control of the In and RE fluxes.

The idea of combining the host of InGaN QDs with the RE luminescence is getting understandable as the injection of carriers into AlN is hindered by the

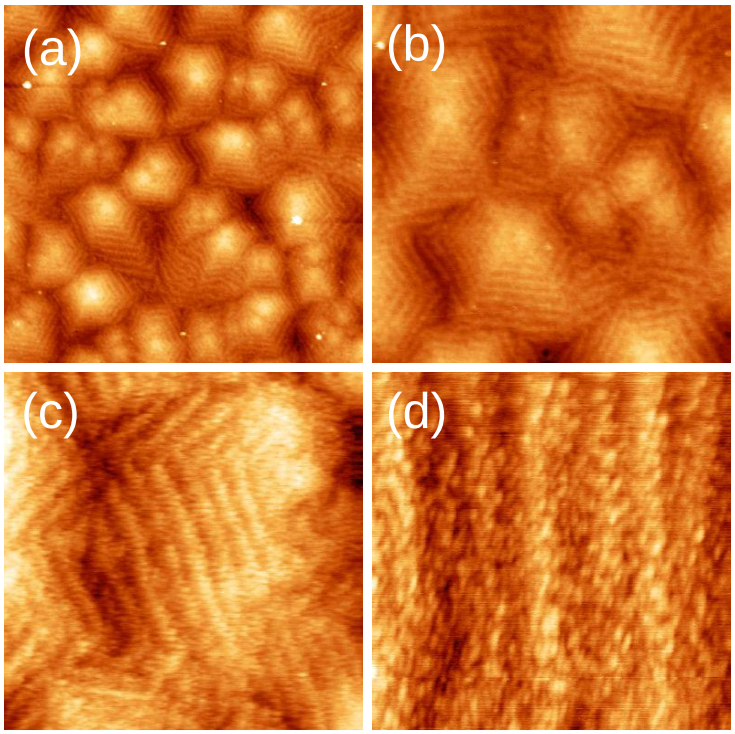

Figure 3.21: *AFM images of InGaN:Eu QDs. Areas of images:* **a)** *4000 x 4000 nm^2 ,* **b)** *2000 x 2000 nm^2,* **c)** *1000 x 1000 nm^2 and* **d)** *500 x 500 nm^2.*

difficulties in p-type and n-type doping of AlN. A solution could be the use of RE doped InGaN QDs grown on GaN for current injection devices, since p- and n-doping of GaN are well controlled by MBE.

For the growth of InGaN QDs a substrate temperature of about 600°C was used. The substrate temperature should not be higher, because of the low desorption temperature of In. The growth of InGaN QDs requires also that the substrate temperature has to be very well controlled as the formation of InGaN QDs is crucially depending on this parameter. InGaN QDs have been grown on a 150 nm thick relaxed GaN buffer grown on AlN pseudo-substrates. The correct growth conditions for InGaN QDs and InGaN:Eu QDs can be controlled by measuring the variation of the intensity of the specular reflected beam in RHEED as shown for one example in Figure 3.20. First in case of undoped InGaN QDs oscillations from 0 s to 60 s are corresponding to the growth of the wetting layer, which is found to have different thicknesses in case of InGaN QDs depending on the In to Ga ratio and substrate temperature. After these oscillations an increase of the RHEED intensity is visible (60 s to 80 s) associated with the 2D/3D transitions. This transition appears only by using of a minimal In concentration of around 20%.

RE metals are influencing the growth of InGaN QDs as they are exhibiting surfactant properties as already demonstrated in the section 3.3. An additional Eu flux during growth of InGaN material is yielding in the shown example to a reduction of the thickness of the wetting-layer, so that the 2D/3D transition can be found earlier. This can be explained as following: A higher Eu flux is simultaneously changing desorption rate of In and Ga and therefore the In to Ga ratio. This has consequences onto the lattice mismatch between GaN and InGaN material. In the shown example (Figure 3.20) the 2D/3D transition can be observed earlier which means that the lattice mismatch is expected to be higher. These conditions are used to grow InGaN:Eu QDs.

However further enlightenment is needed by carring out transmission microscopy measurements to study in depth the growth of InGaN:Eu QDs.

Figure 3.21 shows AFM images of InGaN:Eu QDs in different areas from 4000 x 4000 nm^2 to 500 x 500 nm^2. The surface morphology is characterized by the typical spiral hillocks of GaN (Figure 3.21a and Figure 3.21b. InGaN:Eu QDs are found aligned on the atomic terraces around the hillocks as visible in Figure 3.21b and Figure 3.21c. The higher resolution image of Figure 3.21d shows the InGaN:Eu QDs, which present diameters between 15 nm and 40 nm and rather small height, between 0.4 nm and 1 nm. The quantum dot density was found to be around $1.4 \pm 0.2 \cdot 10^{11}$ cm^{-2}. The heights of InGaN:Eu QDs have been found to be reduced compared to undoped InGaN QDs.

With the here used experiments it is rather hard to measure the In content of the InGaN:Eu QDs. The RBS setup lacks of energetic resolution so that it is difficult to separate In and the Eu signals. One solution to overcome this problem would be to scatter heavier ions, than the He ions. This problem is described in detail in Appendix A.

For achieving superlattices of planes, the InGaN QDs were capped with about 10 nm of non-intentionally doped GaN. In chapter 6 we will discuss in detail the optical properties of InGaN:Eu QDs and we will address the RE location within the InGaN QDs/GaN structure, which is an important issue since Eu has a strong tendency to segregate during MBE growth, so that up to now the final Eu location is unclear. It is possible that also the GaN spacing layer used for capping QDs contains traces of Eu impurities.

References

[Ade00] C. Adelmann, J. Simon, G. Feuillet, N. T. Pelekanos, B. Daudin, and G. Fishmann, *Self-assembled InGaN quantum dots grown by molecularе-beam epitaxy*, Appl. Phys. Lett. **76**, 1570 (2000).

[Ade02] C. Adelmann, J. Brault, D. Jalabert, P. Gentile, H. Mariette, G. Mula, and B. Daudin, *Dynamically stable gallium surface coverages during plasma-assisted molecular beam epitaxy on (0001) GaN*, J. of Appl. Phys. **91**, 9638 (2002).

[Ade03] C. Adelmann, J. Brault, G. Mula, B. Daudin, L. Lymperakis, and J. Neugebauer, *Gallium adsorption on (0001) GaN surfaces*, Phys. Rev. B **67**, 165419 (2003).

[Ade04] C. Adelmann, B. Daudin, R. A. Oliver, G. A. D. Briggs, and R. E. Rudd, *Nucleation and growth of GaN/AlN quantum dots*, Phys. Rev. B **70**, 125427 (2004).

[And05] T. Andreev, Y. Hori, X. Biquard, E. Monroy, D. Jalabert, A. Farchi, M. Tanaka, O. Oda, Le Si Dang, and B. Daudin, *Optical and morphological properties of GaN quantum dots doped with Tm*, Phys. Rev. B **71**, 115310 (2005).

[Ban02] H. Bang, S. Morishima, Z. Li, K. Akimoto, M. Nomura, and E. Yagi, *MBE growth of Eu- or Tb-doped GaN and its optical properties*, J. Cryst. Growth **237-239**, 1027 (2002).

[Ban04] H. Bang, S. Morishima, J. Sawahata, J. Seo, M. Takiguchi, M. Tsunemi, K. Akimoto, and M. Nomura, *Concentration quenching of Eu-related luminescence in Eu-doped GaN*, Appl. Phys. Lett. **85**, 227 (2004).

[Che96] Y. Chen and J. Washburns, *Structural Transition in Large-Lattice-Mismatch Heteroepitaxy*, Phys. Rev. Lett. **77**, 4046 (1996).

[Dau97] B. Daudin, F. Widmann, G. Feuillet, Y. Samson, M. Arlery, and J. L. Rouvière, *Stranski-Krastanov growth mode during the molecular beam epitaxy of highly strained GaN,* Phys. Rev. B **56**, R7069 (1997).

[Don99] K. P. O'Donnell, R. W. Martin, and P. G. Middleton, *Origin of Luminescence from InGaN Diodes*, Phys. Rev. Lett. **82**, 237-240 (1999).

[Eag90] D. J. Eaglesham and M. Cerullo, *Dislocation-free Stranski-Krastanow growth of Ge on Si(100)*, Phys. Rev. Lett. **64**, 1943 (1990).

[Fil04] J. S. Filhol, R. Jones, M. J. Shaw, and P. R. Briddon, *Structural and electrical activity of rare - earth dopants in GaN,* Appl. Phys. Lett. **84**, 2841 (2004).

[Geh99] S. Gehrsitz, H. Sigg, N. Herres, K. Bachem, K. Köhler, and F. K. Reinhart, *Compositional dependence of the elastic constants and the lattice parameter of $Al_xGa_{1-x}As$,* Phys. Rev. B **60**, 11601 (1999).

[Gog03] N. Gogneau, D. Jalabert, E. Monroy, T. Shibata, M. Tanaka, and B. Daudin, *Structure of GaN quantum dots grown under «Modified Stranski-Krastanow« conditions on AlN*, J. Appl. Phys. **94**, 2254 (2003).

[Gog04] N. Gogneau, D. Jalabert, E. Monroy, E. Sarigiannidou, J. L. Rouvière, T. Shibata, M. Tanaka, J. M. Gerard, and B. Daudin, *Influence of AlN*

overgrowth on structural properties of GaN quantum wells and quantum dots grown by plasma-assisted molecular beam epitaxy, J. Appl. Phys. **96**, 1104 (2004).

[Gol85] L. Goldstein, F. Glas, J. Y. Marzin, M. N. Charasse, and G. Le Roux, *Growth by molecular beam epitaxy and characterization of InAs/GaAs strained-layer superlattices*, Appl. Phys. Lett. **47**, 1099 (1985).

[Hey00a] B. Heying, I. Smorchkova, C. Polenz, C. Elsass, P. Fini, S. Den Baars, U. Mishra, and J. S. Speck, *Optimization of the surface morphologies and electron mobilities in GaN grown by plasma-assisted molecular beam epitaxy*, Appl. Phys. Lett. **77**, 2885 (2000).

[Hey00b] B. Heying, R. Averbeck, L. F. Chen, E. Haus, H. Richert, and J. S. Speck, *Control of GaN surface morphologies using plasma-assisted molecular beam epitaxy*, J. Appl. Phys. **88**, 1855 (2000).

[Hir98] H. Hirayama, S. Tanaka, P. Ramvall, and Y. Aoyagi, *Intense photoluminescence from self-assembling InGaN quantum dots artificially fabricated on AlGaN surfaces*, Appl. Phys. Lett. **72**, 1736 (1998).

[Hor04] Y. Hori, X. Biquard, E. Monroy, D. Jalabert, F. Enjalbert, Le Si Dang, M. Tanaka, O. Oda, and B. Daudin, *GaN quantum dots doped with Eu*, Appl. Phys. Lett. **84**, 206 (2004).

[Hor05] Y. Hori, T. Andreev, T. Florian, E. Bellet-Amalric, D. Le Si Dang, M. Tanaka, O. Oda, and B. Daudin, *Undoped and rare-earth doped GaN quantum dots on AlGaN*, submitted to Phys. Stat. Sol.

[Jad01] W. M. Jadwisienczak, H. J. Lozykowski, I. Berishev, A. Bensaoula, and I. G. Brown, *Visible emission from AlN doped with Eu and Tb ions*, J. Appl. Phys. **89**, 4384 (2001).

[Jes98] D. E. Jesson, G. Chen, K. M. Chen, and S. J. Pennycook, *Self-Limiting Growth of Strained Faceted Islands*, Phys. Rev. Lett. **80**, 5156 (1998).

[Kru01] C. Kruse, S. Einfeldt, T. Böttcher, D. Hommel, D. Rudloff, and J. Christen, *Spatially modified layer properties related to the formation of gallium droplets on GaN(0001) surfaces during plasma-assisted molecular-beam epitaxy*, Appl. Phys. Lett. **78**, 3827 (2001).

[Lau04] M. McLaurin, B. Haskell, S. Nakamura, and J. S. Speck, *Gallium adsorption onto a (11-20) gallium nitride surface*, J. Appl. Phys. **96**, 327 (2004).

[Lee02a] D. S. Lee and A. J. Steckl, Ga glux dependence of Er-doped GaN luminescent thin films, Appl. Phys. Lett, **80**, 728 (2002).

[Lee02b] D. S. Lee, J. Heikenfeld, and A. J. Steckl, Growth-temperature dependence of Er-doped GaN luminescent thin films, Appl. Phys. Lett. **80**, 344 (2002).

[Leo93] D. Leonard, M. Krishnamurthy, C. M. Reaves, S. P. Denbaars, and P. M. Petroff, *Direct formation of quantum-sized dots from uniform coherent islands of InGaAs on GaAs surfaces*, Appl. Phys. Lett. **63**, 3203 (1993).

[Liu04] Q. L. Liu, Y. Bando, F. F. Xu, and C. C. Tang, *Effect of growth temperature on morphology, structure and luminescence of Eu-doped GaN thin films*, Appl. Phys. Lett. **85**, 4890 (2004).

[Nak03] M. L. Nakarmi, K. H. Kim, J. Li, J. Y. Lin, and H. X. Jiang, *Enhanced p-type conduction in GaN and AlGaN by Mg-delta-doping*, Appl. Phys. Lett. **82**, 3041 (2003).

[Nak98] S. Nakamura, *The Roles of Structural Imperfections in InGaN-Based Blue Light-Emitting Diodes and Laser Diodes*, Science **281**, 956 (1998).

[Nar99] Y. Narukawa, Y. Kawakami, S. Fujita, and S. Nakamura, *Dimensionality of excitons in laser-diode structures composed of $In_xGa_{1-x}N$ multiple quantum wells*, Phys. Rev. B **59**, 10283 (1999).

[Neu03] J. Neugebauer, T. K. Zywietz, M. Scheffler, J. E. Northrup, H. Chen, and R. M. Feenstra, *Adatom Kinetics On and Below the Surface: The Existence of a New Diffusion Channel*, Phys. Rev. Lett. **90**, 056101 (2003).

[Nor00] J. E. Northrup, J. Neugebauer, R. M. Feenstra, and A. R. Smith, *Structure of GaN(0001): The laterally contracted Ga bilayer model*, Phys. Rev. B **61**, 9932 (2000).

[Mon03] E. Monroy, B. Daudin, E. Bellet-Amalric, N. Gogneau, D. Jalabert, F. Enjalbert, J. Brault, J. Barjon, and Le Si Dang, *Surfactant effect of In for AlGaN growth by plasma-assisted molecular beam epitaxy*, J. Appl. Phys. **93**, 1550 (2003).

[Mul01] Guido Mula, C. Adelmann, S. Moehl, J. Oullier, and B. Daudin, *Surfactant effect of gallium during molecular-beam epitaxy of GaN on AlN (0001)*, Phys. Rev. B **64**, 195406 (2001).

[Rib99] P. Riblet, H. Hirayama, A. Kinoshita, A. Hirata, T. Sugano, and Y. Aoyagi, *Determination of photoluminescence mechanism in InGaN quantum wells*, Appl. Phys. Lett. **75**, 2241 (1999).

[Str37] N. Stranski and L. Krastanow, *Zur Theorie der orientierten Ausscheidung von Ionenkristallen aufeinander*. Sitzungsberichte Abt. IIb **146**, 797 (1937).

[Tac99] K. Tachibana, T. Someya, and Y. Arakawa, *Nanometer-scale InGaN self-assembled quantum dots grown by metalorganic chemical vapor deposition*, Appl. Phys. Lett. **74**, 383 (1999).

[Tar97] E. J. Tarsa B. Heying, X. H. Wu, P. Fini, S. P. DenBaars, and J. S. Speck, *Homoepitaxial growth of GaN under Ga-stable and N-stable conditions by plasma-assisted molecular beam epitaxy*, J. Appl. Phys. **82**, 5472 (1997).

[Wid98] F. Widmann, B. Daudin, G. Feuillet, Y. Samson, J. L. Rouvière, and N. Pelekanos, *Growth kinetics and optical properties of self-organized GaN quantum dots*, J. Appl. Phys. **83**, 7618 (1998).

[Xin96] S. H. Xin, P. D. Wang, Aie Yin, C. Kim, M. Dobrowolska, J. L. Merz, and J. K. Furdyna, *Formation of self-assembling CdSe quantum dots on ZnSe by molecular beam epitaxy*, Appl. Phys. Lett. **69**, 3884 (1996).

[Zhu04] K. Zhu, M. L. Nakarmi, K. H. Kim, J. Y. Lin, and H. X. Jiang, *Silicon doping dependence of highly conductive n-type $Al_{0.7}Ga_{0.3}N$*, Appl. Phys. Lett. **85**, 4669 (2004).

[Zyw98] T. Zywietz, J. Neugebauer, and M. Scheffler, *Adatom diffusion at GaN (0001) and (000-1) surfaces*, Appl. Phys. Lett. **73**, 487 (1998).

4. Optical properties of GaN:Eu layers

Before we start to discuss the optical properties of GaN:RE QDs we put the attention in this chapter onto optical properties of GaN:Eu layers. In section 3.3.1 the growth of GaN:Eu has been discussed. We study now a sample containing 200 nm thin GaN:Eu film grown onto a 200 nm undoped GaN buffer on the AlN pseudo-substrate. Both layers are grown in slightly Ga-rich growth conditions at a substrate temperature of about 720°C. The Eu content of the sample, as determined by RBS is 0.2 %.

This chapter is organized as following: First we discuss the emission spectrum of the GaN:Eu layer (4.1). Then we will address the issue of different Eu^{3+} sites by means of optical characterization (4.2). Because RE atoms in different sites exhibit different optical properties their identification is important for optimization of possible device structures. This identification of RE sites in GaN layers has been also done for Er^{3+} [Dir04] and Nd^{3+} [Kim98] doped layers.

Some of the results are needed for understanding the optical properties of GaN:Eu QDs and especially of InGaN:Eu QDs grown in GaN spacing layers which will be discussed in chapter 6.

4.1 The emission spectrum of GaN:Eu layers

PL spectra at 5 K and 300 K of GaN:Eu layer, excited by 244 nm, are shown in Figure 4.1a. At 5 K the PL spectrum is characterized by sharp Eu^{3+} emissions extending from 470 nm to 850 nm. Note that the PL intensity is presented in logarithmic scale to make visible weak emission lines. In linear scale, only emissions around 620 nm appear clearly. Near-band-gap emission of GaN at 353 nm has been found to be quenched as an evidence that a relatively low Eu concentration of about 0.2 % is sufficient to ensure optimal Eu-related PL. Interestingly, this is a qualitative indication that the layer is of high crystalline quality, associated with a large carrier diffusion length and efficient energy transfer to RE ions. It is worth noticing in relation to this feature that optimum Eu concentration for achieving high Eu emission in GaN layers strongly depends on the chosen growth conditions and was found to be in some cases as high as 2% [Ban04].

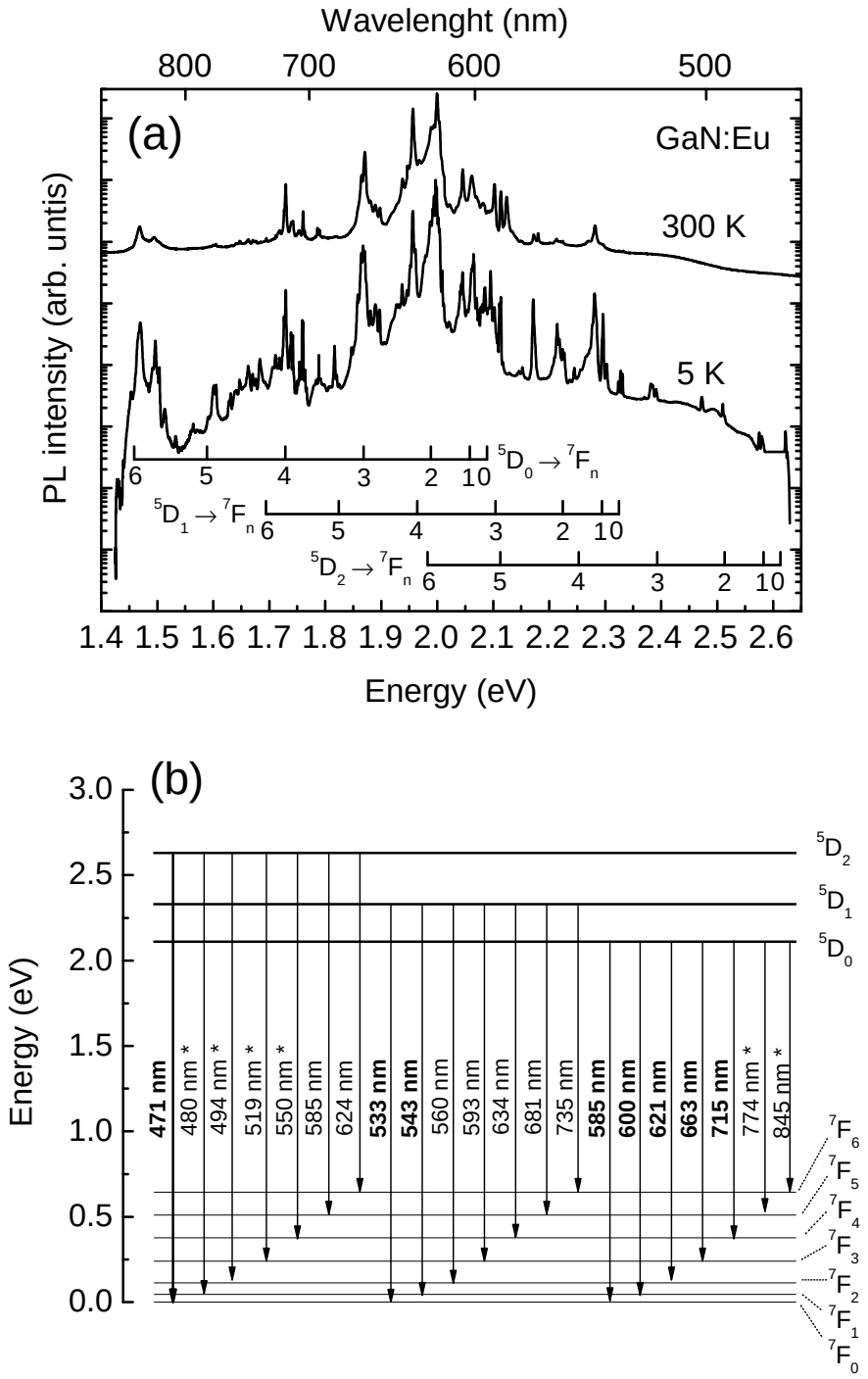

Figure 4.1: *PL spectrum in logarithmic scale of a GaN:Eu layer measured at 5 K with a frequency doubled Ar-ion laser line emitting at 244 nm. The position of the transitions is indicated in the spectrum where ^7F_n means the ground state with n=0 to 6. b) Energy diagram and observed transitions of Eu^{3+} ions in GaN host. Bold plotted emission lines have been already found in literature. Transitions marked by a star (*) are found here for the first time. For other lines only the expected emission wavelength is given. The indicated wavelengths present mean values for transitions.*

The sharp Eu^{3+} emissions in GaN are originating from the three excited states, $^5D_2$, $^5D_1$ and $^5D_0$ which have been already identified in GaN host using direct Eu excitation [Nye03]. Based on PL spectra shown in Figure 4.1a with numerous intra 4f-transitions an energy diagram can be established, as shown in Figure 4.1b [Die68]. It should be noticed that this diagram does not take into account that RE ions may occupy different sites with different local symmetry. Also note that transitions of electrons within 4f-shell are restricted by the selection rules applicable to electric and magnetic dipole/quadrupole, vibronic and phonon processes. The $^5D_0 \rightarrow {}^7F_2$ transition resulting in strong emission lines around 620 nm is J-allowed electric dipole radiation that has been identified by previous authors [Loz00, Kim04, Eye03, Ban04, Shi04, Liu04, Lor04, Pen05]. Some weaker lines (identified by a star * in Figure 4.1b) are identified here for the first time. They originate from intra-f partially allowed transitions. However some transitions are overlapped, as for example the $^5D_0 \rightarrow {}^7F_4$ and $^5D_1 \rightarrow {}^7F_6$ lines and the levels are split so that alternative methods have to be used for further identification. It has to be remarked that the positions of Eu energy levels with respect to GaN band-gap is not clear at this stage. In particular, there is no reason to make coincide arbitrarily the $^7F_0$ ground state with the top of valence band energy. As a matter of fact no emissions from the $^5D_3$ excited state have been found, whereas this $^5D_3$ excited state as positioned in the Dieke diagram should have a lower energy than the band-gap of GaN if the $^7F_0$ ground state is coinciding with the top of the valence band. In the 300 K PL spectrum (Figure 4.1a), hardly any transition from the $^5D_2$ excited state can be found. In addition in the 5 K spectrum a reduction of the splitting can be observed for transitions stemming from the $^5D_2$ excited state which can be explained by the fact that only few sites of Eu^{3+} ions show transitions from this energetically high lying excited state.

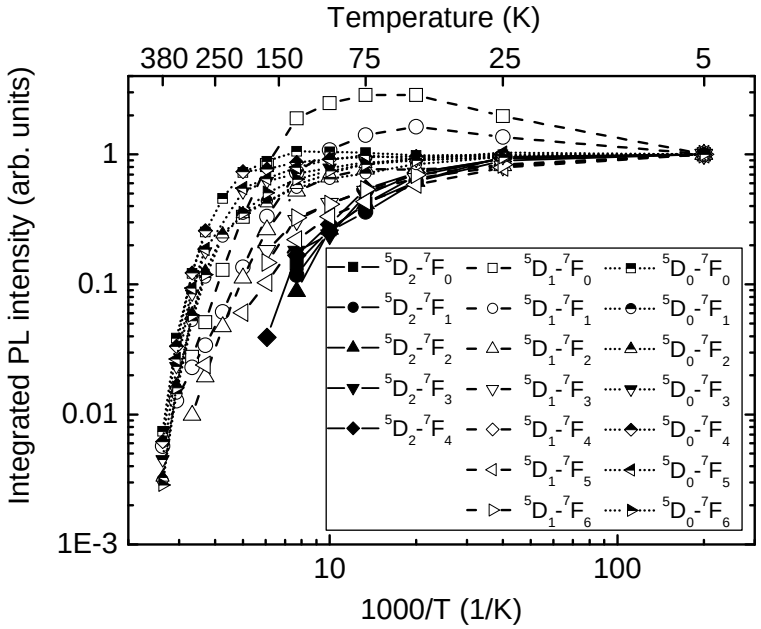

Figure 4.2: *Temperature dependence of the PL intensity of a GaN:Eu layer in double logarithmic scale. The absolute intensity was measured for each transition. Excitation source: 244 nm line of a frequency doubled Ar-ion laser with 10 mW.*

To address this issue and to confirm the assignment of the transitions, the temperature dependence of the PL has been analyzed in Figure 4.2. It is seen that the thermal quenching is different for transitions belonging to different excited states. The temperature dependence of all transitions originating from the $^5D_2$ excited state is rather similar, characterized by the strongest quenching. Consequently, the emission intensity falls under the detection limit of our setup for temperatures higher that 200 K.

Emissions originating from the $^5D_1$ excited state show higher thermal stability and emission from the $^5D_0$ excited state are the most stable. This behavior strongly supports the previous transition assignment. Details of complex thermal quenching are still unclear; however the tendency of increasing quenching with higher-lying levels, namely $^5D_1$ and $^5D_2$, is apparent. The behavior of $^5D_1 \rightarrow {}^7F_0$ transition, which exhibits a slight increase of the emission intensity from 5 K to 75 K is not understood yet. It is worth noticing that strong quenching of the lines originating from $^5D_2$ level could mean that energy of transitions from this level to levels generated by RE doping that are close to the band-edge of GaN is favored, consistent with a possible energy back-transfer (Chapter 2.2).

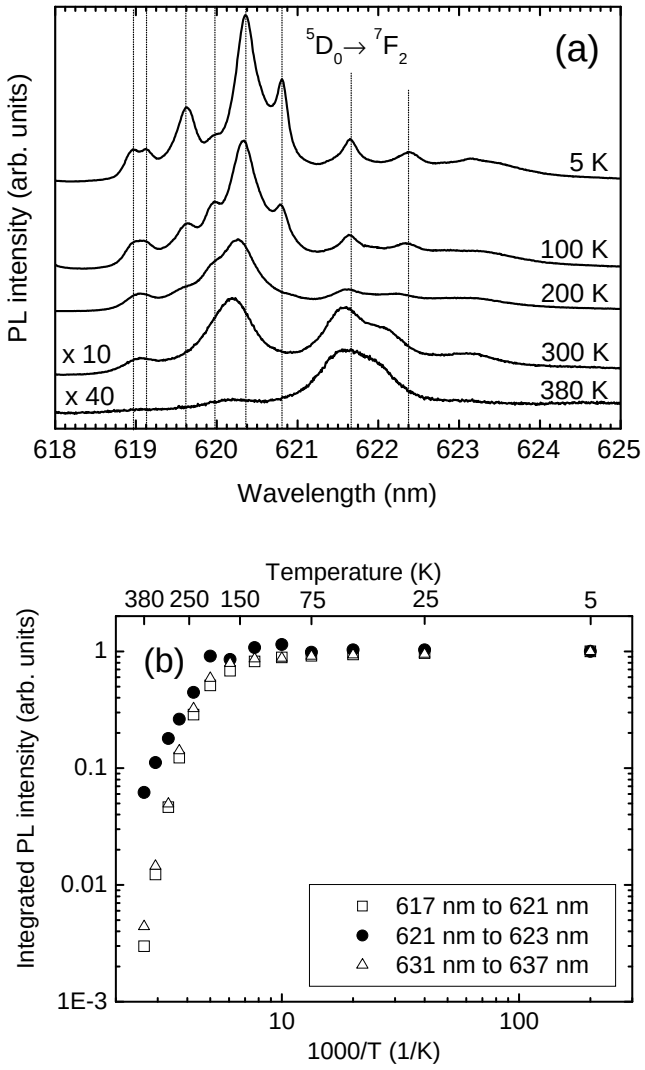

Figure 4.3: a) *PL spectra from GaN:Eu measured at various temperatures between 5 K and 380 K, as indicated. The spectra are normalized by the excitation power density and the integration time for detection. The spectrum at 300 K and 380 K are multiplied by a factor of 10 and 40, respectively, for clarity. The excitation wavelength was 350 nm. The vertical lines are guides to the eye.* **b)** *Integrated PL intensity between 5 K and 380 K of $^5D_0 \rightarrow {}^7F_2$ transition from 616.0 nm to 621.2 nm (unfilled square), from 621.2 nm to 622.8 nm (filled dot), and from 630.0 nm to 637.0 nm (unfilled triangle).*

In a next stage the integrated emission intensity of all intra 4f Eu^{3+} transitions of the GaN:Eu layer has been studied as a function of temperature. The thermal quenching of this quantity is an indication of the efficiency of the energy transfer which may depend on the quality of the grown material as being related to the density of non-radiative recombination centers, but also on the RE concentration since RE ions act as effective carrier trapping centers (Section 2.1). In the present case, PL intensity is reduced by a factor of 2 at 210 K, which favorably compares to recently reported results on GaN:Eu in [Nye03] showing a reduction by the same factor at around 140 K only, as one possible indication of the quality of the material

since the RE content of the here discussed GaN:Eu layer is about 0.2 %, lower than that in the reported article (0.5 to 2%).

It is important to mention that the authors in [Loz00] have grown a GaN:Eu layer which shows thermally stable PL from the $^5D_0 \rightarrow ^7F_2$ transition from liquid helium to room temperature. These significant differences can be explained as already mentioned with different carrier diffusion lengths influenced by different numbers of non-radiative centers and trap levels (RE content).

It is more complicate to consider direct RE excitation which can be also performed with ultra violet excitation due to pumping into continuum states of the RE ions. Experimental results of the authors in [Nye03] are in agreement with this: they found thermally stable Eu luminescence by direct excitation (471 nm) which is easily understandable since non-radiative centers play no role in the excitation mechanism.

Along with the thermal quenching of the emission, a systematic blue shift with increasing temperature was observed. This blue shift was different for each emission line. It was as large as 0.7 nm for emission at 622.4 nm of the $^5D_0 \rightarrow ^7F_2$ transition as shown in Figure 4.3a. The origin of this blue shift is not understood. It is opposite to the usual red shift related to the temperature dependence of the band-gap and the red shift observed for $LaCl_3:Gd^{3+}$ [Pik67].

4.2 Eu sites in GaN:Eu layers and their excitation mechanism

We will now focus our attention on $^5D_0 \rightarrow ^7F_2$ transition, which exhibit luminescence lines in the 617 nm to 628 nm wavelength range. According to the assignment of transition lines, additional emission lines from the $^5D_2 \rightarrow ^7F_6$ transition should be also present in this wavelength range but the emission intensity from this transition is expected to be much lower, especially at room temperature (see Figure 4.2). Therefore, only the $^5D_0 \rightarrow ^7F_2$ transition is considered here. The $^7F_2$ state (J = 2) could be split by local symmetry C_{3v} (hexagonal GaN) into degenerated doublets and singlets or only singlets in lower symmetry. Thus, the $^5D_0 \rightarrow ^7F_2$ transition is expected to give rise to 3 transition lines in GaN material if there exists only one site in C_{3v} symmetry. However as seen that in Figure 4.1a and Figure 4.3a, extra lines are observed, as an evidence of local symmetry lowering and/or that several Eu^{3+} sites are present. Actually, at least, 15 emission lines were identified in the spectral range

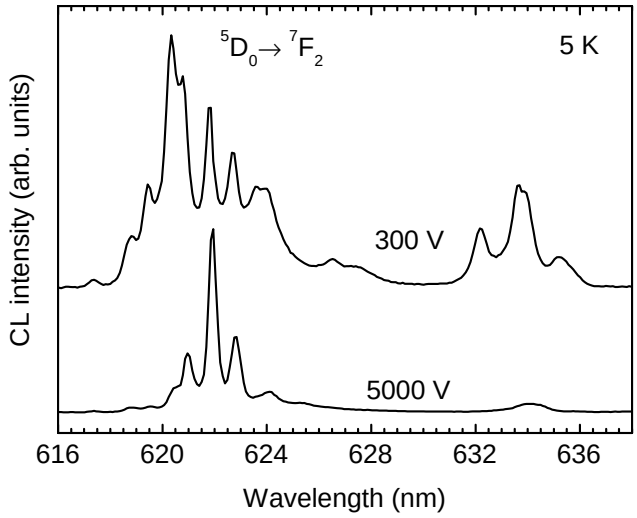

Figure 4.4: *CL at different depths of GaN:Eu measured at 5 K. 300 V and 5000 V were used for excitation near the surface and for the inner sample, respectively. For better clarity the emission intensity has been normalized to its value at 623 nm.*

of 617 nm to 628 nm resulting from the $^5D_0 \rightarrow {}^7F_2$ transition. However for the lowest site-symmetry of Eu^{3+} ion, the $^7F_2$ level can be split into five sub-levels corresponding to the maximum five-fold emission from the $^5D_0 \rightarrow {}^7F_2$ transition.
Then, we assign the extra lines to existence of alternative Eu^{3+} sites, which has been also done in Ref. [Höm03].

To study the different sites of Eu^{3+} ions, the PL of the $^5D_0 \rightarrow {}^7F_2$ transition has been measured form 5 K to 380 K (Figure 4.3a).

Two different sets of Eu^{3+} ions can be identified by comparing the thermal quenching of the various emission lines. The PL spectra in the figure clearly demonstrate faster thermal quenching of emissions at around 620 nm.

This is further illustrated in Figure 4.3b which presents integrated emission at around 620 nm, 633 nm and 622 nm. The emission around 622 nm decreases about one order of magnitude from 5 K to 380 K, however emissions at 620 nm and 633 nm are similarly quenched by nearly 3 orders of magnitude or even not detectable at 380 K. Strong thermal quenching of the 620 nm and 633 nm lines show that they are sensitive to non-radiative channels. Detailed analysis reveals a much more complicated behavior. Emissions at 617.7 nm and 619.9 nm show for instance an increase of the intensity between 5 K and 100 K, followed by a decrease for higher temperatures, which is up to now difficult to explain.

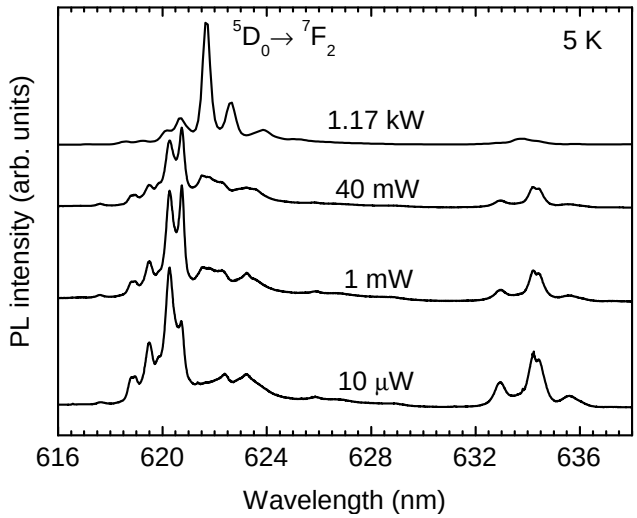

Figure 4.5: *PL spectra of a GaN:Eu layer measured at 5 K with different excitation powers as indicated in the Figure. The spectra are normalized to the emission at 622 nm. The excitation source was a frequency doubled Ar-ion laser line emitting at 244 nm. The radius of the focused Laser spot was 0.2 mm. The spectrum with 1.17 kW excitation power has been measured with a pulsed YAG:Nd laser emitting at 266 nm.*

Clues on the origin of the different Eu^{3+} sites have been obtained by probing luminescence as a function of depth through CL experiments performed as a function of accelerating voltage which is a well known depth sensitive spectroscopic method [Bar03]. Figure 4.4 shows two CL spectra with average diffusion lengths of 100 nm and 5 nm, for accelerating voltage of 5000 V and 300 V, respectively. Well resolved Stark split lines are shown which exhibit remarkable differences.

It is unclear if emissions at 633 nm is originating from a splitting of the $^5D_0 \rightarrow {}^7F_2$ transition, or belongs according to our assignment (see Figure 4.1a and Figure 4.1b) and results in literature to the $^5D_1 \rightarrow {}^7F_4$ transition [Bre67]. As shown in Figure 4.4 emission around 620 nm and 633.5 nm are strongly enhanced for low voltage excitation, i.e. close to the surface of the sample whereas emission at 622 nm is only seen for high voltage excitation, i.e. deep in the volume. This result shows that different Eu^{3+} sites can be found either close to the sample surface or deep in the sample. We will give during this chapter arguments which will further establish this statement.

Coming back to the temperature dependent PL measurement, from the main characteristics of the 620 nm and 633 nm emission lines on one side and of the 622 nm emission lines on the other side, the above mentioned thermal quenching is in agreement with CL results by assuming that emission at 620 nm and 633 nm

originates from the Eu^{3+} ion located near the GaN-layer surface where more non-radiative channels could exist and contribute to the faster thermal quenching.

On the other hand, the 622 nm emission lines is originating from Eu^{3+} ions inside the GaN layer which exhibit less thermal quenching, as observed experimentally.

The above interpretation of results in Figure 4.4 in terms of two populations of Eu^{3+} sites implies that a possible power/acceleration voltage dependence of the rare earth excitation is not significant. As a matter of fact, RE^{3+} ions in nitride host typically exhibit a saturation effect for higher excitation power densities, due to the combined effect of long decay times (~0.2 ms) [Nye03] and the finite number of Eu centers [And04]. Along these views, Figure 4.5 shows PL spectra obtained using different excitation powers (but the same depth penetration because the same excitation wavelength, 244 nm, was used), which are normalized to emission at 622 nm from the Eu^{3+} ion in volume. It is visible that for higher excitation power the emission from Eu inside bulk is more and more pronounced, which can be reasonably explained by the higher number of emitting Eu centers from the inner sample. By contrast the number of Eu^{3+} ions located near the surface is small and constant, so that the saturation effect can be observed earlier. Using a pulsed Nd:YAG laser with a peak power of 1.17 kW (266 nm) Eu emission near the sample surface is almost quenched compared to the volume emission, as a further clue that, for high excitation power, Eu centers near the surface are totally saturated. In the above discussion the assumption has been made that the decay time of both Eu emission lines are rather similar, so that the spectra as a function of excitation power are depending on the number of Eu atoms (more inside bulk, few at the surface).

To check this prediction, time resolved PL measurements have been carried out with a chopped frequency doubled Ar-ion laser (244 nm) and are shown in Figure 4.6. The time resolved PL measurements have been fitted with a double exponential decay; the first decay time is due to the experimental system response (~0.008 ms), the second one is the decay time of the Eu ions. It can be found that the above argumentation can be retained as the decay time of Eu^{3+} ions near the surface, about 0.120 ms at 5 K is rather similar to that of Eu^{3+} ions deeper inside the layer which has been measured to be about 0.150 ms. This similarity is kept in the temperature range between 5 K and 300 K (see the inset in Figure 4.6) The decay time as a function of temperature for the two sets of Eu^{3+} ions provides further information about the

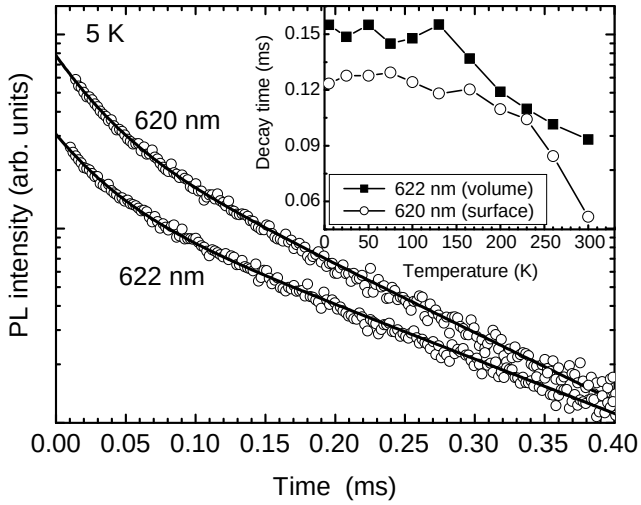

Figure 4.6: *Time resolved PL signal of emission lines at 620 nm (surface) and 622 nm (inside) measured at 5 K. Fitting of the measurements with double exponential decay are plotted bold. The inset shows decay times for both emission lines as a function of temperature.*

excitation dynamics. It can be seen that the they behave similarly; stable between 5 K and 200 K and showing then a decrease by a factor of 2 between 200 K and 300 K.

Having established this, the thermal decrease of emission lines by a factor of ten between 5 K and 300 K shown in Figure 4.3 is not due a mechanism related to the Eu^{3+} ions themselves but is likely due to non-radiative centers of the GaN host, which act before Eu excitation.

Coming back to the results in Figure 4.4 we now want to show how one can calculate the density of generated carriers per volume for the cases of interest, namely 300 V and at 5000 V. The number of electron-hole pairs created per impinging electron can be obtained using the empirical equation $N_{e-h\,Pairs} = U_{acc}/3E_g$ with ($E_{g,GaN} = 3.4eV$). For the used spot size (1 µm) the injected current in nA is proportional to the acceleration voltage according to the formula $I = 1.7 \cdot U_{acc}/1000$, with the acceleration voltage U_{acc} in kV. The evaluation of the excited volume has been obtained using Monte Carlo simulations of electron penetration depth. Then the excited volume is equal to $p(r+d)^2 \cdot d$ with r=500 nm being the radius of the spot size and d being the penetration depth. We found that the density of electron hole pairs created per second ($3 \cdot 10^{25}$ pair/cm^3 and $1 \cdot 10^{26}$ pair/cm^3 for acceleration voltage of 300 V and 5000 V, respectively) is changed only by a factor of 3 for the two used

acceleration voltages as the higher number of injected carriers associated with higher acceleration voltages is compensated by the effect of a strong increase of the excited volume of GaN material (d_{300V} =3 nm, d_{5000V} = 200 nm).

Based on this calculation we conclude that it is legitimate to interpret results in Figure 4.4 as an evidence that two populations of Eu^{3+} ions are present, since the calculated carrier densities for the two acceleration voltages (300 V and 5000 V) are in the same order.

However the estimation is very rough since other influences like electron backscattering and a charge up of the sample have to be considered. Moreover at low acceleration voltages (300 V) it is difficult to measure the spot size of the impinging electron beam, so that high error bars have to be taken into account which are difficult to estimate.

It is interesting to notice that both strong signals from near the surface and inside volume material can be seen in the CL spectrum of the GaN:Eu layer for 300 V acceleration voltage. Observation of CL from volume Eu^{3+} ions is likely related to the diffusion length of created electron-hole pairs, which is nevertheless difficult to quantify at this stage. In the 5000 V acceleration voltage CL spectrum, excitation with higher carrier density and deeper in volume makes emission from the volume Eu^{3+} ions predominant, while that from the surface Eu^{3+} ions saturated.

With the aim of confirming the existence of two populations of Eu^{3+} sites, CL experiments were achieved using two different samples, namely a thick one (200 nm) and a thin one (10 nm). For these two samples Figure 4.7 shows the 622 nm/633 nm line intensity ratio as a function of acceleration voltage. It appears that for thin GaN layer most CL come from Eu^{3+} ions located near the surface while for thick GaN layer the CL comes from Eu^{3+} ions deeper in volume which contributes significantly beside one originating from those near the surface. Not that for acceleration voltages higher than 4 kV the quotient of the 622 nm/633 nm line is slightly decreasing, which is understandable when we keeping in mind that higher acceleration voltages are detrimental to the sample. In order to study the excitation mechanism of the Eu^{3+} ions near the surface and inside the sample, PLE was carried out for emission at 620 nm (633 nm) and 622 nm at 5 K and 300 K. Figure 4.8a present the PLE spectra, which are vertically shifted and grouped in temperature for clarity. In general, the spectra are characterized by strong above- and near-band-edge (at 356.2 nm and 362.4 nm

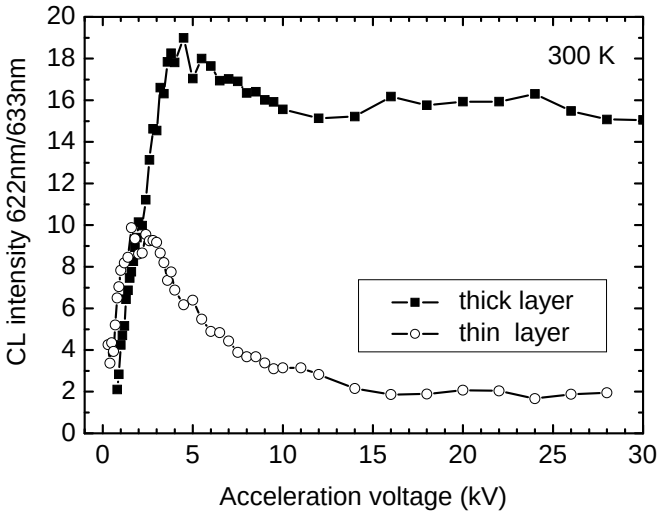

Figure 4.7: *Quotient of CL intensity for emission at 622 nm and 633 nm as a function of the acceleration voltage for a 10 nm thick GaN:Eu layer and the 200 nm thick sample measured at 300 K.*

at 5 K and 300 K, respectively) absorption followed by a stepdecrease at the long wavelength (low energy) side. As a result it can be deduced that Eu^{3+} ions are effectively excited through a GaN near-band-gap excitation mechanism. This result is remarkably different from PLE studies previously reported in literature, for which Eu^{3+} excitation by a defect-related energy transfer mechanism at around 400 nm plays an important role. This defect-related energy states have been identified in literature in MBE grown samples [Pen05] and samples prepared by Eu implantation [Nye03], showing that optical results are depending crucial on the details of sample preparation, e. g. Eu content and defect density of the GaN layer. No well resolved absorption due to a trap level could be found in our GaN:Eu layer. Although the reason for these discrepancies is not clear, it is possible that different sample preparation/synthesis result in different defect type/concentrations that show different features on the PLE spectra. In fact, PLE at 400 nm and longer wavelength (not shown) is more than 100 times weaker, and only exists in the case of the emission around 622 nm, indicating that most Eu^{3+} atoms are excited by an energy transfer mechanism via the host band-gap and/or very shallow traps closed to the band-edge. The PLE at 633.5 nm shows similar characteristics to the 620 nmemission. A small redshift from 5 K to 300 K of the near-band-edge resonance is assigned to a thermal narrowing effect.

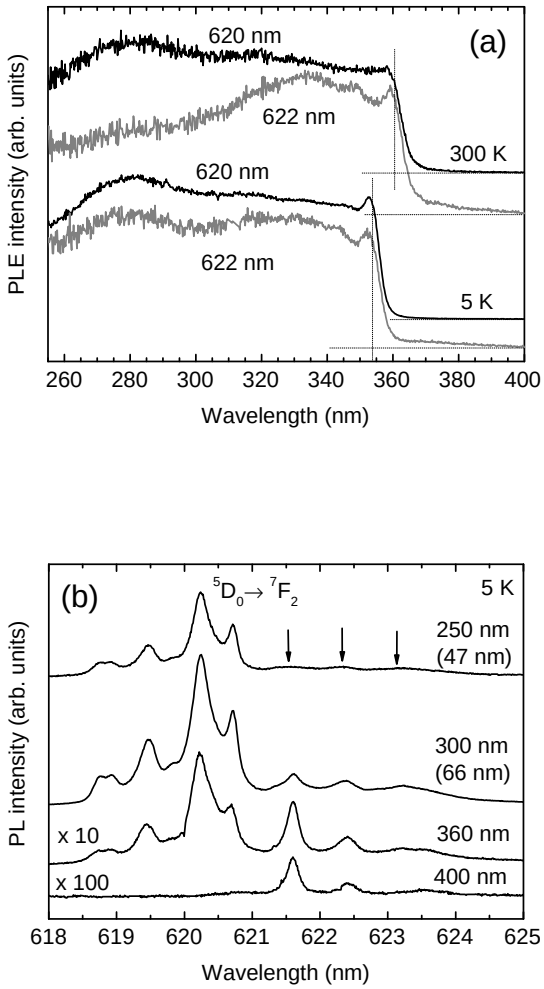

Figure 4.8: a) *PLE spectra of a GaN:Eu layer for Eu emissions at 620.0 nm and 621. 7 nm (measured at 300 K) and at 620.3 nm and 622.0 nm (measured at 5 K). The horizontally dotted lines are PLE base lines. The vertically dotted lines show the band-gap energy of GaN* **b)** *PL spectra of a GaN:Eu measured at 5 K with different excitation wavelengths (indicated in the curves). The penetration depths until 1/e as indicated in the figure is calculated using values from Ref. [Mut99]. The spectra are normalized to the excitation power density and the integration time for detection. The spectra under 360 nm and 400 nm excitation are multiplied by a factor of 10 and 100, respectively, for clarity. The arrows indicate the 622 nm lines assigned to Eu^{3+} ions from the volume.*

These PLE results show that carrier-mediated energy transfer between the GaN host and Eu^{3+} ions is the dominant mechanism. The sample quality is directly reflected by the linewidth of the Eu emission lines. We found for the $^5D_2 \rightarrow {}^7F_0$ transitions a line width of 0.1 nm and for the $^5D_0 \rightarrow {}^7F_2$ transition a line width of about 0.3 nm, depending on the emission. These line widths are much sharper than those recently reported in literature (FWHM 1.6 nm) indicating an unperturbed local environment of Eu atoms [Nye03].

PLE below the band-gap energy shows interesting difference between Eu^{3+} emission at 620 nm and 622 nm, namely a low energy tail for 622 nm excitation with respect to the 620 nm (and 633 nm spectrum which is not shown here). This difference is again assigned to the existence of two Eu^{3+} sites, namely near the surface and inside the sample depth. Furthermore we suggest that the bump observed around 280 nm in the 300 K PLE spectrum for 620 nm emission, which is not present in the PLE at 622 nm, is another clue of the excitation of two types of sites. However the origin of the difference in absorption at 300 K is not clear at this stage. At 5 K, the PLE spectra for the 620 nm and 622 nm emissions look rather similar around the mentioned region which is possibly associated with the temperature-dependent carrier population in shallow traps after excitation.

Further enlightenment is provided by PL experiments which are shown in Figure 4.8b. Increasing the wavelength i.e. the penetration depth of the light, we observed a progressive increase in the intensity of the line at 622 nm, which is assigned to the volume Eu^{3+} site, in agreement with CL experiments in Figure 4.4. This is surely the strongest argument for the surface/volume interpretation as the tunable excitation source was a 500 W Xe lamp filtered by a double grating monochromator, with typical excitation densities below 200 $\mu W/cm^2$. Therefore these measurements at very low excitation should not induce any saturation effect (as shown in Figure 4.5), and the only varying parameter was the absorption depth of the excitation beam. This depth depends on the chosen excitation wavelength, which would be smaller than 10 nm to 20 nm for above band gap excitation at 250 nm to 300 nm (because of the strong optical absorption), and would extend deeper in the volume for below band gap excitation at 360 nm to 400 nm.

Also noticeable, below band-gap excitation at 400 nm shows only emission from inside the sample, consistent with the presence of the PLE tail further than 360 nm shown in Figure 4.8a.

It is interesting to notice that a GaN layer grown by MOCVD implanted with Eu atoms show no emission at around 620 nm which is understandable because Eu ions are implanted typically deeper inside the sample [Wan05], leading to a lack of Eu close to the surface and, consequently, to the absence of the lines identified in the present work as being related to a site close to the surface.

References

[And04] T. Andreev, Y. Hori, X. Biquard, E. Monroy, D. Jalabert, A. Farchi, M. Tanaka, O. Oda, Le Si Dang, and B. Daudin, *Optical and structural properties of rare earth doped GaN quantum dots*, Superlattices and Microstructures, **36**, 707 (2004).

[Ban04] H. Bang, S. Morishima, J. Sawahata, J. Seo, M. Takiguchi, M. Tsunemi, K. Akimoto, and M. Nomura, *Concentration quenching of Eu-related luminescence in Eu-doped GaN*, Appl. Phys. Lett. **85**, 227 (2004).

[Bar03] J. Barjon, J. Brault, B. Daudin, D. Jalabert, and B. Sieber, *Cathodoluminescence study of carrier diffusion in AlGaN*, J. Appl Phys. **94**, 2755 (2003).

[Bre67] C. Brecher, H. Samelson, A. Lempicki, R. Riley, and T. Peters, *Polarized Spectra and Crystal-Field Parameters of Eu^{3+} in YVO_4*, Phys. Rev. **155**, 178 (1967).

[Die68] G. H. Dieke, *Spectra and Energy levels of Rare Earth Ions in Crystals* (Wiley, New York, 1968).

[Dir04] V. Dierolf, C. Sandmann, J. Zavada, P. Chow, and B. Hertog, *Site-selective spectroscopy of Er in GaN*, J. of Appl. Phys. **95**, 5464 (2004).

[Höm03] U. Hömmerich, Ei Ei Nyein, D. S. Lee, J. Heikenfeld, A. J. Steckl, and J. M. Zavada, *Photoluminescence studies of rare earth (Er, Eu, Tm) in situ doped GaN*, Mater. Sci. Eng. **B105**, 91 (2003).

[Kim98] S. Kim, S. J. Rhee, X. Li, J. J. Coleman, and S. G. Bishop, *Photoluminescence and photoluminescence excitation spectroscopy of multiple Nd^{3+} sites in Nd-implanted GaN*, Phys. Rev B **57**, 14588 (1998).

[Kim04] J. H. Kim and P. H. Holloway, *Room-temperature photoluminescence and electroluminescence properties of sputter-grown gallium nitride doped with europium*, J. Appl. Phys. **95**, 4787 (2004).

[Lor04] K. Lorenz, U. Wahl, E. Alves, S. Dalmasso, R. W. Martin, K. P. O'Donnell, S. Ruffenach, and O. Briot, *High-temperature annealing and optical activation of Eu-implanted GaN*, Appl. Phys. Lett. **85**, 2712 (2004).

[Loz00] H. J. Lozykowski, W. M. Jadwisienczak, J. Han, and I. G. Brown, *Luminescence properties of GaN and $Al_{0.14}Ga_{0.86}N$/GaN superlattice doped with europium*, Appl. Phys. Lett. **77**, 767 (2000).

[Liu04] Q. L. Liu, Y. Bando, F. F. Xu, and C. C. Tang, *Effect of growth temperature on morphology, structure and luminescence of Eu-doped GaN thin films*, Appl. Phys. Lett. **85**, 4890 (2004).

[Mut99] J. F. Muth, J. D. Braun, M. A. L. Johnson, Zhonghai YU, R. M. Kolbas, J. W. Cook, J. R. and J. F. Schetzina, *Absorption coefficient and refractive index of GaN, AlN and AlGaN alloys*, MRS J. Nitride Semicond. Res. 4S1, G5.2 (1999).

[Nye03] Ei Ei Nyein, U. Hömmerich, J. Heikenfeld, D. S. Lee, A. J. Steckl, and J. M. Zavada, *Spectral and time-resolved photoluminescence studies of Eu-doped GaN*, Appl. Phys. Lett. **82**, 1655 (2003).

[Pen05] H. Y. Peng, C. W. Lee, H. O. Everitt, D. S. Lee, A. J. Steckl, and J. M. Zavada, *Effect of optical excitation energy on the red luminescence of Eu^{3+} in GaN*, Appl. Phys. Lett. **86**, 051110 (2005).

[Pik67] A. H. Piksis, G. H. Dieke, and H. M. Crosswhite, *Energy Levels and Crystal Field of $LaCl_3:Gd^{3+}$,* J. Chem. Phys. **47**, 5083 (1967).

[Shi04] S. Shirakata, R. Sasaki, and T. Kataoka, *Photoluminescence of Eu-doped GaN thin films prepared by radio frequency magnetron sputtering*, Appl. Phys. Lett. **85**, 2247 (2004).

[Wan05] K. Wang, R. W. Martin, K. P. O'Donnell, V. Katchkanov, E. Nogales, K. Lorenz, E. Alves, S. Ruffenach, and O. Briot, *Selectively excited photoluminescence from Eu-implanted GaN*, Appl. Phys. Lett. **87**, 112107 (2005).

5. Optical properties of GaN QDs doped with Eu

In this chapter we will discuss optical properties of GaN:Eu QDs grown on AlN. EXAFS experiments have shown that Eu atoms are located inside GaN QDs, in contrast to Tm doped GaN QDs for which Tm atoms are better found at the interface between GaN QDs and AlN spacer (See section 3.4). For this reason it is suitable to begin the discussion of the optical properties with GaN:Eu QDs.

We will first discuss the influence of the Eu concentration on the optical properties (Section 5.1). Then the temperature dependency of the PL will help to show the capability of Eu doped GaN QDs for devices working at room temperature. Within this chapter the energy transfer mechanisms from GaN QD host to the Eu atoms will be also discussed tentatively.

5.1 The influence of the Eu concentration on the emission spectrum

Figure 5.1 shows a CL overview spectrum from GaN:Eu QDs measured at 300 K. As in case of the GaN:Eu layer sharp emission lines are visible extending from about 470 nm to 860 nm. The dominant intra Eu^{3+} transition is also here the $^5D_0 \rightarrow {}^7F_2$ transition at around 622 nm. The wide emission ranging from 280 nm to 350 nm can be attributed to the fundamental emissions of the QDs. At this stage it is rather hard to compare the optical output of GaN:Eu QDs with that of a GaN:Eu layer, as absorption coefficients have to be taken into account which have not yet been fully studied for GaN QDs.

In case of GaN:Eu layer we have already seen that a Eu content of 0.2 % is sufficient to totally quench the near band-gap emission from the host material (Section 3.4.6). We now want to discuss the influence of the Eu content on the emission spectrum of GaN:Eu QDs in a comparative PL study. Figure 5.2 shows the integrated QDs emission divided by the integrated Eu^{3+} luminescence for a series of samples grown with different Eu content. The samples consist of 10 stacks of Eu doped QDs. It is visible that for low Eu concentration the spectrum is dominated by fundamental emission from QDs. With increasing Eu^{3+} concentration the emission

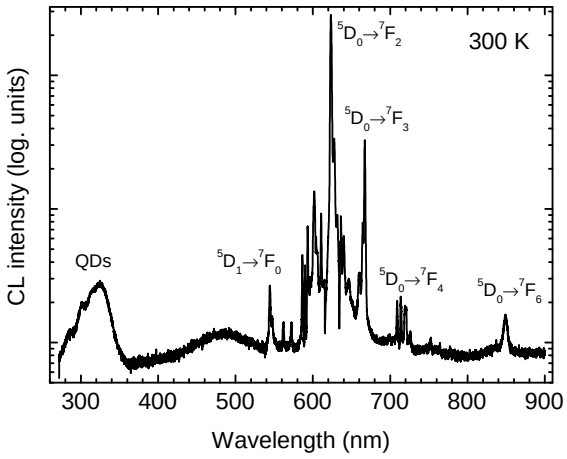

Figure 5.1: *Overview CL spectrum in logarithmic scale of GaN:Eu QDs measured at 300 K. Assigned transitions from Eu^{3+} ions are indicated in the figure.*

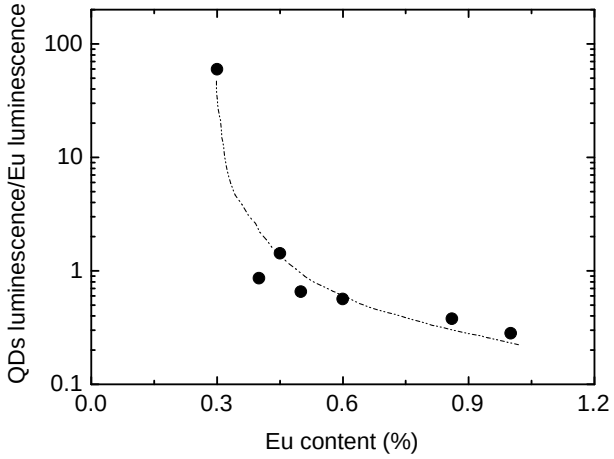

Figure 5.2: *Integrated QD luminescence versus the integrated Eu luminescence in logarithmic scale measured in a comparative PL study for a series of samples containing different Eu contents. Excitation source YAG:Nd Laser emitting at 266 nm. Diameter of the focal point: 0.5 mm. The measurement has been performed at room temperature. The dashed line is a guide to the eye. The samples contain 10 stacks of GaN:Eu QDs.*

from QDs is starting to quench and Eu^{3+} emission is getting more and more important until luminescence from QDs is dominated by Eu^{3+} emission. From this measurement, important information can be deduced: First Eu^{3+} emission is correlated to fundamental emission from QDs. This means that an energy transfer from the GaN QDs host to the Eu^{3+} ions exists. For a Eu content between 0.4 % and 1% the Eu^{3+} emission is increasing linearly. This means that the optical output is proportional to the number of Eu atoms. For Eu concentrations lower than 0.4 % the ratio of QDs

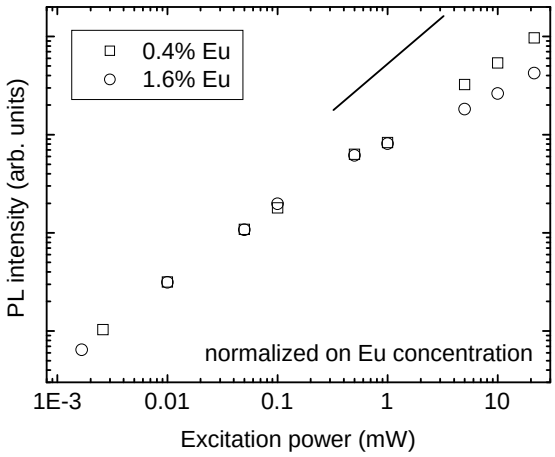

Figure 5.3: *Integrated red Eu PL measured as a function of the excitation power for two samples containing 1.6% Eu (circles) and 0.4% Eu (squares). The Eu emission is normalized to the Eu content obtained by RBS measurements. The line is showing a linear behavior in the double logarithmic scale. The measurement has been performed at 300 K.*

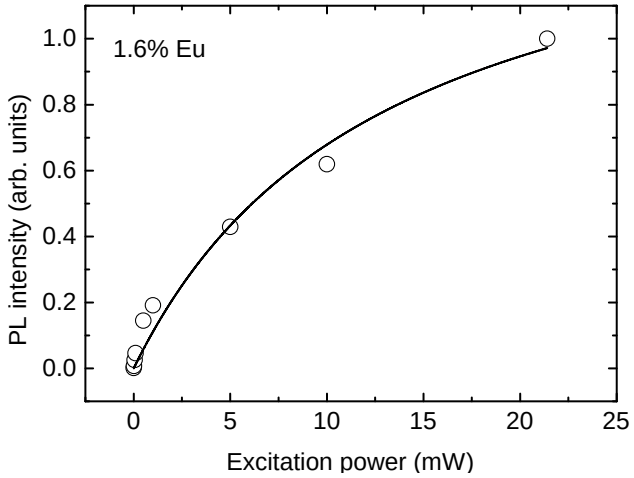

Figure 5.4: *Integrated PL intensity from the red Eu transitions measured with various excitation powers (open circles). The solid line corresponds to a fit from model described in the text. The sample was excited with the 305 nm line of an Ar-ion laser. The measurement has been performed at 300 K.*

emission versus Eu emission is non-linear. It is reasonable to assume that PL inactive Eu centers are existing in the sample with 0.3%.

In a next stage we want to discuss how red Eu emission is behaving as a function of the excitation power. For this in Figure 5.3 the integrated red Eu PL has been measured for various excitation powers and is shown in double logarithmic scale for two samples containing 1.6 % and 0.4 % Eu. The Eu^{3+} emission has been normalized to the Eu content as measured by RBS. It is visible that the key parameter for the Eu^{3+} emission is the number of Eu^{3+} ions per QDs as the intensity of Eu^{3+} emission is coinciding when normalized to the Eu content. Next a strong saturation effect is clearly observed, which is to be expected since the number of

Eu^{3+} ions in each QD is finite. This behavior can be described by the following equation:

$$\frac{dn}{dt} = P(N-n) - n/t \qquad (4.1)$$

Here N is the total number of Eu ions in QDs, typically 1300 for 1% Eu-doped QD, n is the number of excited Eu ions, P is proportional to the photon flux of the pumping laser and t the radiative decay time of Eu ions (of the order of 300 µs see below). In stationary case we obtain:

$$n = \frac{t\,PN}{1+t\,P}. \qquad (4.2)$$

In the limit of low power, i.e. $t\,P << 1$, n, which is proportional to the PL intensity, shows a linear increase with power $n \approx t\,P\,N$. In the upper limit of $t\,P >> 1$ all the rare earth ions are excited, so that a saturation of the luminescence intensity is observed $n \approx N$. This simple model gives a reasonable fit to the saturation measurements, as shown by the solid line in Figure 5.4. A decay time of 325 µs has been deduced from the fit, consistent with the measured decay time (370 µs see below).

Coming back to Figure 5.3, we can observe for higher excitation powers that the red Eu^{3+} emission normalized to the Eu content is higher for the sample with lower Eu content (0.4%) than for the sample with higher one (1.6%). For explaining this small effect the decay time of the Eu^{3+} ions has to be known, with respect to the excitation power [Loz93] and the Eu content which is discussed in section 5.3.

5.2 Temperature dependent PL of GaN:Eu QDs

We now want to discuss the thermal quenching of GaN:Eu QDs to measure the Eu radiative quantum efficiency. Figure 5.5 compares the integrated Eu^{3+} PL of undoped GaN QDs, Eu doped GaN QDs and a thick GaN:Eu layer from liquid helium temperature to room temperature. As discussed in section 4 for the thick GaN:Eu layer the decrease of the PL with temperature is almost one order of magnitude, explained by a high number of non radiative channels from a high defect

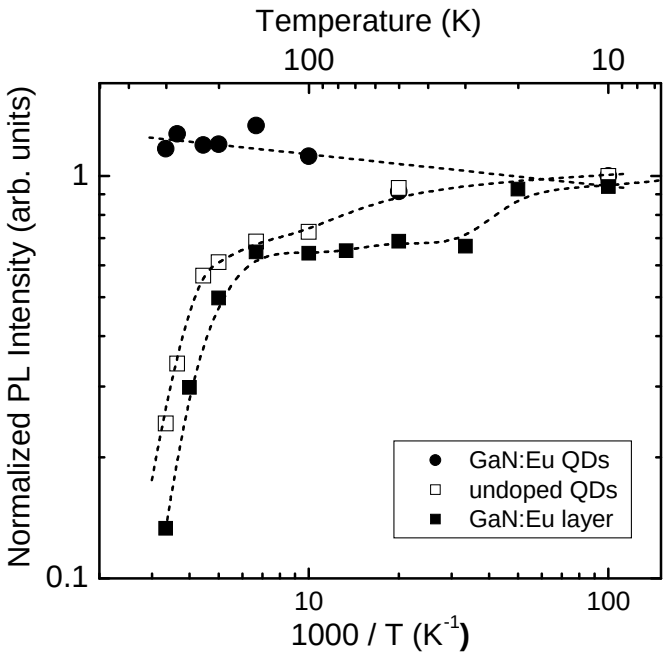

Figure 5.5: *Temperature dependence of the PL intensity for Eu-doped GaN QDs (filled circles), undoped GaN QDs (unfilled squares), and a thick GaN layer (filled squares). The dashed lines are used to guide the eye. The Eu content in GaN QDs was 1.6 %. The samples have been excited with a Nd:YAG laser (266 nm).*

density[2]. As shown in Figure 5.5, the PL of undoped GaN QDs exhibits also a decrease, although a bit weaker (by about 30%) in agreement with results reported in ref. [Yon02, Sim03].

By contrast, the Eu related PL of GaN:Eu QDs is almost constant as a function of temperature. This remarkable behavior would be understandable if carrier recombination through Eu excitation were fast enough to be dominant over possible non-radiative and radiative processes in QDs. It is possible, on the other hand, that trapping of carriers by Eu atoms is very fast. This would result in strong localization of carriers in the vicinity of Eu atoms prior to recombination, therefore further supporting the exclusion of nonradiative recombination paths. In other words, carrier trapping by Eu^{3+} ions is much more effective in GaN:Eu QDs than in Eu doped thick layers since QDs are defect free regions. These Eu-trapped carriers are more localized than

[2] Note that the used Nd:YAG laser has a very high excitation peak power of about 1 kW, which has been focused through a spot with a diameter of minimum 0.5 mm, so that most excited Eu^{3+} ions have been located deep in the GaN:Eu layer (Section 4.2).

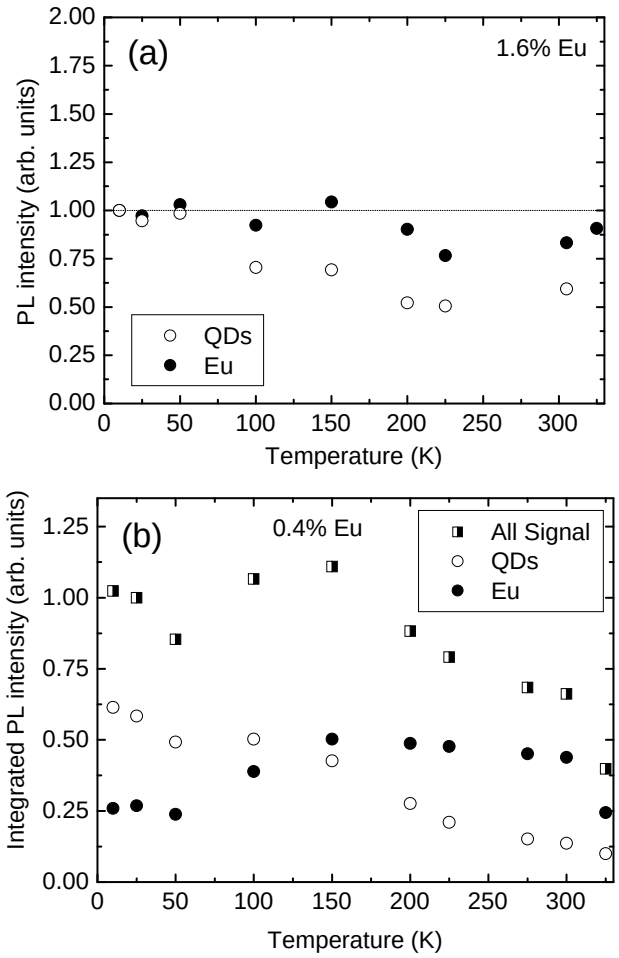

Figure 5.6: *Temperature dependence of the PL intensity for Eu-doped GaN QDs. Filled circles show the integrated red Eu^{3+} PL and open circles the residual integrated QD emission in blue to ultraviolet spectral range from the sample (Figure 5.1) for a sample containing* **a)** *1.6% Eu and* **b)** *0.4% Eu. The half filled squares in b) show the integrated PL intensity from both QD related emission and that from Eu^{3+} ions. The dashed line in a) is a guide to the eye. Both samples have been excited with an Ar-ion Laser emitting at 305 nm (Used excitation power 1 mW).*

carriers trapped in QDs, and should be less sensitive to non-radiative recombination. Note also that the thermal quenching of near band-gap emission from an undoped GaN layer is much higher than those of the Eu emission in a Eu doped layer, which is in good agreement with the above discussion [Ler99].

5.2.1 Temperature dependent PL of GaN:Eu QDs with different contents

To study in more detail the thermal behavior of the PL of Eu doped GaN QDs the residual emission from QDs is shown together with the Eu^{3+} PL from 5 K to 325 K in Figure 5.6a for a sample with low near band-gap related emission (1.6 % Eu). It can be found that both red Eu^{3+} PL emission and residual QD PL emission are stable from liquid helium to room temperature. This is interesting as for undoped GaN QDs

near band gap related emission is starting to quench already at 50 K as we have seen in section 5.2. This result demonstrates again the strong carrier trapping efficiency due to Eu doping.

A temperature dependent PL study has been also performed on a sample containing a rather low Eu content (0.4%). A very interesting thermal behavior can be found for this sample as the Eu^{3+} emission is increasing by a factor of about 2 in the temperature range between 50 K and 150 K to be then thermally stable up to room temperature. Moreover, consistent with the increase of Eu emission, QD related PL shows a decrease by the same order. This result is again strongly supporting that an energy transfer from the QDs host to the Eu^{3+} ions is existing. However, the thermal increase of the Eu emission between 50 K and 150 K shows the complexity of energy transfer mechanism. One possible explanation is that the $^5D_0$ excited state is gaining energy due to relaxation process from higher excited states, although it is difficult to explain why this process is more likely for lower Eu concentration. For more information see the discussion in chapter 7.

5.3 Time resolved PL of GaN:Eu QDs

In a next stage time resolved measurements have been performed for the two samples of interest, namely 10 stacks of GaN:Eu QDs doped with 1.6% and 0.4% Eu. The time resolved measurements have been carried out as in case of the GaN:Eu layer with the chopped 244 nm line of a frequency doubled Ar-ion laser. The measured data are shown in Figure 5.7a, which have been fitted with a double exponential decay. The first decay time is originating from the experimental setup (0.008 ms) and the second one from the Eu^{3+} ions. A good agreement between the fit and the measured data can be found in more than two orders of magnitude.

Figure 5.7b shows decay time measurements of the $^5D_0 \rightarrow {}^7F_2$ transitions of GaN:Eu QDs with the two Eu concentrations. At first it is visible that the excited Eu^{3+} ions show systematically about 20% longer decay times in the sample with the higher Eu content. This can be tentatively explained by possible cross relaxation processes between Eu^{3+} ions, e. g. after rare earth excitation a backtransfer occurs to the trap level, or another excited state of a neighbor rare earth ion. Such a mechanism has

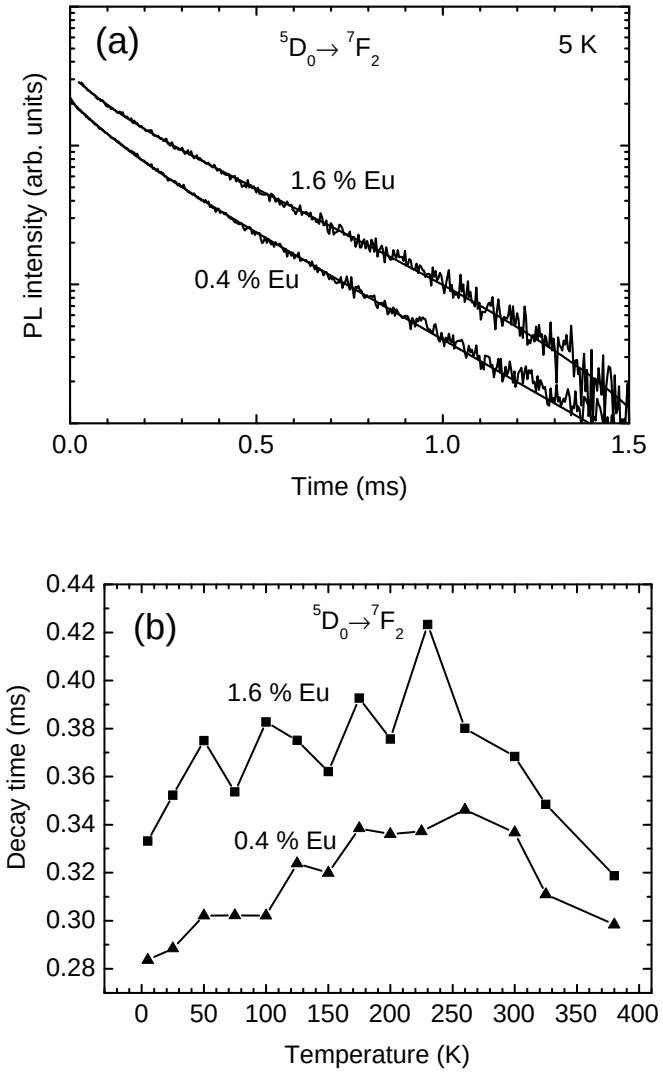

Figure 5.7: a) *Time resolved PL signal of the $^5D_0 \rightarrow {}^7F_2$ transtion measured at 5 K for GaN:Eu QDs with a concentration of 1.6% and 0.4%. Fitting of the measurements with double exponential decay are plotted bold.* **b)** *Decay times as a function of temperatures of the two samples.*

been recently invoked in Eu doped fluoride glasses [Dej95]. Next, for the two samples, an increase of about 20 % of the decay time can be observed between liquid helium temperature and 250 K. This interesting feature is at this stage puzzling, as usually the decay time is decreasing with temperature due to non-radiative mechanisms. One interpretation could be higher cross relaxation rates with temperature which are however unlikely for samples with low RE concentrations. However, the Eu concentration is rather low (0.4 %), so that again the question of microscopic Eu location in GaN QDs comes out. In other words, the cross relaxation rate is not only depending onto the absolute Eu content in GaN QDs, but onto the distance between two Eu ions. In chapter 3.4.2 we have already remarked that

EXAFS data do not allow to conclude on Eu environment as fare as 4 shells round the Eu ions. This shows that Eu atoms are not homogeneously distributed in the QDs, as otherwise a simulation with only Ga fourth next neighbors would fit experimental data, so that other metal neighbors have to be considered perhaps Eu ions, so that cross relaxation can occur.

Even if the above discussion is very speculative, the results are in agreement with the fact that for the GaN:Eu layer the decay time (0.150 ms at 5 K) is about a factor of 2 shorter, and the Eu content also much lower (0.2%). It is clear that in a GaN:Eu layer Eu ions have a different local environment (no Al and perhaps less Eu atoms). The influence of the high polarization field in QDs onto the decay time is yet unclear.

Coming back to the decay time measurements as a function of temperature shown in Figure 5.7b a decrease can be then found for the two samples for temperatures higher than 250 K. This can be explained by the fact that at elevated temperatures non-radiative processes in QDs, perhaps due to phonons, have to be considered.

5.4 The effect of the GaN QDs size onto the Eu emission

To gain in more detail information about Eu location inside GaN:Eu QDs and onto the excitation mechanism a sample with 100 stacks of Eu doped GaN QDs has been grown. The high emission intensity of this sample allows measuring the PLE to get information about the excitation mechanism as shown in Figure 5.8. A sloping absorption edge can be found at around 300 nm corresponding to an excitation mechanism via the size distributed QDs. Moreover below the band-gap of the QDs no direct adsorption from Eu^{3+} ions can be seen, due to the low emission intensity of the used Xe-lamp PLE setup. Slight oscillations are superimposed to the PLE spectrum. At first glance they can be associated with different excited states from QDs. Comparative PL spectra of GaN:Eu QDs with different excitation wavelengths are shown in Figure 5.9. The spectra exhibit only a broad emission line (FWHM 0.9 nm) at 622 nm, interestingly at the spectral position assigned to Eu^{3+} located in

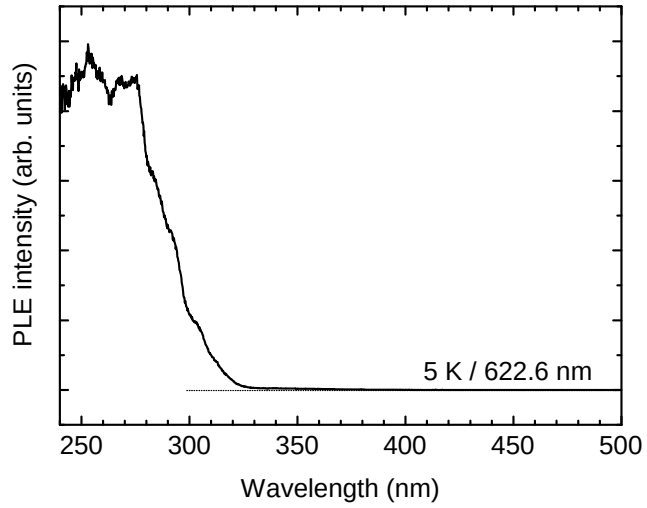

Figure 5.8: *PLE of the 622.6 nm emission line of Eu doped GaN QDs measured at 5 K.*

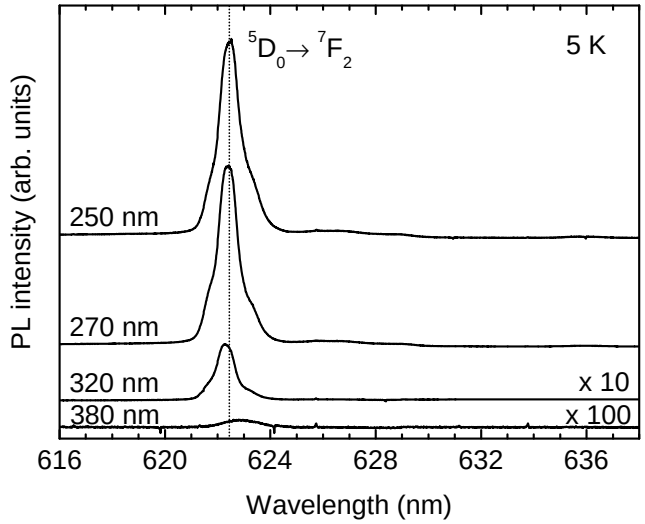

Figure 5.9: *PL spectra for GaN:Eu QDs measured at 5 K with different excitation wavelengths.*

the bulk of the GaN layer (FWHM 0.3 nm). The broader linewidth could be explained by a strong internal electric field inside GaN QDs, which was found to be in the order of 7 MV/cm [And00, Sim03]. Another reasonable explanation for the broader linewidth is the inhomogeneous strain inside GaN QDs. The reduction of the emission intensity is simply due to the fact that the excited QD density of states is getting smaller and smaller for longer wavelengths in agreement with the PLE study shown in Figure 5.8. With excitation wavelengths longer than 320 nm a drastic reduction of the emission intensity is observed, although the linewidth is unaffected. An excitation below the fundamental transitions of GaN QDs (380 nm) shows only very weak emission.

In general smaller QDs have higher transition energies than bigger dots. The grown GaN:Eu QDs are typically distributed in height and diameter as one can see in the AFM images shown in Figure 3.10. According to this situation higher excitation wavelengths (320 nm) can only excite bigger QDs, which have different properties like larger internal electric fields acting on Eu atoms [And00]. Note that it is difficult to know, which QDs are preferably excited with smaller excitation wavelength as also higher excited states of bigger QDs can play a role.

As a result it can be concluded; that Eu related PL seems to be only very little influenced by the size of excited QDs as the spectral shap is not significantly infuenced.

From the emission spectrum in Figure 5.9 only one optical active site from Eu inside GaN QDs can be identified. For more information see the discussion in chapter 4.

References

[And00] A. D. Andreev and E. P. O'Reilly, *Theory of the electronic structure of GaN/AlN hexagonal quantum dots*, Phys. Rev. B **62**, 15851 (2000).

[Dej95] M. Dejneka, E. Snitzer, and R. E. Riman, *Blue, green and red fluorescence and energy transfer of Eu^{3+} in fluoride glasses*, J. of Luminescence **65**, 227 (1995).

[Ler99] M. Leroux, N. Grandjean, B. Beaumont, G. Nataf, F. Semond, J. Massies, and P. Gibart, *Temperature quenching of photoluminescence intensities in undoped and doped GaN*, J. of Appl. Phys. **86**, 3721 (1999).

[Loz93] H. J. Lozykowski, *Kinetics of luminescence of isoelectronic rare-earth ions in III-V semiconductors,* Phys. Rev. B **48**, 17758 (1993).

[Sim03] J. Simon, N. T. Pelekanos, C. Adelmann, E. Martinez-Guerrero, R. André, B. Daudin, and Le Si Dang, and H. Mariette, *Direct comparison of recombination dynamics in cubic and hexagonal GaN/AlN quantum dots*, Phys. Rev. B **68**, 035312 (2003).

6. Optical properties of InGaN QDs doped with Eu

In section 2.5 we discussed the growth of InGaN:Eu QDs on GaN. In this section we will try to answer the key question: Are InGaN QDs really doped? And if not, where are the Eu^{3+} atoms located in the InGaN QDs/GaN structure? At least it is reasonable that the GaN spacing layer contains traces of Eu impurities as we have seen that Eu has a strong tendency to segregate during growth (section 3.3.1).

To find out the RE location in RE doped GaN QDs grown on AlN, structural characterisations like EXAFS are the methods of choice, besides optical characterisation. The identification of nearest next neighbours gives information about the RE location as we have seen in case of Eu and Tm doping of GaN QDs (Sec. 3.4). In case of InGaN QDs the situation is far more complex, because Ga atoms are located in InGaN QDs with unknown In content and in the GaN spacing layer.

The here studied sample consists of 165 stacks of InGaN:Eu QD planes, each capped with about 10 nm of GaN. From the chosen growth conditions, we estimate an Eu content of about 1% in the InGaN:Eu QDs.

6.1 Eu location in InGaN QDs sandwiched in GaN spacing layers

Figure 6.1 shows PL spectra in the red spectral range around the $^5D_0 \rightarrow {}^7F_2$ transition of Eu^{3+} ions, measured for a GaN:Eu layer, GaN:Eu QDs and InGaN:Eu QDs at room temperature, using above-bandgap excitation at 360 nm, 300 nm and 360 nm respectively. The PL spectrum of InGaN:Eu QDs exhibits several lines at around 620 nm, 622 nm, and 633.5 nm, where the 622 nm line clearly consists of many lines on the low energy side. Apart from some line width and intensity variation, the PL spectrum of InGaN:Eu QDs is quite similar to that of the GaN:Eu thick layer, by contrast to that of GaN:Eu QDs, which presents only an intense line at 622.5 nm (See also chapter 4 and 5). The emission lines are very sharp, e. g. below 0.5 nm of FWHM at room temperature in GaN:Eu layer (chapter 4). For GaN:Eu QDs as well as InGaN:Eu QDs, Eu lines are slightly broader due to internal strain and electric field distributions (Chapter. 5).

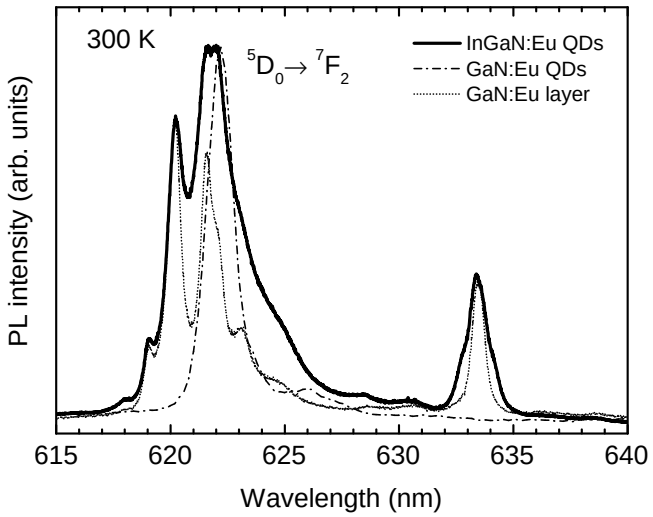

Figure 6.1: *PL spectra of InGaN:Eu QDs (solid line), GaN:Eu QDs (dashed dotted line) and GaN:Eu layer (dotted line) measured at 300 K for excitation at 360, 300 and 360 nm respectively.*

According to our transition assignment discussed in section 4.1, emission lines shown in Figure 6.1 originate from the $^5D_0 \rightarrow {}^7F_2$ transition, the number of lines being dependent on the Eu local site symmetry (Sec. 4 and 5). Figure 6.1 shows that Eu ions can occupy different sites in Eu-doped GaN layer. Only one Eu sites has been found for Eu doped GaN QDs so that it is reasonable to assume that one site is existing inside InGaN QDs, namely the coinciding emission line at 622 nm. If this is true also for the InGaN:Eu QDs sample, then the 622 nm line in the PL spectrum of InGaN:Eu QDs could be assigned to Eu ions in InGaN QDs, and the 620 nm and 633.5 nm lines to Eu ions in the GaN barrier layer. Such a spreading of RE dopants out of the doped QDs, most probably due to segregation effects, has been already discussed in section 3.4.4 for Tm-doped GaN QDs grown in AlN matrix.

To address the issues of different Eu^{3+} locations in the InGaN:Eu QDs sample, the PLE spectra for the 620 nm, 622 nm, and 633 nm lines at various temperatures, as shown in Figure 6.2a and Figure 6.2b have been measured. A common feature of the PLE spectra is a pronounced peak, at around 360 nm at 5 K, corresponding to the enhanced absorption of correlated electron-hole pairs at the band edge of the GaN barrier and spacer layer. However, they also display a few remarkable differences that can be reasonably explained if, as earlier, one assumes that the 620 nm and 633.5 nm lines are related to Eu^{3+} ions in the GaN spacer layer and the 622 nm line to Eu^{3+} ions in InGaN QDs. Firstly, the PLE spectra for the 620 nm and

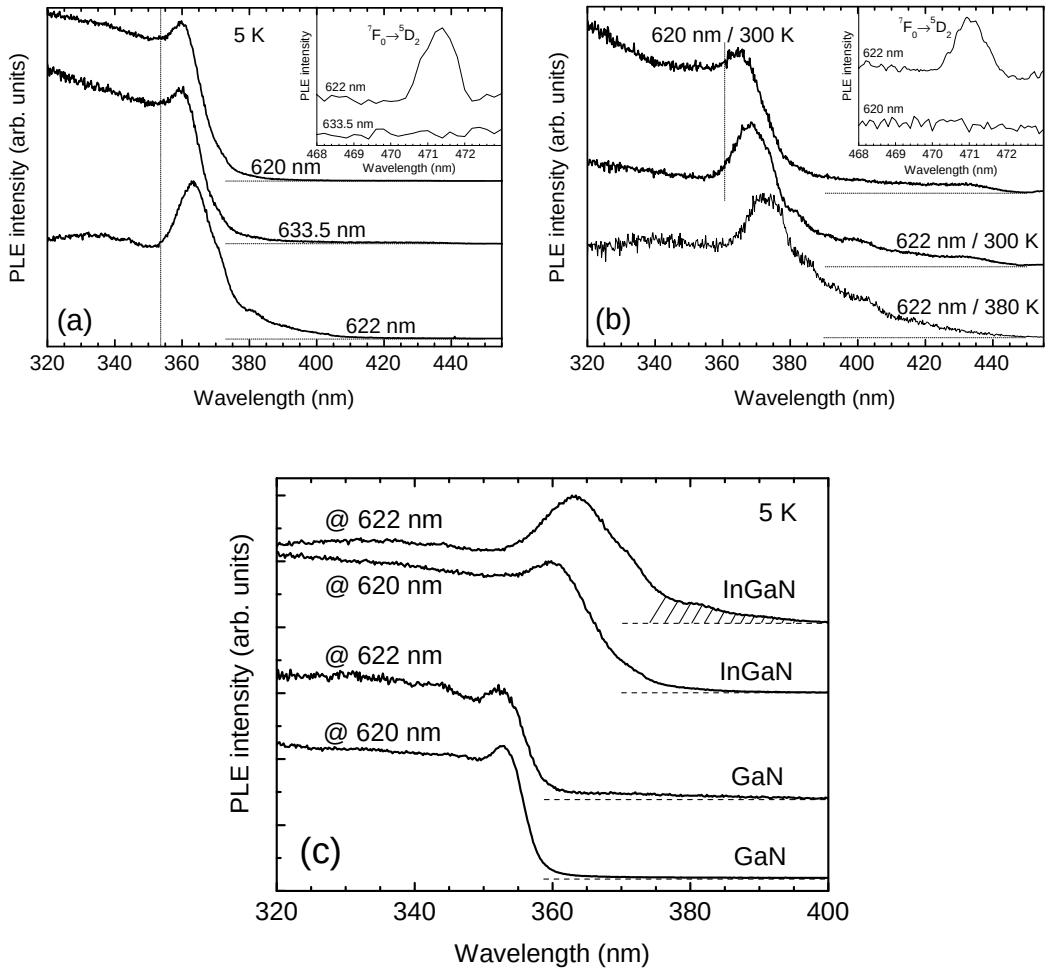

Figure 6.2: *PLE spectra for Eu emissions at 620.0 nm, 622.3 nm and 633.5 nm in InGaN:Eu QDs, measured at* **a)** *5 K and* **b)** *300 K and 380 K. The horizontally dotted lines are PLE base lines. The vertically dotted lines show the bandgap energy of GaN given in [Vis98]. The insets show the PLE spectra in the spectral range of the intra-4f absorption ($^7F_0 \rightarrow {}^5D_2$) of Eu^{3+} for emissions at 622 nm, 622 nm and 633.5 nm, measured at* **a)** *5 K and* **b)** *300 K.* **c)** *PLE spectra for Eu emissions at 622 nm and 620 nm in InGaN:Eu QDs (upper) and GaN:Eu layer at 622 nm and 620 nm (lower) measured at 5 K. The horizontally dotted lines are PLE base lines. The dashed part illustrates Eu emission by exciting InGaN QDs with certain size/shape distribution.*

633.5 nm lines are very similar (Figure 6.2a), which is consistent with the assumption that these two lines are from Eu^{3+} ions located in the same host, probably the GaN spacing layer in agreement with studies on GaN:Eu layer as discussed in section 4.2. Secondly, the band-edge peak in the PLE spectra is the most pronounced for the 622 nm line, indicating a more efficient energy transfer to Eu^{3+} ions. This supports the assumption of Eu location in QDs since carrier-mediated energy transfer to RE ions is much more efficient for RE ions located in GaN QDs than in GaN layers [Hor04].

Finally, the PLE band edge-peak for the 622 nm line extends farther in the gap, beyond 400 nm. Again this is consistent with the QD assumption since the PLE

spectrum of self-assembled QDs should display, in order of increasing energy, increased absorption into the distribution of excited states of an inhomogeneous ensemble of QDs, then into the wetting layer and the barrier (Compare also the AFM images in Figure 3.21). For InAs/GaAs QDs, the energy separation between absorption into the InAs wetting layer and the GaAs barrier is about 0.1 eV [Ste96, Hei97], which is roughly the width observed for the band-edge peak in the PLE spectrum of the 622 nm line. The PLE spectra at 300 K (Figure 6.2b) exhibit a small redshift of the near-band-edge resonance due to the usual band gap thermal narrowing effect.

Figure 6.2c shows for better understanding the PLE for emission at 620 nm and 622 nm for a GaN:Eu layer and the InGaN:Eu QDs at 5 K in the same scale. The GaN:Eu layer exhibits rather similar PLE spectra for emissions at 620 nm, 622 nm, and 633.5 nm (For more details see section 4), comparable to those of emission at 620 nm and 633.5 nm from the InGaN QDs sample, whereas emission at 622 nm, probably originating from Eu atoms inside InGaN QDs, exhibits a pronounced low energy tail as we have already seen. Note that the small redshift of 40 meV of this peak as compared to the PLE of the 620 nm and 633.5 nm lines could be induced by some In diffusion, say less than 1 % [Don04], into the GaN spacer.

PLE below the band-gap opens the possibility to resolve sharp intra-4f absorption lines by exciting directly the RE atoms [Ney04]. Although the excitation density of the used Xe lamp system is rather low in case of emission at 622 nm the $^7F_0 \rightarrow {}^5D_2$ transition can be well resolved even at room temperature. It is surprising that the emission at 471 nm can only be observed in the PLE of the 622 nm line in InGaN:Eu QDs (see inset of Figure 6.2a and Figure 6.2b). It is also absent in the PLE spectra of 620 nm, 622 nm and 633.5 nm lines from GaN:Eu QDs and GaN:Eu layer, even though the concentration of Eu ions is of the same order in these samples.

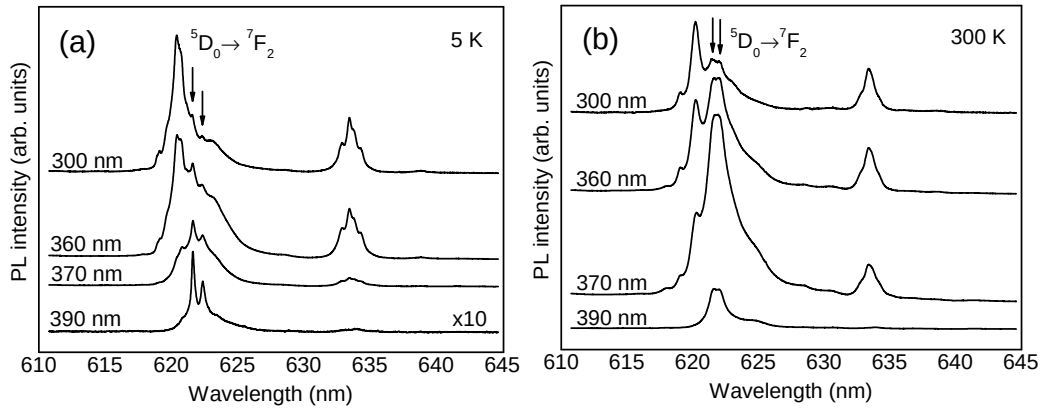

Figure 6.3: *PL spectra from InGaN:Eu QDs measured at* **(a)** *5 K and* **(b)** *300 K with different excitation wavelengths (indicated at the curves). The spectra are normalized by the excitation power density and the integration time for detection. The 5-K spectrum under 390 nm excitation is multiplied by a factor of 10 for clarity. The arrows indicate the 622 nm lines assigned to Eu ions inside InGaN QDs (see text).*

As a further check of the different Eu locations in InGaN:Eu QDs the PL was measured as a function of the excitation wavelength. The results are displayed in Figure 6.3a and Figure 6.3b for 5 K and 300 K, respectively. At 5 K, the 620 nm and 633.5 nm lines are strongly favored by exciting above the band gap of the GaN spacer layer (see the top spectrum in Figure 6.3a). For this type of excitation, carriers are created in the spacer layer so that any carrier-mediated energy transfer to Eu ions is expected to be more effective for Eu^{3+} ions located in the spacer than in QDs. This is because, in the latter case, one needs the additional process of carrier capture in QDs. In Figure 6.3, it is interesting to note that exciting well below the band gap of GaN at 390 nm produces only the 622 nm line. This observation is not a definite proof that the 622 nm line is due to Eu ions in QDs, but it is consistent with this assumption. At room temperature, the same tendency is found in selectively excited PL spectra, and the above general discussion remains valid.

Next, the 400 nm light (below the band-gap of GaN) was used to excite InGaN:Eu QDs and GaN:Eu layer samples in order to directly compare the emission lines. Figure 6.4 shows the different PL spectra. The PL integration time was longer by two orders of magnitude in the case of the GaN layer as compared to InGaN QDs.

This shows, as discussed in chapter 4.2, that defect related excitation mechanisms are very weak in our GaN layer and that on the other hand a significant part of the InGaN QD distribution can be still excited at 400 nm. In case of the GaN:Eu layer $^5D_0 \rightarrow {}^7F_2$ transition displays only emission at around 622 nm consisting

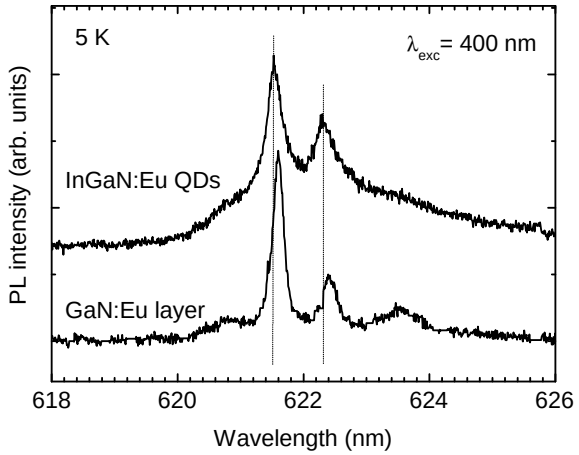

Figure 6.4: *PL spectra of InGaN:Eu QDs (upper spectrum) and GaN:Eu layer (lower spectrum) with the 400 nm excitation at 5 K. The vertical dotted lines guide to the eye. Spikes have been removed manually from the PL spectrum of the GaN:Eu layer.*

of two sharp lines with FWHM smaller than 0.3 nm. The InGaN QDs sample also shows these two sharp lines, slightly broadened and blue-shifted by about 0.1 nm, probably due to internal strain and electric field effects. A detailed view on the PL spectrum of the InGaN QDs shows a broad underlying signal. As this emission is not observed in case of the GaN layer it may come from Eu inside the InGaN QDs. As the broad emission is not yet understood, we will next study the temperature dependence in order to reveal the Eu location in the InGaN QDs/GaN sample.

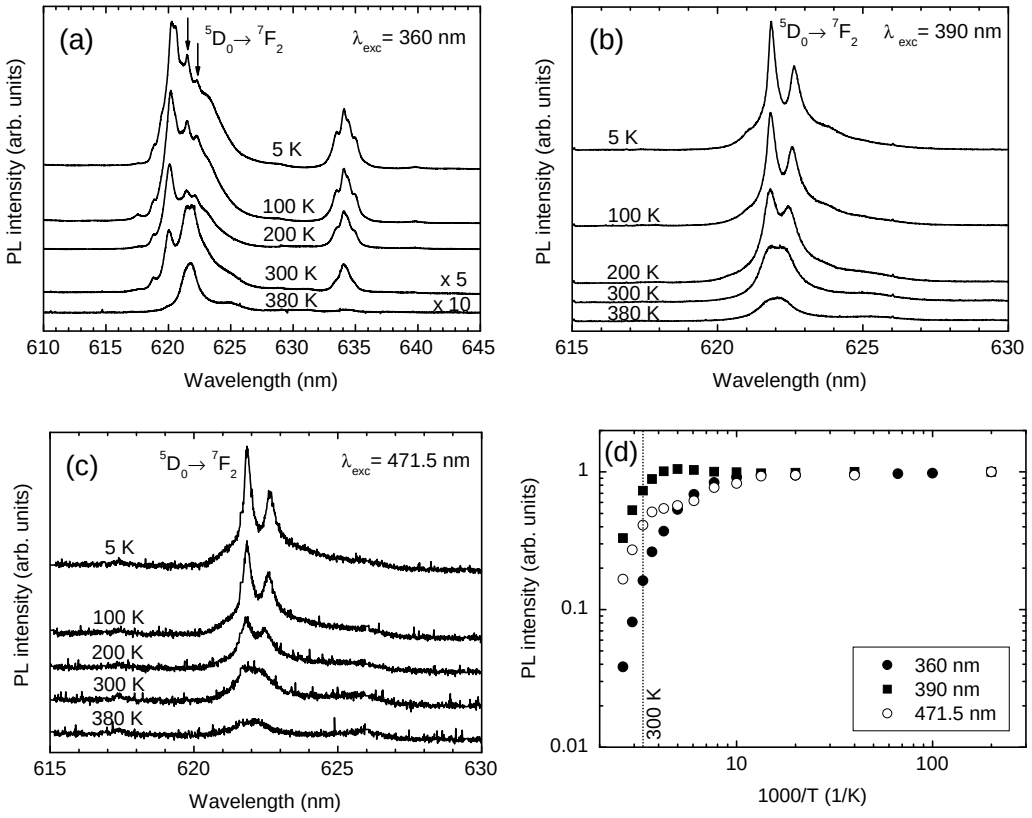

Figure 6.5: *PL spectra of InGaN:Eu QDs measured for temperatures between 5 K and 380 K using a excitation wavelengths of* **(a)** *360 nm* **(b)** *390 nm and* **(c)** *471.5 nm. The spectra are normalized by the excitation power density and the integration time for detection. The arrows in indicate the 622 nm lines assigned to Eu ions inside InGaN QDs. The spectra are measured with another gating than those shown in Fig. 3, so that the spectral position and the line width can be slightly different. In* **(d)** *the integrated intensity of InGaN:Eu QDs for emissions at 622 nm between 5 K to 380 K is shown in double logarithmic scale. The excitation wavelength was 360 nm (filled circle), 390 (filled square) and 471.5 (unfilled square) corresponding to results shown in* **(a-c)***. The vertical line marks 300 K for clarity.*

6.2 Temperature dependence of the Eu^{3+} PL of InGaN:Eu QDs

We now discuss the different characteristics of the thermal quenching originating from different Eu^{3+} ion locations. The thermal behavior of PL has been measured using excitation wavelength of 360 nm, 390 nm and 471.5 nm, and thus well above the band-gap of the spacing layer (360 nm), only by exciting the InGaN QDs (390 nm) and by directly exciting the Eu atoms (471.5 nm). Figure 6.5 shows the results with interesting features.

In agreement with our assumption, it is found that the 620 nm and 633.5 nm emission lines from above band-gap excitation of the GaN spacing layer are similarly

quenched whereas the 622 nm line remains more stable which is visible in Figure 6.5a[3]. At 380 K only the 622 nm line remains in the InGaN:Eu PL spectrum, which confirms the different origin of the line.

By exciting only the InGaN QDs (390 nm, Figure 6.5b), two sharp emission lines on a bump can be found and the PL is almost stable up to room-temperature. A detailed look shows that the sharp emission at lower energy position is shifting with temperature to the one at higher energy position. This thermal blue shift can be found for all emissions under various excitation wavelengths, but less pronounced than in this case. Its different amplitude might be a sign of different locations of Eu^{3+} ions in InGaN QDs itself.

Under direct RE excitation (471.5 nm, Figure 6.5c), emission spectra look similar to those measured by exciting only InGaN QDs (390 nm, Figure 6.5b), which is in agreement with the above discussed PLE study. Here emission intensity has been found about 100 times lower, which shows the efficiency of the band-gap related energy transfer.

Figure 6.5d shows the integrated emission intensity for emission assigned to Eu^{3+} ions inside InGaN QDs for the three discussed excitation wavelengths (360 nm, 390 nm and 471.5 nm) between 5 K and 380 K. The highest thermal quenching can be found by exciting the sample with shorter wavelength, namely 360 nm, which can be explained by the assumption that here Eu^{3+} atoms from InGaN QDs as well as from the GaN spacing layer are excited as discussed above.

A reduced thermal quenching can be found for excitation below the band gap of the GaN spacing layer. This is due to the fact that electron and hole pairs are directly injected and confined in QDs, that should significantly reduce their capture by non-radiative recombination centers at elevated temperatures (Compare to the argumentation for GaN QDs/AlN in section 5.2). Furthermore, the weak thermal quenching suggests that the carrier-mediated energy transfer to RE^{3+} ions in QDs should be faster than non-radiative recombination channels experienced by carriers in QDs, which are found to be on a time scale of 1 ns for carriers in GaN/AlN QDs as reported by Simon et al. [Sim03].

[3] Compare the thermal quenching of GaN:Eu, where emission at 622 nm (assigned to bulk material) has been found also more stable than emission at 620 nm and 633.5 nm (assigned to Eu^{3+} ions near the surface). However the thermal stability of the PL is about a factor 5 higher in case of InGaN QDs, when measuring the Eu emission intensity between 5 K and 380 K.

Using direct Eu^{3+} excitation, results are similar to those obtained for exciting below the band-gap of the GaN spacing layer, which is in agreement with the above discussed PLE study. One specific difference is a slight decrease of emission intensity at about 140 K, which suggests the existence of a second activation energy, whereas its origin is yet unclear. This effect could be explained by the fact that also Eu atoms from the spacing layer are directly excited, as the thermal decrease from 5 K to 140 K is similar to the one using the 360 nm excitation line. However, for understanding this effect further investigation is required. One main difficulty was that the used PLE setup did not allow us to excite Eu atoms from the GaN:Eu reference sample directly.

6.3 Applicability of InGaN:RE QDs for full color devices

We have given arguments to support the fact that InGaN QDs are most probably doped with Eu. The observed red Eu emission only exhibits a low thermal quenching from liquid helium to 380 K. This makes the InGaN:Eu QDs interesting for red devices operating at room temperature.

However, doping of InGaN QDs with other REs, especially for the blue emission, will be rather hard. The energy transfer would be hindered by too low band-gap energy from InGaN QDs host which is even lower than that of GaN layers. Furthermore in chaper 7 we will see that blue Tm emission from GaN layers, is very weak, assigned to a low band-gap energy of the host.

In order to overcome these problems and to achieve white light emission from RE atoms inside InGaN QDs one could imagine to use undoped InGaN QDs for blue emission and to realize the red and green colors by RE doping, for example Eu for red and Tb, Er or Ho for green.

References

[Don04] K. P. Donnell, I. Fernandez-Torrente, P. R. Edwards, and R. W. Martin, J. of Cryst. Growth, *The composition dependence of the $In_xGa_{1-x}N$ bandgap*, **269** 100 (2004).

[Hor04] Y. Hori, X. Biquard, E. Monroy, F. Enjalbert, Le Si Dang, M. Tanaka, O. Oda and B. Daudin, *GaN quantum dots doped with Eu*, Appl. Phys. Lett. **84**, 206 (2004).

[Hei97] R. Heitz, M. Veit, N. N. Ledentsov, A. Hoffmann, D. Bimberg, V. M. Ustinov, P. S. Kop'ev, and Zh. I. Alferov, *Energy relaxation by multiphonon processes in InAs/GaAs quantum dots*, Phys. Rev. B **56**, 10435 (1997).

[Nye03] Ei Ei Nyein, U. Hömmerich, J. Heikenfeld, D. S. Lee, A. J. Steckl and J. M. Zavada, *Spectral and time-resolved photoluminescence studies of Eu-doped GaN*, Appl. Phys. Lett. **82**, 1655 (2003).

[Sim03] J. Simon, N. T. Pelekanos, C. Adelmann, E. Martinez-Guerrero, R. André, B. Daudin, and Le Si Dang and H. Mariette, *Direct comparison of recombination dynamics in cubic and hexagonal GaN/AlN quantum dots*, Phys. Rev. B **68**, 035312 (2003).

[Ste96] M. Steer, D. J. Mowbray, W. R. Tribe, M. S. Skolnick, M. D. Sturge, M. Hopkinson, A. G. Cullis, C. R. Whitehouse and R. Murray, *Electronic energy levels and energy relaxation mechanisms in self-organized InAs/GaAs quantum dots*, Phys. Rev. B **54**, 17738 (1996).

[Vis98] A. K. Viswanath, J. I. Lee, S. Yu, D. Kim, Y, Choi, C. Hong, *Photoluminescence studies of excitonic transitions in GaN epitaxial layers*, J. of Appl. Phys. **84**, 3848 (1998).

7. Optical properties of GaN:Tm QDs

In this chapter we will discuss optical properties of GaN:Tm QDs grown on AlN which are interesting for blue light emission. In Section 3.4.4 we have seen, in a combined EXAFS and RBS study, that most Tm atoms are located inside AlN in the GaN QDs/AlN structure, in particular at the interface. We want to show in this chapter that QDs are also doped with Tm. For this we have performed optical studies using selective excitation, to excite only the GaN QDs in PL and the whole heterostructure in CL. We will also compare the optical properties of AlN:Tm, GaN:Tm, and GaN:Tm QD samples in order to get more insight into the location of Tm^{3+} ions in doped QDs, and to estimate their radiative quantum efficiency with respect to doped thick layers. This will help to discuss the capability of this system for device applications.

Next we want to study in more details the optical properties of Tm doped GaN QDs. Decay time measurement and PLE studies are shown to study the energy transfer mechanism from the GaN QDs energy levels to the QDs excited states.

In the end of this chapter comparative data on AlGaN:Tm will be discussed.

7.1 Tm^{3+} location within the GaN:Tm QDs/AlN structure

The here studied sample is containing 50 stacks of Tm doped QDs with a concentration of about 3% as measured by RBS (The same sample is studied in section 3.4.4). A 60 nm thick AlN:Tm sample layer and a 200 nm thick GaN:Tm layer were grown on an AlN and GaN buffer respectively to be used as reference samples.

In PL, only energy levels below 4.6 eV can be excited by the fourth harmonic of the Nd:YAG laser (266 nm). This limiting value corresponds to about the energy of the wetting layer of GaN/AlN QD samples, but is smaller than the band gap of AlN [Ade03]. Thus PL spectra would mainly display optical transitions from GaN QDs. By contrast, in CL, the generation volume of electrons and holes deeply extends in the sample, typically 500 nm (1 µm) deep in a GaN (AlN) layer for a 10 kV electron beam. As a result, radiative recombinations from both GaN QDs and AlN barriers can be observed which could provide complementary information about the location of Tm^{3+} ions. As shown in Figure 7.1a, the PL spectrum at 5 K of a GaN:Tm thick layer

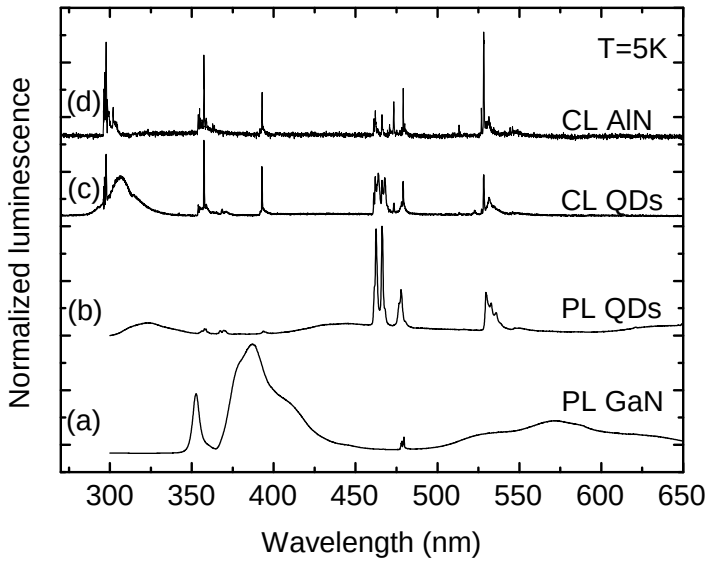

Figure 7.1: a) *PL of a GaN:Tm layer, b) PL of GaN:Tm QDs,* **c)** *CL of GaN:Tm QDs and d) CL of AlN:Tm at 5 K. In case of the PL spectra, a long-pass filter at 300 nm was used to protect the monochromator from direct laser exposure.*

with 2% Tm is dominated by a near band edge emission at 355 nm, a strong broad band at 390 nm, and the yellow band at 575 nm. The 390 nm band, not observed in undoped samples, could be related either to some defects induced by Tm doping or to Tm^{2+} ions since divalent rare earth ions are known to be more sensitive to local crystal field effects than trivalent rare earth ions. Additional sharp lines at 480 nm and 805 nm are also observed with considerably weaker intensity (see also Figure 7.1b and Figure 7.1d. Using the energy diagram proposed in Ref. [Höm03a], they have been identified as originating from to the $^1G_4$ and $^3H_4$ level of Tm^{3+} (see Figure 7.2). In this diagram it can be seen that the $^1D_2$ level is nearly resonant to the band gap of GaN. However, no transitions related to this level are observed, in agreement with published literature [Höm03a, Höm03b, Lee03, Loz99]. We will come back to the identification of Tm transition lines at the end of this section.

For Tm-doped QD samples, the situation is markedly different. The 5 K PL spectrum of a GaN QD sample doped with 3% Tm is displayed in Figure 7.2b. First, the spectrum extends further into the UV, well above the band gap of bulk GaN. Indeed, such a blue shift could be predicted since AFM data in Figure 3.10 show that Tm-doped QDs are small, with typical heights less than 1 nm for 3% Tm doping. As a result, in spite of the huge internal electric field in the order of 7 MV/cm in GaN/AlN

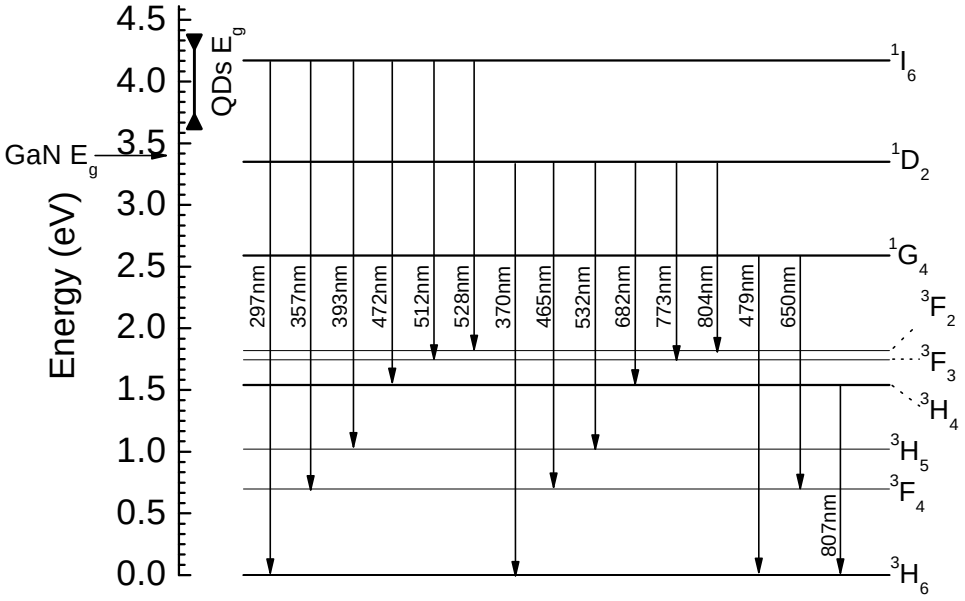

Figure 7.2: *Energy diagram of Tm^{3+} ions and observed transitions in AlN host. The energetic position of intra QD transitions is marked with the arrow at the energy scale. The band gap of GaN at 3.4 eV is also indicated in the figure. Note that the energy scale can have an offset with respect to all excited and ground states.*

QDs [Sim03], carrier confinement effects should be dominant over the quantum confined Stark effect. Therefore we assign the band at 320 nm in Figure 7.1b to the radiative recombination of electron-hole pairs in QDs. Actually this band peaks at shorter wavelength (i.e. 310 nm), as shown in the CL spectrum in Figure 7.2c, due to the fact that the UV region of the PL spectrum is severely distorted by the use of a low band pass filter at 300 nm to protect the detection system from direct laser exposure. Another striking feature in the PL spectrum is the presence of intense sharp lines related to the $^1I_6$, $^1D_2$, and $^1G_4$ levels in the blue-green region (450-550 nm). These lines, which are not observed for the Tm-doped GaN thick layer (see Figure 7.1a), are a clear evidence of Tm ions in QDs. In fact previous studies of Tm doping in AlGaN alloys have shown that these transition lines can only be detected when the Al concentration is larger than 30%, that is when the material band gap becomes larger than 4 eV [Lee03]. Indeed this is the case of GaN QDs (310 nm=4 eV) doped with Tm^{3+} ions, which suggests that band gap engineering in semiconductor nanostructures can be used to tune the optical properties of rare earth ions.

So far we have shown that Tm^{3+} ions are located in doped QDs. However, the carrier-mediated energy transfer to Tm^{3+} ions is not as complete as for Eu-doped QDs, since band to band recombination is clearly observed in QDs with 3% Tm

(Figure 7.1b) whereas it is not detectable in QDs with 1.5% Eu [Hor04] (See also chapter 5). The incomplete energy transfer in Tm-doped QDs cannot be due to a slow energy transfer process, since intense PL of Tm^{3+} is observed at room temperature (see below). This suggests that the Tm concentration in QDs is actually much lower than 3%, implying that most doped Tm^{3+} ions are not in the QDs but in the AlN barrier spacer, which is in agreement with the combined EXAFS and RBS study in the sections 3.3.3 and 3.4.4.

More information about Tm^{3+} location is provided by CL measurements, which probe both GaN and AlN parts of the sample. With respect to the PL spectrum in Figure 7.1b, the CL spectrum in Figure 7.1c of the same doped QD sample indeed exhibits additional lines, next to those of the PL spectrum, but extremely sharp (see details in Figure 7.3. These lines are found to coincide with those of the CL spectrum of AlN:Tm (see Fig. Figure 7.1d) which clearly demonstrates that, in doped QDs, Tm^{3+} ions are also present in the AlN barrier layer.

In Figure 7.1 and Figure 7.3, it can be seen that Tm^{3+} lines in QDs are spectrally broader and redshifted by about 2-3 nm in the blue-green region when compared to AlN:Tm samples. The minimum FWHM is about 1.2 nm and 0.3 nm in GaN:Tm QDs and AlN:Tm, respectively. This is not so surprising considering the fact that Tm^{3+} in QDs should experience not only strain as large as 1% but also a huge internal electric field of the order of 7 MV/cm. These fields are not uniformly distributed in QDs, which should induce a spectral broadening of Tm^{3+} transition lines. Our FWHM values for AlN:Tm are clearly in the lower limit when compared to results in literature for nitrides doped with rare earth ions [Gru04].

Concerning the spectral shift, it is interesting to note that a Stark shift of about 200 KHz/(V/cm) has been reported for the $^4I_{15/2} \rightarrow {}^4F_{9/2}$ line of Er^{3+} in $YAlO_3$ by application of an external electric field of 200 V/cm [Wan92]. Assuming a similar Stark effect, a shift of the order of 0.1 nm would be expected for transition lines in the blue in GaN QDs. Although this rough estimate is smaller by one order of magnitude than measured data, one should keep in mind that electric fields in QDs are on the

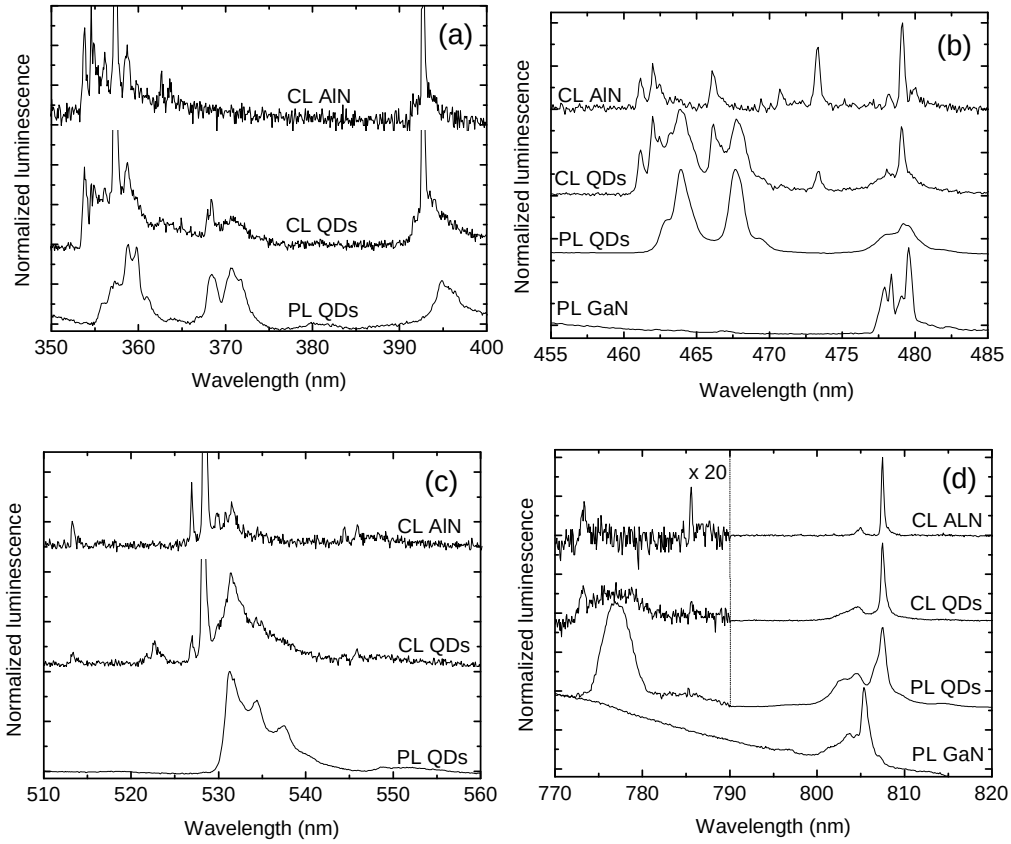

Figure 7.3: *High resolution CL and PL spectra of GaN:Tm, GaN:Tm QDs and AlN:Tm in expended scales* **a)** *from 350 nm to 400 nm,* **b)** *from 455 nm to 485 nm,* **c)** *from 510 nm to 560 nm and* **d)** *from 770 nm to 820 nm. The measurements were performed at 5 K.*

MV/cm scale, which is four orders of magnitude larger than the external applied field. In such a case, non-linear Stark effects should take place and induce a larger spectral shift.

7.2 Temperature dependent PL of GaN:Tm QDs

The key issue of radiative quantum efficiency of doped QDs has been investigated by measuring the temperature dependence of Tm^{3+} PL lines, and results are reported in Figure 7.4 and Figure 7.5. Figure 7.4a and Figure 7.4b show the spectra at 10 K and 300 K, where some transition lines become weaker and some others are completely quenched. As displayed in Figure 7.4c, transitions related to the $^1D_2$ level are remarkably stable with respect to the temperature whereas those

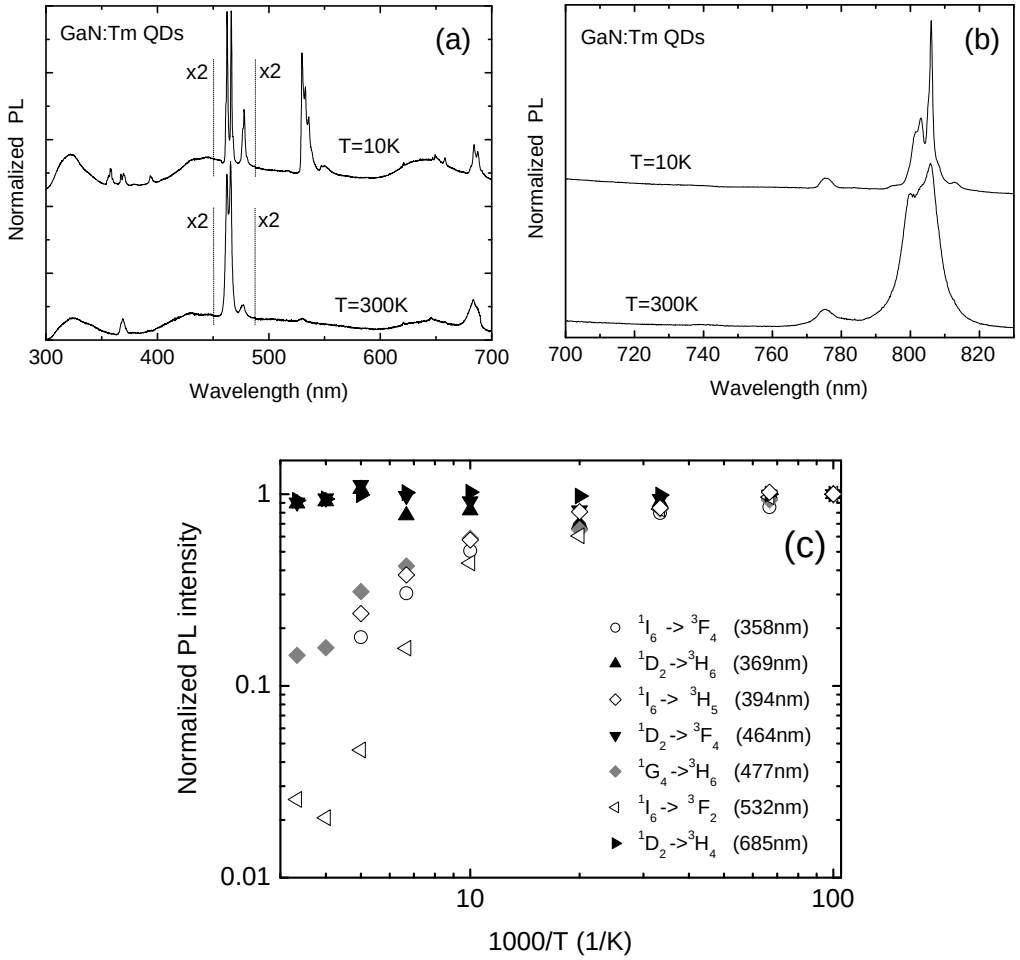

Figure 7.4 a) *PL of GaN:Tm QDs measured at 10 K and 300 K. The second order of QD signal is observed at around 650 nm.* **b)** *PL spectrum in the infrared region at 10 K and 300 K. Excitation source: 305 nm line of an Ar^+ laser* **c)** *Temperature dependence of the PL intensity for GaN:Tm QDs. The integrated intensity was measured corresponding to each transition. For temperatures higher than 200K the emission from the $^1I_6 \rightarrow ^3H_5$ and $^1I_6 \rightarrow ^3F_4$ transitions was under the detection limit. Excitation source: 266 nm from a Nd:YAG laser.*

related to the $^1I_6$ level are thermally unstable, and those related to the $^3H_4$ and $^1G_4$ levels exhibit an intermediate behavior. It should be noted that, even though the $^3H_4$ and $^1G_4$ levels are deeper in the band gap than the $^1D_2$ level, the carrier-mediated energy transfer is much more efficient to the $^1D_2$ level.

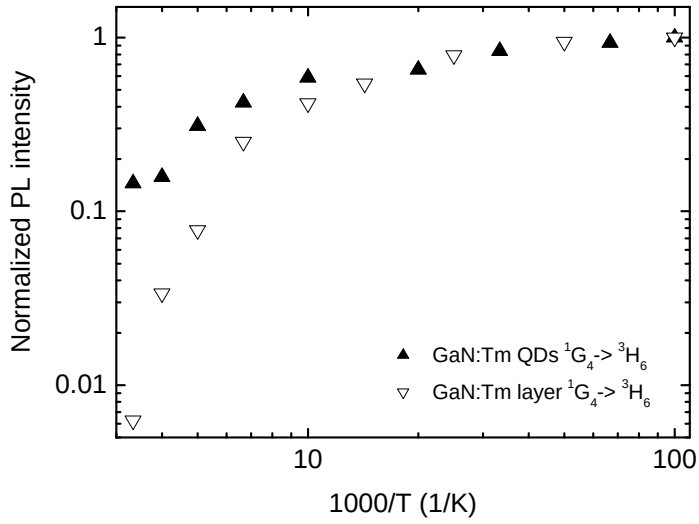

Figure 7.5: *Temperature dependence of the PL for the $^1G_4 \rightarrow {}^3H_6$ transition in a GaN:Tm layer and in GaN:Tm QDs.*

In Figure 7.5, we compare the temperature dependence of the $^1G_4 \rightarrow {}^3H_6$ Tm^{3+} transition at 480 nm in a GaN layer and in GaN QDs. The superior radiative quantum efficiency of doped QDs is again demonstrated. As discussed for Eu doped GaN QDs, it can be explained by the high carrier capture cross section of QDs which should enhance any carrier-mediated energy transfer to rare earth ions. Thus doped QDs appear to be a particularly attractive design structure for light emitters.

All transitions identified in this work are summarized in the energy diagram of Figure 7.2. The transition wavelengths are those measured in AlN:Tm. Intra Tm^{3+} transitions in nitrides are assigned to four excited states, namely the $^1I_6$, $^1D_2$, $^1G_4$ and the $^3H_4$ states. However a final identification of the transitions requires further investigation. This is particularly the case for transitions starting from the $^1I_6$ and $^3P_0$ level [Loz99 Hom03a, Sel93].

As mentioned above, the temperature dependence of transition lines is a good indication of their origins. For example in doped QDs, transitions related to the $^1D_2$ level are remarkably stable with respect to the temperature, whereas those related to the $^1I_6$ level are strongly quenched at room temperature (see Figure 7.4a). On the other hand at low temperature, the $^1I_6$ transitions are dominant in the CL spectra of AlN:Tm and doped QDs, but much weaker in the PL spectrum of doped QDs. This illustrates the complexity of the carrier-mediated energy transfer.

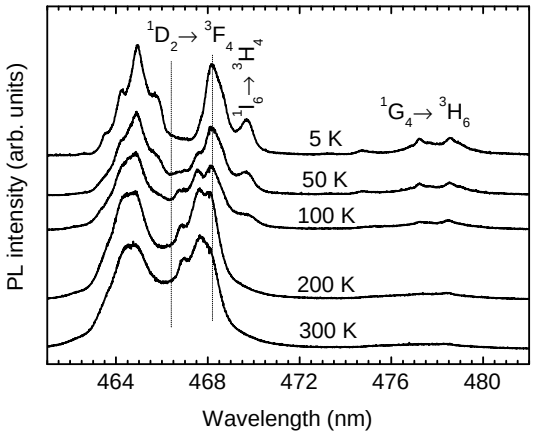

Figure 7.6: *High resolution PL spectra at various temperatures of Tm doped GaN QDs for the blue spectral range. The spectra are normalised to the accumulation time. Excitation: 250 nm from the Xe-lamp. Assigned transitions are indicated in the figure. The vertical dotted lines are shown as a guide for the eyes.*

In CL experiments, carriers can be excited in AlN, which could favor their capture into a Tm-related trap for energy-transfer to the $^1I_6$ level of Tm ions in AlN. In PL experiments, carriers are only excited in QDs and our results suggest that the energy transfer takes place via the $^1D_2$ level rather than the $^1I_6$ level of Tm in QDs.

As a whole, from the comparison of optical data obtained by the two experimental methods, namely PL and CL, we can conclude that Tm is incorporated inside the GaN QDs and also in the AlN spacer. Specific QD-related intra Tm transitions also exist, which was demonstrated by the comparison of the AlN:Tm layer and the GaN:Tm QDs in CL. This was confirmed by PL, which revealed that Tm transitions related to QDs show constant PL as a function of temperature.

7.3 Excitation mechanism in Tm doped GaN QDs

In this section we want to go further into discussion of the excitation mechanism of Tm doped GaN QDs. We found in section 7.2 that intra 4f Tm transitions from $^1I_6$, $^1D_2$, $^1G_4$ and $^3H_4$ excited states have different thermal quenching behavior depending on its relative energetic position. In more detail: PL from the $^1I_6$ level is fast quenched and hardly observed at temperatures higher than 100 K, whereas those starting from the $^1D_2$ are stable between liquid helium and room temperature. An intermediate quenching is observed for the blue $^1G_4 \rightarrow {}^3H_6$ and infrared $^3H_4 \rightarrow {}^3H_6$ transitions. Detailed thermal behavior for the blue spectral range is displayed in the high resolution PL spectra in Figure 7.2. This spectral range is of particular interest as it

involves transitions stemming from $^1D_2$ and from $^1I_6$, and $^1G_4$ mostly responsible for the blue light emission.

Emissions in the spectral range of 463 nm to 471 nm where both the $^1D_2 \rightarrow {}^3F_4$ and $^1I_6 \rightarrow {}^3H_4$ transitions can exist and give strong luminescence will be analyzed in more detail. It is clearly seen in Figure 7.6 that most of the emission lines in the mentioned range are stable with temperature because the $^1D_2$ level is located at much lower energy than $^1I_6$, in agreement with published data [Gru04]. We assigned it to $^1D_2 \rightarrow {}^3F_4$ transition. By contrast the line at the longer wavelength side (469.5 nm) is fast quenched and hardly observed at temperatures higher than 100 K. Thus, this emission line is assigned as stemming from the higher-lying $^1I_6$ state. The fast thermal quenching of PL originating from $^1I_6$ may result from various processes: (i) From phonon emission to relax down to lower-lying states of Tm^{3+} ion. This process is unlikely as many phonons are needed to fill the energy gap between the starting and final discrete levels. (ii) by phonon-assisted de-excitation to the host material. This is a most reasonable process because transitions from high-lying $^1I_6$ state can release an energy comparable to the energy range of the fundamental energy of GaN QDs. Though it is not possible to determine the exact levels of the RE^{3+} ion corresponding to the fundamental edge of the semiconductor host, the near resonance energy of the $^1I_6 \rightarrow {}^3H_6$ transition and fundamental gap of the host GaN QD at least makes more likely Auger transfer with phonon assistance. Population of LO-phonons follows Bose-Einstein distribution, increasing fast at temperatures higher than 100 K hence being responsible for thermal quenching of this emission. Similar result has been reported for InP:Yb [Loz94, Tag92, Tag96, Kli02] in which the temperature activated the energy back-transfer from the guest RE ions to the host semiconductor. Some other processes like cross-relaxation between adjacent Tm atoms for resonant $^1I_6 \rightarrow {}^3H_4$ and $^3H_6 \rightarrow {}^1G_4$ (this process takes place with increasing Tm concentration) or emitting spontaneous IR to lower levels could be also responsible for the observed quenching [Dej95].

Note that the phonon-assisted de-excitation from the $^1D_2$ level to the GaN QDs host is much less effective because any transition from the $^1D_2$ to lower levels corresponds to an energy, which is small, compared to the fundamental energy of the host. On the other hand, the $^1D_2$ excited state at lower energy can benefit from re-population from other higher-lying levels during their quenching with temperature.

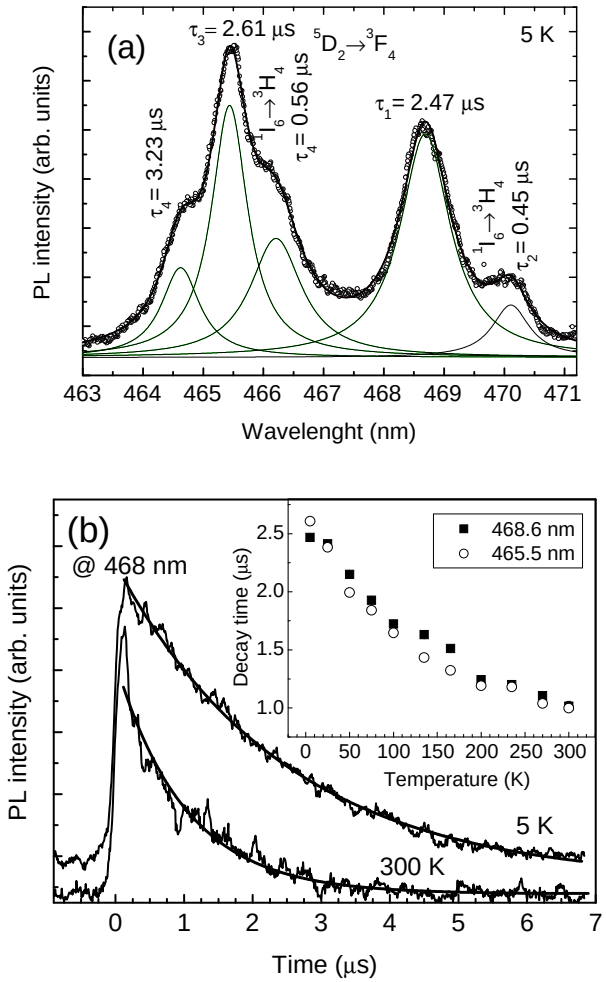

Figure 7.7 *a) The open circles correspond to the PL from GaN:Tm QDs measured at 5 K with the time resolved setup (see experimental part). The spectrum has been fitted with a multiple Lorentzian containing 5 peaks. Measured decay times and assigned transitions are also indicated in the figure. b) Time resolved PL signal of the $^1D_2$-$^3F_4$ transition measured at 468 nm at 5 K (upper curve) and 300 K (lower curve). Fitting of the measurements with mono exponential decay are plotted bold. The inset shows decay times for the $^1D_2$-$^3F_4$ transition at 468 nm and 465 nm as a function of temperatures.*

The above mentioned facts are possible reasons for the temperature stability of emission lines from the $^1D_2$ excited state. In Figure 7.6 also several emission lines between 465 nm and 468 nm are see, whose intensity increase with temperature. These are believed to be Stark-split levels which are PL-observable depending on the temperature-dependent population factor. The temperature dependent population of energetic levels has been also experimentally observed for AlN:Tm in reference [Gru04].

The intermediate thermal quenching was observed for the blue $^1G_4 \rightarrow {}^3H_6$ transition and for the infrared $^3H_4 \rightarrow {}^3H_6$ transition. This can be explained assuming that transitions from $^1G_4$ or $^3H_4$ are not in resonance for de-excitation processes and

are not likely to benefit from re-population with temperature so that the excitation mechanism is temperature independent. In this case, the thermal quenching is likely due to thermally activated non-radiative de-excitation only.

Further information can be gained about the excitation and de-excitation of Tm^{3+} ion in GaN QD host based on time-resolved PL measurements. As the blue and green spectral regions are concerned, two sets of transitions result in emission lines at very similar energies in steady-state PL spectra, but exhibit distinct decay times, namely ~0.5 μs for the emissions at 466.3 nm, 469.7 nm, 534.5 nm, 537.5 nm (Figure 7.7 and Figure 7.9b) and ~1.2 μs for the emission at 532 nm (Figure 7.9b). The former emission group has been identified as resulting from the $^1I_6$ level ($^1I_6 \rightarrow {}^3H_4$ for the 466.3 nm and 469.7 nm lines, and $^1I_6 \rightarrow {}^3F_3$ for the 531 nm, 534.5 nm and 537.5 nm lines in agreement with the different thermal quenching of the PL. As the emission lines in the 463-471 nm range are overlapped, before analyzing the decay times the spectra have been de-convoluted with a multiple Lorentzian curve fit (Figure 7.7). For the two strongest isolated lines (at 465.5 nm and 468.6 nm), the PL decays could be well fitted with a monoexponential function. Fig. 4b presents the measured and fitted curves for the PL decays of the 468.6 nm emission line at 5 K and 300 K using the typical equation: $y = Ae^{-t/t}$, where t is the decay time, t the elapsed time after the laser pulse and A a fitting parameter. For lines that include a contribution from nearby stronger lines (for which a monoexponential decay fit could be done) the PL decay was fitted as the sum of a known exponential decay (stemming from the overlapping stronger line) and another exponential (that gives the decay time of the line of interest). For the two main blue emission lines at 468.6 nm and 465.5 nm and the one at the higher energy side (464.5 nm) the decay times obtained at 5 K are similar, i.e. respectively 3.2 μs, 2.6 μs and 2.5 μs. This is to be expected since the three mentioned lines are just originating from the Stark-splitting in C_{3v} symmetry of the $^1D_2 \rightarrow {}^3F_4$ transition. However, it is worth noticing that even if the three mentioned lines originate from the same $^1D_2 \rightarrow {}^3F_4$ transition, there is a trend to observe longer decay time for the higher-energy Stark component. This feature has been also observed for the Stark-splitting components of the $^1I_6 \rightarrow {}^3H_4$ transition that result in the 466.2 nm (0.56 μs) and 470 nm (0.45 μs) lines; and the $^1I_6 \rightarrow {}^3F_3$ transition that result in the 531.6 nm (1.2 μs), 534.5 nm (0.6 μs) and 537.5 nm (0.5 μs) lines. No explanation of this result can be given at the moment. However the decay time of the $^1D_2 \rightarrow {}^3F_4$ transition at 5 K has been found to be ~2.6 μs which is

longer than those for the $^1I_6 \rightarrow {}^3F_3$ (1.2 μs). This is likely due to the fact that the $^1D_2 \rightarrow {}^3F_4$ transition is spin-forbidden as in the case of the $^1I_6 \rightarrow {}^3F_3$ transition; in addition the $^1D_2$ state is located much below the $^1I_6$ so that energy released from the $^1D_2$ transitions to any manifolds is far from resonances with fundamental energy of the host material or near-fundamental-edge traps to favor the back-energy transfer which generally contributes to the reduction of the measured decay time. Note that a similar trend, i.e a longer decay time for the $^1D_2$ excited state compared to $^1I_6$ was observed in Tm-doped AlGaN [Höm03a]. Although the longest decay time has been found for emissions resulting from the $^1D_2 \rightarrow {}^3F_4$ transition, as a result of the reduced energy back-transfer to the host material, a reduction of the decay time has been found when increasing temperature, from ~2.6 μs at 5 K to ~1 μs at 300 K. This reduction in decay time can be attributed to an increase in non-radiative recombination with increasing temperature due to an increased back-transfer to the host [Loz94]. This increase in the non-radiative recombination rate is however not correlated with a corresponding decrease in luminescence intensity. Indeed, from 4 K to 300 K, the luminescence intensity for the $^1D_2 \rightarrow {}^3F_4$ transition is constant within ± 20%. As we are in the low excitation regime (well below saturation of the transitions), this suggests that the excitation efficiency of the $^1D_2$ level increases with increasing temperature and that this effect compensates for the non-radiative losses. In particular, $^1D_2$ could benefit from depopulation of $^1I_6$ with temperature, as already discussed above. The excitation scheme proposed for the 468 nm emission is as follows: (i) photo-excited/generated carriers (in host GaN QDs) → (ii) traps (isoelectronic Tm^{3+} ions) → (iii) 4f-electrons of Tm^{3+} ions (by near resonant energy transfer to high-lying states like $^1I_6$ and $^3P_1$ and/or non-resonant process to $^1D_2$) → (iv) transitions (e.g $^1D_2 \rightarrow {}^3F_2$) to emit light. One can expect that processes (i) – (iii) occur in nanosecond range and they all contribute to the rise-time in the time-resolved PL measurement. From the time-resolved spectra taken at 5 K and 300 K (Figure 7.7b), it appears that the rise-time is shorter than 50 ns. This value can be accounted for by the energy transfer rate from GaN QDs to the 4f-electrons of Tm^{3+} ions. As the energy transfer processes from the QDs to the RE^{3+} ions take place faster than other non-radiative processes, one can practically expect high efficiency luminescence from the RE-doped GaN QDs. This is also consistent with the fact that we did not observe the fundamental level emission for GaN QDs doped with Tm

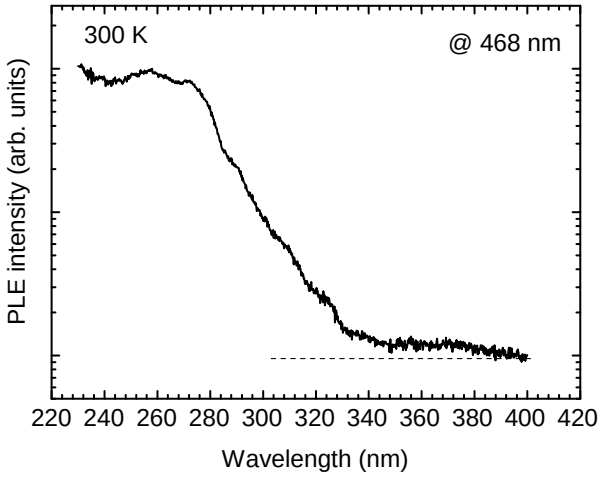

Figure 7.8: *PLE spectrum at 300 K for the 468 nm emission line of Tm^{3+} ion in GaN QDs. The spectra has been normalized to the excitation intensity and presented in logarithmic scale. The horizontally dotted line is a guide to the eye. Note absorption between 260 nm and 330 nm can be associated with GaN QDs.*

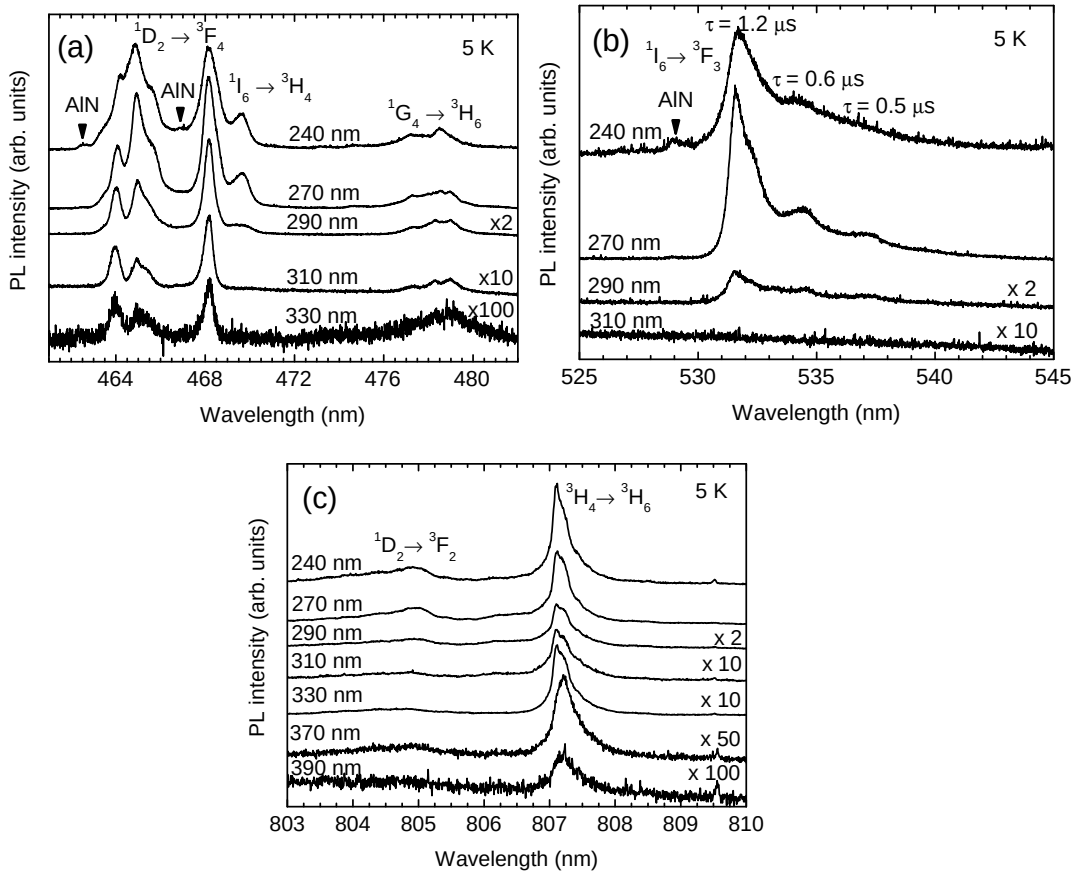

Figure 7.9: *PL spectra at 5 K for GaN:Tm QDs measured with different excitation wavelengths (indicated at the curves) in the a) blue, b) green and c) infrared spectral region. The spectra are normalized by the excitation power density and the integration time for detection. Spectra with low emission intensity are multiplied by a factor for clarity. The arrows indicate Tm^{3+} emission from the AlN spacing layer (see text). Assigned transitions are shown in the figure. The decay times for the green spectral region are also indicated in Fig. b) with respect to its measured wavelength position.*

because energy transfer processes to Tm^{3+} ions are much faster than other possible processes in QDs.

As already observed for GaN QDs doped with Eu (Section 5), the photoluminescence excitation spectra for Tm doped GaN QDs at 300 K display a gradual absorption edge related to the QD absorption, which can be seen in Figure 7.8 . This confirms that the transfer to the Tm states is indeed mediated by the QD states, and that in these samples the QDs have rather high energy levels (absorption below 330 nm).

To gain more insight in the excitation mechanism, we checked how the different emissions behave in PL as a function of the excitation wavelength in a range extending from 230 nm to 330 nm to cover the whole band gap energy values corresponding to the QDs size distribution. The results are shown in Figure 7.9a-c for the most intense emissions. In the blue spectral range (Figure 7.9a) the emission lines at 464.5 nm, 465.5 nm and 468.6 nm have been assigned to the $^1D_2 \rightarrow {}^3F_4$ transition. Also in agreement with the above discussion of the thermal quenching (Figure 7.6) is the $^1I_6 \rightarrow {}^3H_4$ transition emitting around 466.2 nm and 470 nm, and the $^1G_4 \rightarrow {}^3H_6$ emission at 479 nm. Emissions from the higher excited states ($^1I_6$) tend to be weakened when using longer excitation wavelengths. As a consequence the corresponding emissions from the $^1I_6 \rightarrow {}^3H_4$ transition and the $^1I_6 \rightarrow {}^3F_3$ transition could not be detected by exciting the sample at 310 nm (see Figure 7.9a and Figure 7.9b). In agreement with this behavior transitions from the $^1D_2$ excited state show very weak intensity for excitation wavelengths longer than 310 nm, while the infrared $^3H_4 \rightarrow {}^3H_6$ transition could be well detected at an excitation wavelength of 380 nm. It is possible that the excitation wavelength-dependent effect be assigned to the GaN QDs size-distribution because the excitation energy transfer to the high-lying levels of Tm^{3+} ions needs a relatively high energy from GaN QDs, which corresponds to the smaller size dots. By exciting the sample with shorter wavelength (240 nm), Tm^{3+} ion luminescence from the AlN spacer is visible (Figure 7.9a and Figure 7.9b). In agreement with cathodoluminescence studies discussed in section 7.1 (Figure 7.3), the weak emissions at 462.5 nm and 467 nm are consistent with the presence of Tm^{3+} ions in the AlN spacing layer that contains some defect-related energy states

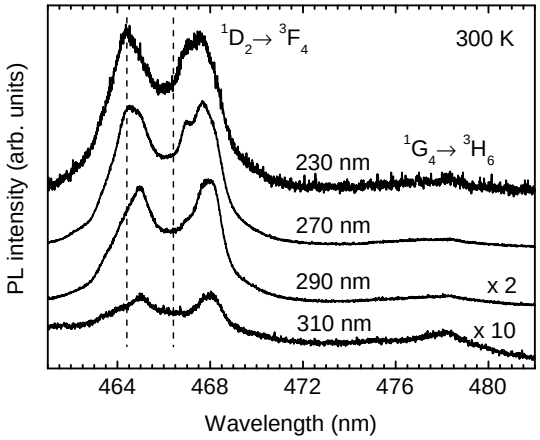

Figure 7.10: *High resolution PL spectra in blue spectral range for Tm doped GaN QDs measured at 300 K with various excitation wavelengths as indicated in the figure. The spectra are normalized to the power density and the accumulation time. The spectra under 290 nm and 310 nm excitation are multiplied with a factor 2 and 10 for clarity. Assigned transitions are also indicated in the figure.*

where carriers can be captured so that they can transfer their energy to Tm^{3+} ions. It has to be noticed that the exact wavelength position in Figure 7.9a and Figure 7.3 is slightly different due to the use of different light detection systems. One point we would like to mention regarding the temperature-activated emission lines (within 466.5 nm to 467.5 nm) is that they are observable only at short excitation wavelength (230 nm to 270 nm) and high temperatures (Figure 7.6 and Figure 7.10). At long excitation wavelengths these lines did not appear. This again supports the assumption that they come from the high-lying $^1I_6$ state that is not likely to be excited with long excitation wavelength.

It is interesting to note that emission from the $^1D_2$ excited state can be detected, using excitation energy (380 nm) even below its energetic position (370 nm). This could be explained by two photon processes, however further studies are required to confirm this hypothesis.

7.4 Optical properties of AlGaN doped with Tm

Now we want to compare the optical properties of GaN:Tm QDs with those of an AlGaN:Tm film. We have shown above that GaN host exhibits too low band gap energy to excite the $^1D_2$ and higher lying excited states. Thus for studying nitride layers doped with Tm, $Al_xGa_{x-1}N$ seems to be an interesting host material. Cf. also Ref. [Höm03a] and [Lee03]. We have chosen an Al and Ga content of about 50 %, to get a band gap energy close to the transition energy of our grown QDs. Also the Tm

flux was comparable to the one used during QDs growth. During growth of this reference sample the RHEED has shown typical bi-dimensional growth, whereas also a 2x4 reconstruction has been observed.

Figure 7.11a shows the low temperature PL of an AlGaN:Tm layer. Strong near band gap emission can be found at 264.5 nm with a FWHM of less than 7 nm indicating that AlGaN material is with 120 meV of good quality. Compare ref. [Mon03]. A broad signal can be found at 323 nm which we have also seen above in GaN:Tm layers and which has been tentatively assigned to defect levels or to Tm^{2+} ions since they exhibit typically broad emission as they are characterized by outer shell transitions, so that the influence of the host material is getting important. Another possibility could be that this emission is originating from defects induced during Tm doping. Next also Tm^{3+} transitions can be found originating from the $^1D_2$ and $^1I_6$ excited state, but intensity ratio shows that in this sample emission from the $^1I_6$ excited state is relatively lower.

For studying deeper the optical properties of AlGaN:Tm the decay times and relative PL intensity have been measured for the $^1D_2 \rightarrow {}^3F_4$ and are illustrated in Figure 7.11b for comparative study. First the decay time at 5 K is 1.3 µs which is a factor 2 lower than in the case of GaN:Tm QDs indicating that non radiative recombinations are less important in QDs, so that the radiative quantum efficiency is higher for Tm in QDs than for Tm in $Al_{0.5}Ga_{0.5}N$. With increasing temperature the decay time decreases down to 0.45 µs at 300 K. The results also show that a change of the decay time is correlated with the decrease of PL emission intensity. Thus the decrease of the PL can be explained by the activation of non-radiative channels with increasing temperature. If we assume that the excitation efficiency is not temperature dependent, then the decay time reduction should lead to a decrease by a factor of 2

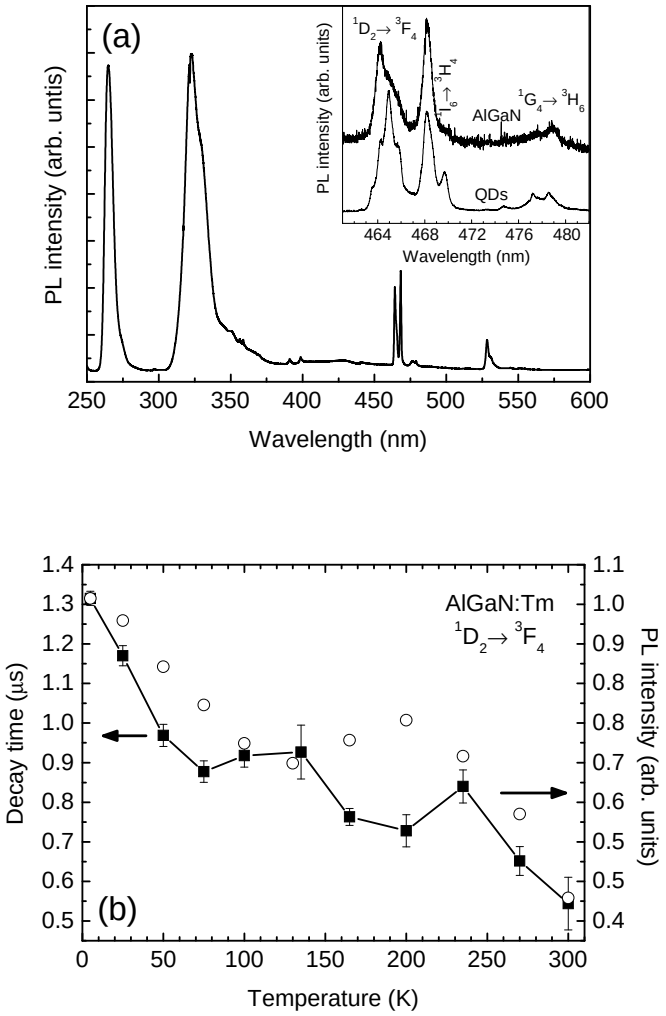

Figure 7.11: a)*PL of AlGaN:Tm measured at 5 K with the frequency doubled Ar^+ laser (244 nm) with an excitation power density of about 0.8 W/cm^2. The inset shows the blue spectral region for AlGaN:Tm and GaN:Tm QDs for comparison. b) PL as a function of temperature (right scale) and decay times (left scale) for the $^1D_2 \rightarrow {}^3F_4$ transition. The error bars are calculated from the R factors of fits.*

of the emitted PL. As a factor of 3 decrease is observed, we can assume that the excitation efficiency for this particular transition is also slightly reduced as temperature is increased.

The inset of Figure 7.11a shows for comparison the PL of blue spectral range of both GaN:Tm QDs and AlGaN:Tm and it can be found that same emission lines at similar positions are existing but with different intensity ratios. Note that AlN:Tm shows Tm^{3+} emission lines at different positions and with a different Stark splitting.

It might be possible that during growth of AlGaN material Tm doping induces GaN clustering so that the structure around the Tm atoms is getting QD like. For

confirming this possibility it is interesting to carry out EXAFS experiments to get an idea about the local environment of Tm^{3+} atoms. The explanation of the existence of a QD like structure around Tm atoms is also confirmed by the rather low thermal quenching, which has been found much more more pronounced in RE doped layers studied here and in literature [Nye03].

References

[Ade03] C. Adelmann, E. Sarigiannidou, D. Jalabert, Y. Hori, J. –L. Rouvière, B Daudin, S. Fanget, C. Bru-Chevallier, T. Shibata, and M. Tanaka, *Growth and optical properties of GaN/AlN quantum wells*, Appl. Phys. Lett. **82**, 4154 (2003).

[Dej95] M. Dejneka, E. Snitzer, and R. E. Riman, *Blue, green and red fluorescence and energy transfer of Eu^{3+} in fluoride glasses*, J. of Luminescence **65**, 227 (1995).

[Dej95] M. Dejneka, E. Snitzer, R. E. Riman, J. of Luminecence **65**, 227 (1995).

[Die68] G. H. Dieke, *Spectra and Energy levels of Rare Earth Ions in Crystals,* (Wiley, New York, 1968).

[Gru04] J. B. Gruber, U. Vetter, H. Hofsäss B. Zandi M. F. Reid, *Spectra and energy levels of $Tm^{3+}(^4f_{12})$ in AlN*, Phys. Rev. B **70**, 245108 (2004).

[Höm03a] U. Hömmerich, Ei Ei Nyein, D. S. Lee, A. J. Steckl, and J. M. Zavada, *Photoluminescence properties of in situ Tm-doped AlxGa1–xN*, Appl. Phys. Lett. **83**, 4556 (2003).

[Höm03b] U. Hömmerich, Ei Ei Nyein, D. S. Lee, J. Heikenfeld, A. J. Steckl, and J. M. Zavada, *Photoluminescence studies of rare earth (Er, Eu, Tm) in situ doped GaN*, Mater. Sci. Eng. B **105**, 91 (2003).

[Hor04] Y. Hori, X. Biquard, D. Jalabert, E. Monroy, F. Enjalbert, Le Si Dang, M. Tanaka, O. Oda, and B. Daudin, *GaN quantum dots doped with Eu*, Appl. Phys. Lett. **84**, 206 (2004).

[Kli02] M. A. J. Klik, T. Gregorkiewicz, I. V. Bradley, and J-P. R. Wells, *Optically Induced Deexcitation of Rare-Earth Ions in a Semiconductor Matrix*, Phys. Rev. Lett. **89**, 227401 (2002).

[Lee03] D. S. Lee and A. J. Steckl, *Enhanced blue emission from Tm-doped $Al_xGa_{1-x}N$ electroluminescent thin films*, Appl. Phys. Lett **83**, 2094 (2003).

[Loz94] H. J. Lozykowski, A. K. Alshawa, and I. Brown, *Kinetics and quenching mechanisms of photoluminescence in Yb-doped InP*, J. Appl. Phys. **76**, 4836 (1994).

[Loz99] H. J. Lozykowski, M. Jadwisienczak, and I. Brown, *Visible cathodoluminescence of GaN doped with Dy, Er, and Tm*, Appl. Phys. Lett. **74**, 1129 (1999).

[Mon03] E. Monroy, B. Daudin, E. Bellet-Amalric, N. Gogneau, D. Jalabert, F. Enjalbert, J. Brault, J. Barjon, and Le Si Dang, J. Appl. Phys. 93, 1550 (2003)

[Nye03] Ei Ei Nyein, U. Hömmerich, J. Heikenfeld, D. S. Lee, A. J. Steckl, and J. M. Zavada, *Spectral and time-resolved photoluminescence studies of Eu-doped GaN*, Appl. Phys. Lett. **82**, 1655 (2003).

[Sel93] M. D. Seltzer, J. B. Gruber, M. E. Hills, G. J. Quarles, and C. A. Morrison, *Multisite optical spectra and energy levels of trivalent thulium ions in yttrium scandium gallium garnet*, J. Appl. Phys. 74, 2821 (1993).

[Sim03] Simon, N. T. Pelekanos, C. Adelmann, E. Martinez-Guerrero, R. André, B. Daudin, and Le Si Dang, *Direct comparison of recombination dynamics in cubic and hexagonal GaN/AlN quantum dots*, Phys. Rev. B 68, 035312 (2003).

[Tag92] A. Taguchi, M. Taniguchi, and K. Takahei, *Direct verification of energy back transfer from Yb 4f-shell to InP host*, Appl. Phys. Lett. **60**, 965 (1992).

[Tag96] A. Taguchi and K. Takahei, *Band-edge-related luminescence due to the energy backtransfer in Yb-doped InP*, J. of Appl. Phys. **79**, 3261 (1996).

[Wan92] Y. P. Wang and R. S. Meltzer, *Modulation of photon-echo intensities by electric fields: Pseudo-Stark splittings in alexandrite and $YAlO_3:Er^{3+}$*, Phys. Rev. B **45**, 10119 (1992).

8. Optical properties of GaN QDs doped with Tb

We have demonstrated in the chapters 5 and 7 red and blue PL form GaN QDs grown on AlN. To fulfill the set of colors for white light emission, the green color is needed. Inner shell transitions in the green spectral range can be found from Er^{3+}, Ho^{3+} and Tb^{3+} ions, although in this work only weak luminescence has been found for Er and Ho doped GaN QDs. In contrast, Tb doped GaN QDs have shown intense green PL visible with bare eye.

In this chapter we will discuss first (8.1) the optical properties of GaN:Tb layers. It will be shown that this system is problematic for achieving high optical output. Then we will address the optical properties of GaN:Tb QDs, and give arguments in favor of successfully doping of the GaN QDs.

8.1 Optical properties of GaN:Tb layers

Before discussing optical properties of GaN:Tb QDs we want first illustrate that green light emission from Tb-doped MBE grown GaN films is difficult to extract. The PL spectrum of a 100 nm thin GaN:Tb layer measured at liquid helium temperature is shown in Figure 8.1. The spectrum is characterized by near band gap emission at about 360 nm. At lower energy, at about 390 nm, another broad signal can be found, although its origin remains unclear. Then the typical yellow band can be observed between 500 nm and 800 nm, superimposed to very weak sharp emission lines from RE atoms. Emission at about 620 nm originates from residual Eu contamination in the MBE system. Other emissions could originate from Tb^{3+} inner shell transitions. Is has to be remarked that the PL system has been well aligned and the accumulation time has been more than 10 min, which is very long compared to other spectra measured in this work (For the GaN:Eu layer studied in chapter 4 about 0.1 s).

In agreement with our results Bang et al. reported that their Tb-doped GaN thick layers presented very weak PL emission [Ban02]. The authors checked that Tb was well incorporated, and they characterized the sample quality by XRD which showed values compatible with high quality GaN. The authors explained this poor radiative quantum efficency by means of EXAFS measurement, which revealed that the Tb ion

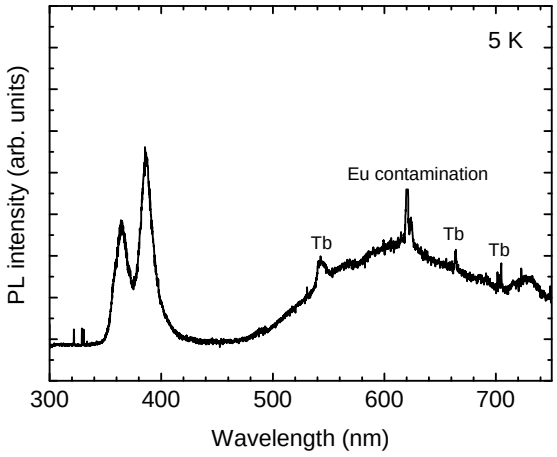

Figure 8.1: PL of a about 100 nm thin GaN:Tb layer measured at 5 K. The excitation source has been a Nd:YAG laser.

occupies a Ga site in the tetrahedral coordination and the bond length of Tb-N was the same as that of Ga-N. This highly symmetrical structure suppresses the inner-4f transition.

On the other hand, an optical study of Tb^{3+} ions implanted in GaN layer has been also reported, where sharp and intense transitions were observed [Loz00, Gru02]. It is possible that after the implantation the Tb^{3+} ions sites are different from those during in-situ doping. This could be due to the fact that the local symmetry of Tb^{3+} ions in this type of material system can be as low as D_2 [Gru02]. This statement however requires further investigations.

8.2 Optical properties in GaN:Tb QDs grown on AlN

Figure 8.2a shows PL spectra of GaN:Tb QDs measured at 10 K and 300 K. The narrow lines at 490 nm, 550 nm, 580 nm and 620 nm are assigned to the $^5D_4 \rightarrow {}^7F_J$ (J=6, 5, 4, 3, respectively) intra-4f transitions of Tb^{3+} ions, schematically shown in the energy diagram of Figure 8.2b. Other intra-4f transitions of $^5D_4 \rightarrow {}^7F_J$ (J=2, 1, 0) and the $^5D_3 \rightarrow {}^7F_J$ (J=6 to 1) are also observed and can be found in the expended scales in Figure 8.3. It is worth noticing that in spite of the complex emission spectrum, the laser-excited sample looks green to naked eye.

The intense luminescence of Tb^{3+} ions from Tb-doped GaN QDs can be explained by a disturbance of the local site symmetry resulting from the internal strain

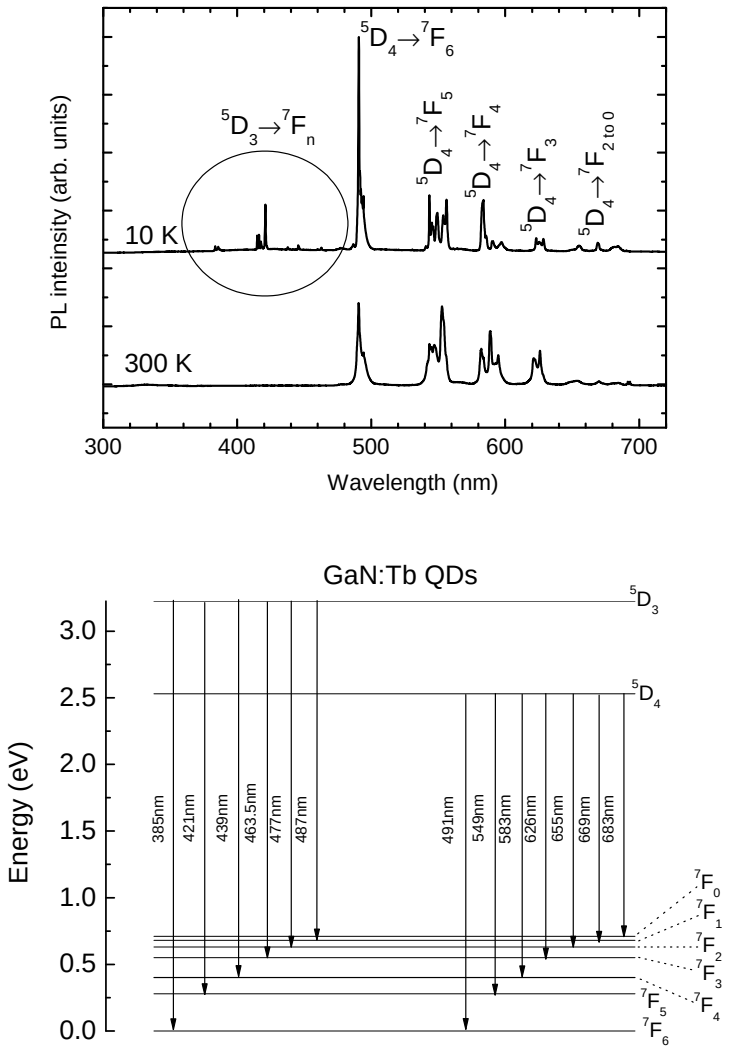

Figure 8.2: **a)** *PL spectra of Tb doped GaN QDs measured at 10 K (upper spectrum) and 300 K (downer spectrum) with an Nd:YAG laser (266 nm). Assigned transitions are also indicated in the figure.* **b)** *Energy diagram of Tb^{3+} ions and observed transitions in GaN QDs and AlN host. Note that the energy scale can have an offset with respect to all excited and ground states.*

as well as internal electric field that is experienced by the GaN QDs in an AlN matrix [Sim03]. In the PL spectrum in Figure 8.2 no near band gap related emission from GaN QDs has been observed which shows an efficient energy transfer is from the QDs host to the Tb^{3+} ions.

However the Tb location inside the Tb doped GaN QDs embedded in AlN spacing-layers is not easy to access, as AlN:Tb shows strong luminescence, similar to the case of Tm doped AlN. To address this, as in case of Tm doped QDs (Figure 7.3) a comparative CL and PL study has been performed on AlN:Tb and GaN:Tb

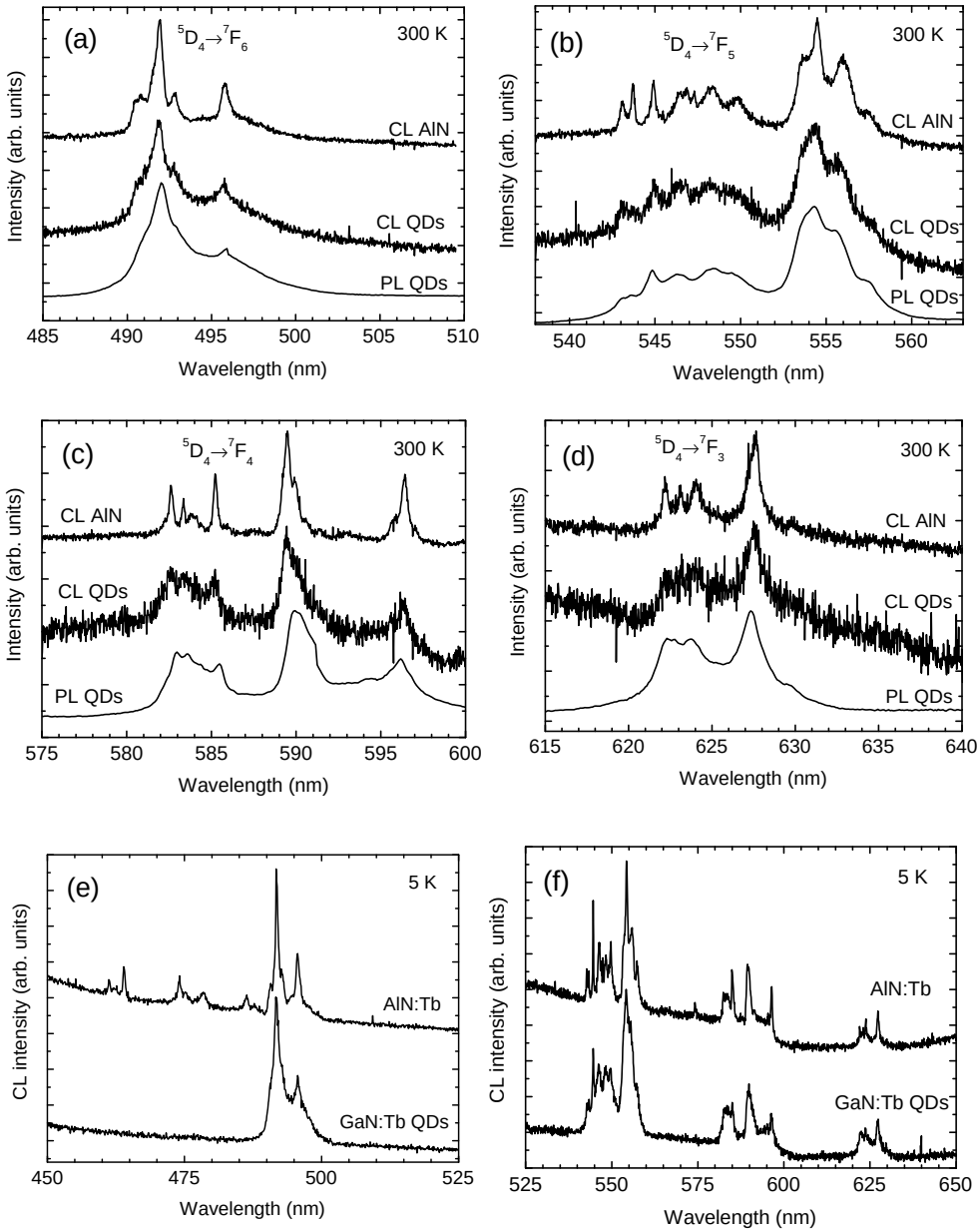

Figure 8.3: *High resolution CL and PL spectra of GaN:Tb QDs and AlN:Tb in expended scales* **a)** *from 480 nm to 510 nm,* **b)** *from 538 nm to 563 nm,* **c)** *from 575 nm to 600 nm and d) from 615 nm to 640 nm measured at 300 K.* **e-f)** *from 450 to 525 nm and 525 to 650 nm high resolution CL spectra of AlN:Tb and GaN:Tb QDs measured at 5 K. For PL measurements a Nd:YAG laser (266 nm) has been used. The high noise of the CL spectra is due to the use of a high resolution grating.*

QDs with the idea to excite either the QDs without AlN spacer (PL) and the whole heterostructure in CL. Figure 8.3 shows these spectra in expended scales. Results show only minor differences, in no way comparable to the case of Tm doping where strong differences were observed during similar study. The most important feature is a broadening of line width, when comparing the spectra for Tb doped GaN QDs and AlN. This can be induced by a higher internal electric field inside dots, or lower crystalline quality. No remarkable difference in splitting has been observed. It seems that in the case of Tb doping also the AlN spacing layer can be excited with the pumping laser. This result is in agremment with PL on AlN:Tb, where intense transitions have been found as an indication of an excitation mechanism possibly via defect related energy states from the AlN. Comparing emission spectra of AlN:Tb and GaN:Tb QDs in PL, the main different feature is the line width, which has been found in case of Tb-doped AlN to be about 0.05 nm (not shown). In addition to this the emission intensity of GaN:Tb QDs have been found always higher (more than a factor of 10) with respect to the amount of excited material.

Comparing the emission spectrum from GaN:Tb QDs a remarkable difference can be found with respect to that of the GaN layer containing impanted Tb atoms. It is interesting that for the implanted GaN layer, transitions of $^5D_3$ and $^5D_4$ excited state were both observed with rather similar intensity rations [Loz00, Gru02], whereas from the GaN:Tb QD sample only weak emission at low temperature from transitions originating from the $^5D_3$ excited states have been found. Responsible mechanisms are at this stage complicate to clarify.

An analysis of the temperature dependence of Tb emission in GaN:Tb QDs is given in Figure 8.4a and b. At first it is visible that transitions starting from the $^5D_3$ excited state are totally quenched at room temperature. By contrast in the case of the $^5D_4$ excited state, the PL intensity is stable over the whole temperature range comparable to RE emission from Eu- and Tm-doped GaN QDs. It is important that the total emission intensity from lines starting from the D_3 excited state is very low compared to those from the $^5D_4$ excited state so that the total emission intensity is stable (See Figure 8.2a). In detail the thermal behavior of emission starting from the $^5D_4$ excited state is more complicate as one can see in Figure 8.4b. This complicate behavior can be explained by thermal changes of the transition probability.

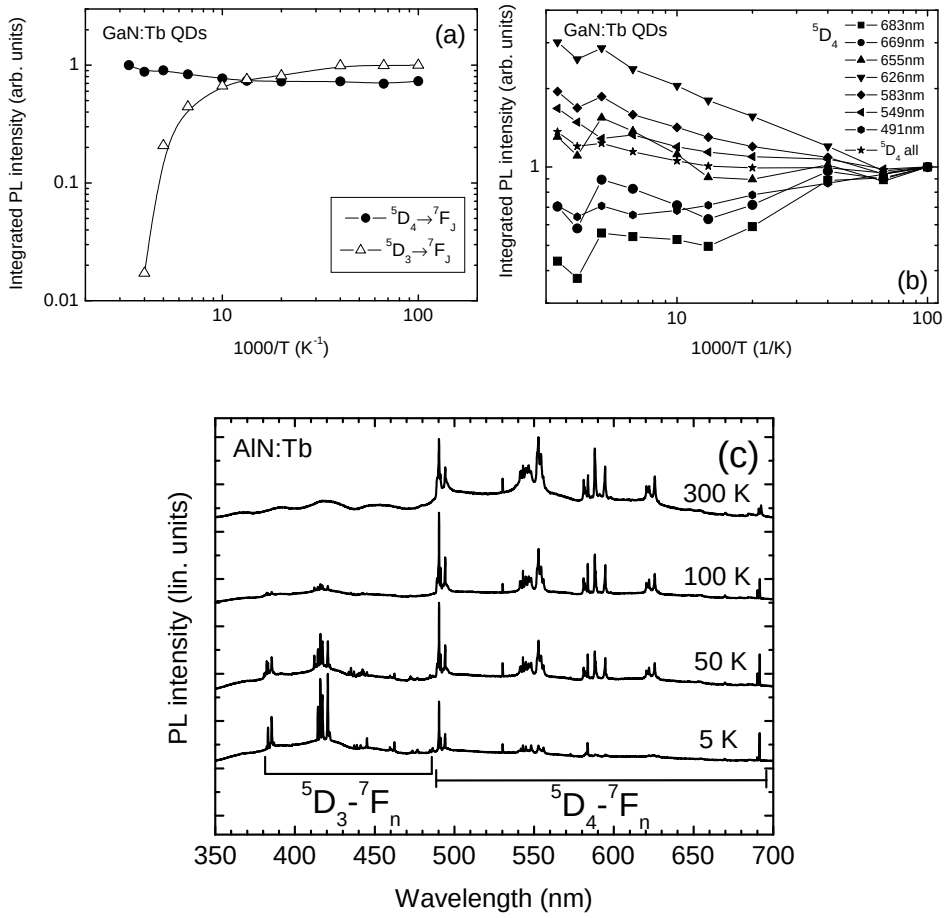

Figure 8.4: a) *Temperature dependence of PL intensities for Tb-doped GaN QDs. Closed and open circle represent the total integrated intensities of transitions from $^5D_4$ and $^5D_3$ excited states, respectively.* **b)** *Temperature dependence of PL intensities for Tb-doped GaN QDs for transition starting from the $^5D_4$ excited states.* **c)** *PL spectra of AlN:Tb measured at various temperatures as indicated in the figure. The spectra are normalized on the accumulation time. The exitation scource of all measurements has been a Nd:YAG laser (266).*

The $^5D_3$ level is about 3.2 eV higher than that of the $^7F_0$ ground state which is smaller than the band gap energy of GaN (3.6 eV) and energy states of GaN QDs (4 eV) so that it is difficult to assume energy backtranfer processes which could be responsible for the thermal quenching.

One possibility to explain the strong thermal quenching of the $^5D_3$ emission lines are some relaxation processes from the $^5D_3$ to the $^5D_4$ excited state. Compare for more details the discussion for GaN:Eu in chapter 4 and GaN:Tm QDs in chapter 7 where the energy backtransfer process and other deexcitation processes are discussed in more detail.

To clarify this thermal quenching issue and to address further on the Tb location, Figure 8.4c shows the temperature dependence of the Tb emission in AlN:Tb layer. The quenching of the transitions from $^5D_3$ is more than two orders of magnitude

between room temperature and 5 K. By contrast, transitions stemming from the $^5D_4$ excited state increase from liquid helium to room temperature by a factor of more than 3.

So on the transitions from $^5D_3$ are dominant at low temperature, on the other hand, the transitions from $^5D_4$ are more intense at room temperature, but the total PL intensity is constant over the entire temperature range.

Thus the thermal quenching of the $^5D_3$ emission in AlN:Tb layer could be the result of some energy transfer from the $^5D_3$ excited state to the lower lying $^5D_4$ excited state. However in detail the thermal quenching of AlN:Tb is difficult to analyze as the lines are very narrow and each emission has different characteristics in its detail.

Nevertheless, this observation shows that the thermal stability of the $^5D_4$ emission in GaN:Tb QDs is due to another process. These clear differences in the PL of AlN:Tb and in GaN:Tb QDs provide a support to the incorporation of Tb^{3+} ions in QDs in Tb-doped GaN QDs.

One way of interpretation can be that emissions starting from $^5D_3$ excited state from GaN:Tb QDs sample are from Tb in the AlN spacing layer. This is supported by the fact that emission from the $^5D_3$ excited state are rather similarly quenched in GaN:Tb QDs and AlN:Tb and that these emission are found only very weak in the QDs sample. This is also in agreement with the fact that Tb has, as Eu and Tm, a tendency to segregate during growth, and incorporates into AlN.

The fact that the line widths of lines from the $^5D_3$ excited state are sharper than those from the $^5D_4$ exited state on the QDs sample would be also in agreement with this statement since it can be assumed that the linewidth of RE emission from GaN QDs are broader than that of RE^{3+} ions inside AlN, as a result of the high internal electric field and strain effects which we have seen for Tm doping in chapter 7. If this is true, it would then indicate that GaN QDs are doped with Tb and that some Tb^{3+} ions can be found in the AlN spacing layer. A final proof for this statement would be to address the Tb location issue means structural methods like EXAFS.

References

[Ban02] H. Bang, S. Morishima, Z. Li, K. Akimoto, M. Nomura, and E. Yagi, *MBE growth of Eu- or Tb-doped GaN and its optical properties*, J. Cryst. Growth **237-239**, 1027 (2002).

[Gru02] J. B. Gruber, B. Zandi, H. J. Lozykowski, and W. M. Jadwisienczak, *Spectra and energy levels of Tb^{3+} in GaN*, J. Appl. Phys. **92**, 5127 (2002).

[Lee03] D. S. Lee and A. J. Steckl, *Enhanced blue emission from Tm-doped $Al_xGa_{1-x}N$ electroluminescent thin films*, Appl. Phys. Lett **83**, 2094 (2003).

[Loz00] H. J. Lozykowski, W. M. Jadwisienczak, and I Brown, *Photoluminescence and cathodoluminescence of GaN doped with Tb*, Appl. Phys. Lett. **76**, 861 (2000).

[Sim03] J. Simon, N. T. Pelekanos, C. Adelmann, E. Martinez-Guerrero, R. André, B. Daudin, and Le Si Dang, *Direct comparison of recombination dynamics in cubic and hexagonal GaN/AlN quantum dots*, Phys. Rev. B **68**, 035312 (2003).

9. White luminescence from rare earth doped GaN QDs

In the previous chapters we have seen that it is possible to obtain red, blue and green PL from QDs doped with Eu, Tm and Tb respectively. The aim of this chapter is to show the potential of these materials for white light emission. For this, two different strategies can be performed. The first one would be to co-dope the GaN QDs with RE atoms which means that during growth of QDs, 3 RE cells have to be opened at the same time. This method would be for industrial application the method of choice, as it is most easy to perform. However the disadvantage could be that the RE atoms interact during growth in an uncontrollable way. Also Co-doped materials show very complicate excitation processes as cross relaxation processes can occur [Dej95]. To avoid these problems the samples studied here contain just stacks of QDs planes, each stack being doped with only one sort of RE atom which could be even problematic as we have seen that the RE atoms can segregate during growth even over the AlN capping-layer (Eu) so that interaction between RE atoms can be still possible (Section 3.3.1 and 3.3.2).

Figure 9.1 shows a photo of 3 samples excited with a Nd:YAG laser (266 nm) containing 100 planes of QDs doped with Tm, Eu, Tb and 1 sample containing 288 planes of GaN QDs where the RE colors have been combined to get out white light emission. A corresponding PL spectrum of a sample with white PL is shown in Figure 9.2a. Emission lines from the three RE ions can be identified. The temperature dependence of the PL has been measured from liquid helium temperature to more than 410 K in order to check the thermal stability of the white color. From liquid helium to room temperature all emission lines from higher lying excited states are quenched, which is in agreement with the detailed studies of the Eu, Tm and Tb doped QDs (chapter 5,7 and 8). From 300 K to 450 K the residual emission lines, namely the $^5D_0 \rightarrow {}^7F_2$ for Eu, $^1D_2 \rightarrow {}^3H_4$ for Tm and $^5D_4 \rightarrow {}^7F_J$ J=1 to 6 for Tb, of the RE atoms have been found rather stable with a Eu and Tb emission decrease by about 50% whereas blue Tm emission seems even to increase.

Figure 9.1: *Photo of the PL of samples (from the left to the right) containing 100 stacks of GaN:Tm QDs, 100 stacks of GaN:Eu QDs, 100 stacks of GaN:Tb QDs and 24 x (4 stacks of GaN:Tm QDs, 6 stacks of GaN:Tb QDs and 2 stacks of GaN:Eu QDs).*

For obtaining a well defined color output the sensitivity of the light detection system has been adjusted using a white reference lamp. Then the spectra have been corrected with respect to the response function of the setup. This finally allowed to analyze each component with its proper weight. Then the resulting point in the chromaticity diagram can be calculated by adding different contributions, which is shown in Figure 9.2c. In this diagram we can find for typical working temperatures of a device (270 K to 450 K) that color is changing only slightly. The whitest sample, which has been grown during this work, is also indicated in the diagram. It can be found that the whiteness can easily compete with the color of a typical tube fluorescent . It has to be remarked that with a correct color adjustment in principle all emission colors from near infrared to deep blue can be produced which could be interesting also for other device applications.

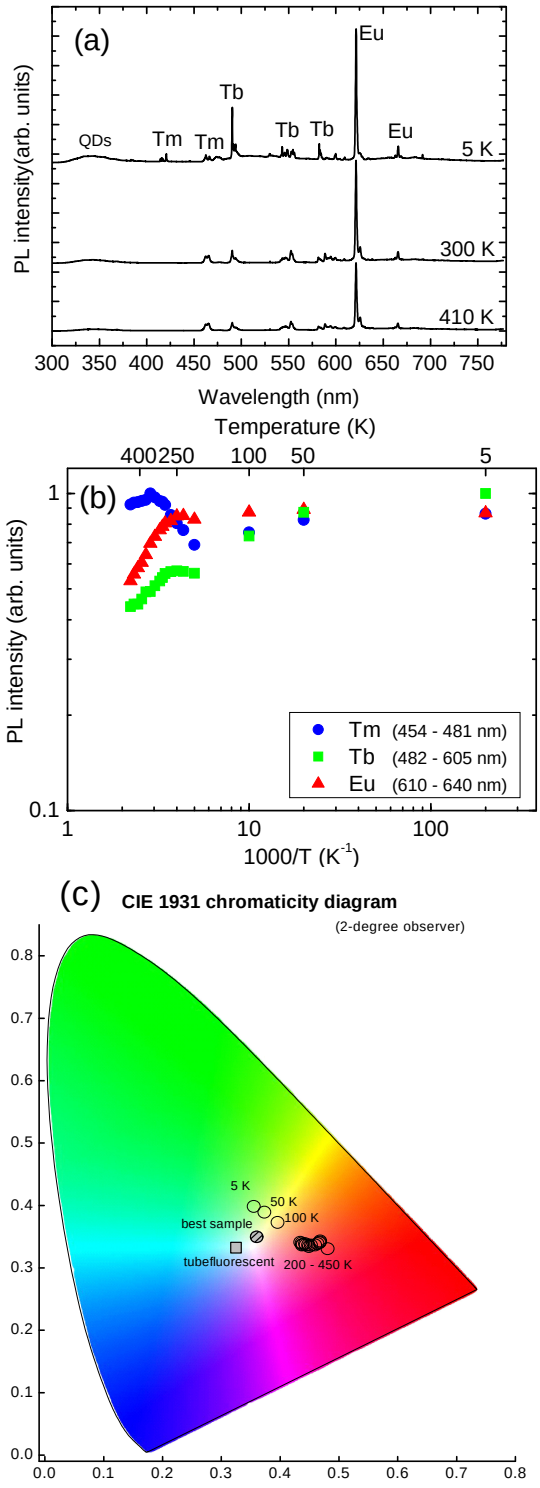

Figure 9.2: a) *PL spectra of a sample containing 7 x (4 stacks of GaN:Tm QDs, 10 stacks of GaN:Tb QDs and 3 stacks of GaN:Eu QDs) measured at indicated temperatures. The excitation source was a Nd:YAG laser (266 nm). The spectra are normalized to the accumulation time.* **b)** *Temperature dependency of the PL of RE lines of the sample studied in a.* **c)** *Change of the color of the PL in a chromaticity diagram (open circles). The color of a typical tube fluorescent is indicated by a square. The color measured at room temperature from the "whitest" grown sample in this work, containing a similar superlattice to the sample studied with temperature is also shown in the figure.*

9.1 Current injection via a metal semiconductor contact

A first step to current injection devices has been performed by depositing a metal contact (30 nm Ni / 200 nm Au) on the semiconductor. The idea is that electrons tunneling through a Schottky barrier into an active region, in our case GaN:Eu QDs grown on $Al_{0.5}Ga_{0.5}N$ doped with Si. Si has been used to achieve n-type conductivity of the material. Figure 9.3 shows a photo of the EL. A corresponding spectrum in shown in Figure 9.4 and compared with a PL spectrum carried out with the frequency doubled Ar-ion laser (244 nm). Interestingly emission lines are observed at higher energy (lower wavelenght) and are more pronounced in case of the EL which makes the emitting color more orange, compared to the deep red color observed by direct laser excitation (Figure 9.1). This is a sign that the excitation density is higher in EL than in PL as the emission lines at higher energy are starting typically to increase for higher excitation densities. It is interesting to notice that in the PL spectrum also emission from undoped QDs are observable at around 350 nm, which is not existing in the EL spectrum.

For better understanding further investigations have to be performed as at this stage it is unclear how the injected electrons are exciting the Eu atoms.

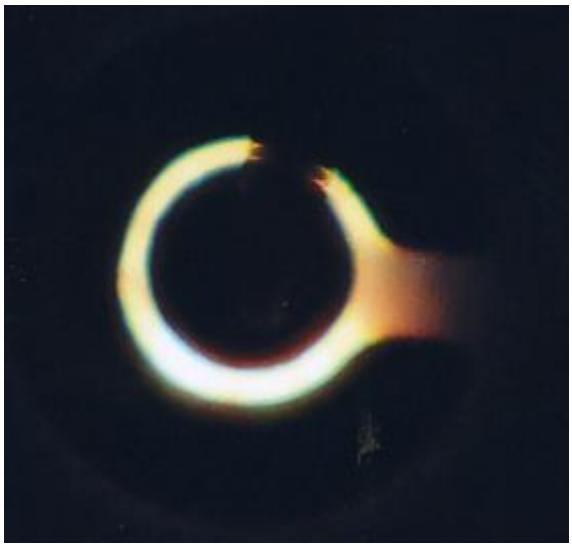

Figure 9.3: *Photo of the EL from 5 stacks of GaN:Eu QDs capped with 10 nm $Al_{0.5}Ga_{0.5}N$:Si.*

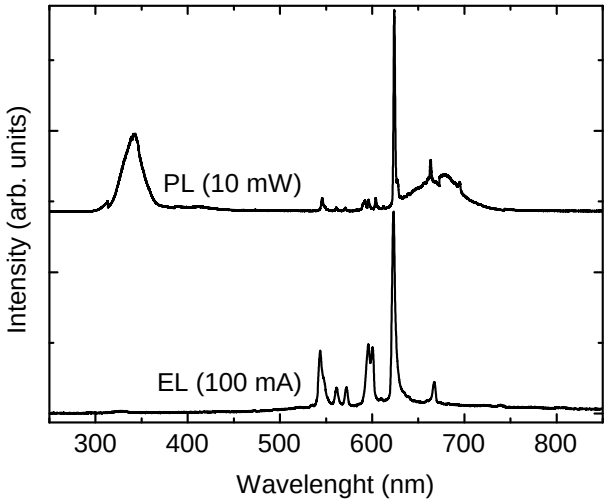

Figure 9.4: *Normalized PL and EL spectra to compare to relative intensities of the emission lines for an excitation power of 10 mW (244 nm) and a current of 100 mA. The broad emission at around 675 nm is the second order of the QD emission. The spectra have been measured at a similar sample positions.*

References

[Dej95] M. Dejneka, E. Snitzer, and R. E. Riman, *Blue, green and red fluorescence and energy transfer of Eu^{3+} in fluoride glasses*, J. of Luminescence **65**, 227 (1995).

10. Conclusion

In conclusion we have discussed MBE growth, optical and structural properties of Eu, Tm and Tb doped GaN and InGaN QDs and related materials.

We have seen that growth of QDs is drastically affected by the presence of Eu which is explained by a strong tendency of Eu to segregate on the growing surface. EXAFS studies and optical characterizations have been in agreement to demonstrate that GaN QDs are doped with Eu, whereby no Eu centers have been identified in the surrounding AlN spacing-layer.

In case of InGaN QDs, Eu location has been established in both InGaN QDs and the GaN spacing layer by systematic PL and PLE studies.

The situation is more complicate in the case of GaN:Tm QDs where we have demonstrated that Tm atoms are partially located in GaN QDs and partially at the GaN/AlN interface. This has been established by structural characterizations, namely EXAFS and RBS combined with an optical study where selective excitation of the AlN capping layer and the GaN QDs has been performed.

Tb^{3+} ions have been found inside GaN QDs by comparing the thermal behavior of the PL with that of an AlN:Tb layer which is remarkably different. Transition lines from Tb ions inside QDs show thermally stable PL between liquid helium and room temperature, whereas emission lines of the AlN:Tb layer show a complicate thermal behavior, as some emission lines are quenched and other lines show an increase with temperature.

Due to the established location of RE ions in (In)GaN QDs structures, different Eu sites have been found in GaN:Eu layers where depth sensitive CL and PL experiment have put in evidence two different sites of Eu^{3+} ions near to the sample surface and deeper in the volume, characterized by different crystal field splitting, thermal quenching, wavelength and electron beam acceleration dependent excitations. Intra 4f-transitions of Eu^{3+} ions starting from the $^5D_2$, $^5D_1$ and $^5D_0$ excited states have been identified and show different thermal quenching in PL. We have shown that below-band-gap excitation of the Eu^{3+} ions is more than 100 times weaker than near- or above-band-gap excitation and has been found only for the Eu^{3+} ions located deeper from the sample surface.

For GaN:Eu QDs the PL intensity is linearly increasing with the Eu content. A saturation effect of the Eu emission has been observed for higher excitation powers,

explained with a simple model taking into account the decay time of the Eu ions. Eu PL from GaN QDs and InGaN QDs has been found thermally stable between liquid helium and room temperature showing the high quantum efficiency of these structures.

Tm doped GaN QDs show bright emission from Tm^{3+} ions under optical excitation above the fundamental energy of GaN QDs. The PL as a function of temperature was fast quenched for transition from the high-lying manifolds state but stable for the blue $^1D_2 \rightarrow {}^3F_4$ transition. Based on the decay times of emissions we have discussed mechanisms for excitation to and de-excitation from Tm^{3+} ions.

The first step to a real device has been shown by the demonstration of thermal stable white light emission up to 400 K by combining different stacks of RE doped QDs and by the demonstration of current injection via a metal semiconductor contact.

11. Appendix A

This appendix gives a short summary about the experiments used during this work. The appendix can be structured into four sub-sections. At first the samples are grown by molecular beam epitaxy (Section 11.1) with in situ reflection high electron diffraction control (Section 11.2).

For structural characterization Rutherford backscattering spectroscopy (Section 11.3) and extended X-ray adsorption fine structure have been used. The surface morphology was studied with different kinds of microscopes, mainly an atomic force microscope (Section 11.4). Optical characterizations have been carried out by photoluminescence and cathodoluminescence measurements (A4). The aim of this Appendix is to give a short physical description of each method, with respect to the used setups.

11.1 Molecular beam epitaxy

Molecular beam epitaxy (MBE) is a common technique to deposit mono-crystalline thin films with a well defined orientation on a substrate. During growth, shutters from Knudsen cells can be opened and closed to expose the sample surface to a well controlled flux of elements. The idea of MBE is that the atoms are not scattered during the trajectory from the source cell to the sample. This has advantages like a well controlled growth rate and low incorporation of impurities. To realize this, UHV conditions are necessary. However the growth rate (typically in the order of 100 nm/h) is lower as compared to other techniques, e.g. MOCVD (typically 1 µm/h).

During this work a MECA 2000 MBE machine was built up and put in operation (Figure 11.1). The machine consists of an introduction system, a preparation chamber, especially for heating the substrates and an epitaxy chamber for the final growth. The epitaxy chamber is equipped with Ga (2 cells), Al, In, and 3 different rare earth Knudsen effusion cells like Eu, Tm, Tb, Ho, Er and a Si and Mg cell for n and p-doping respectively. Active nitrogen is produced by a nitrogen plasma cell. The required UHV conditions are realized by a complex pumping system consisting of turbo molecular pumps, ion getter pumps and titan sublimation pumps.

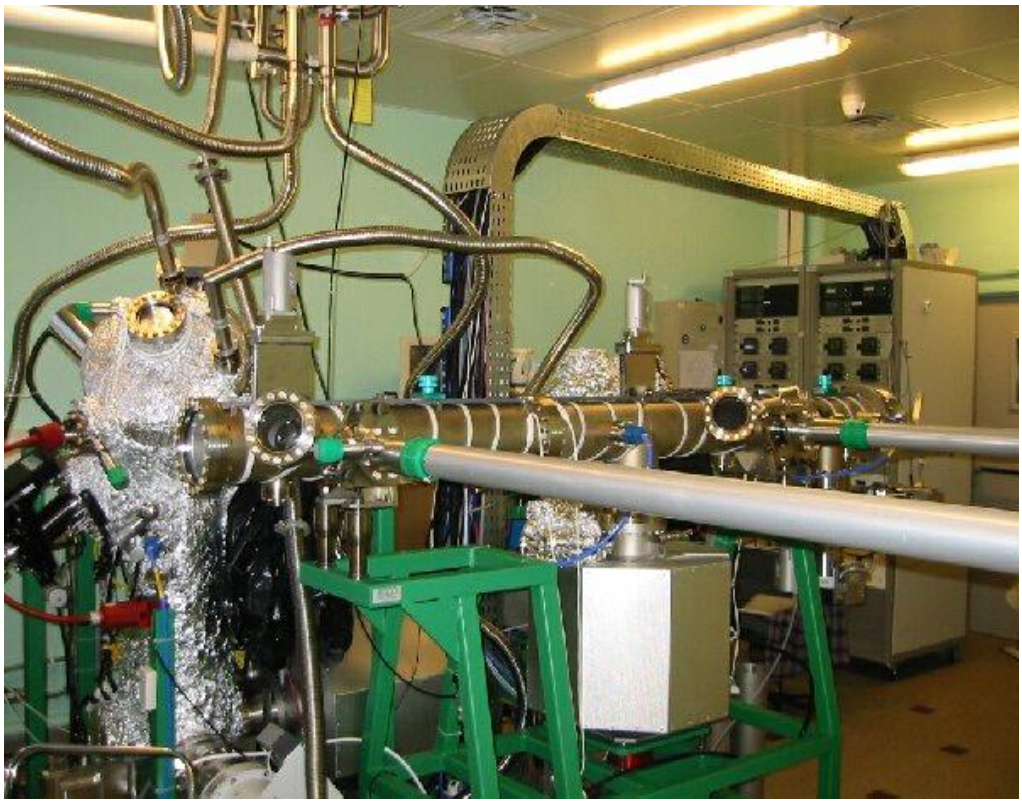

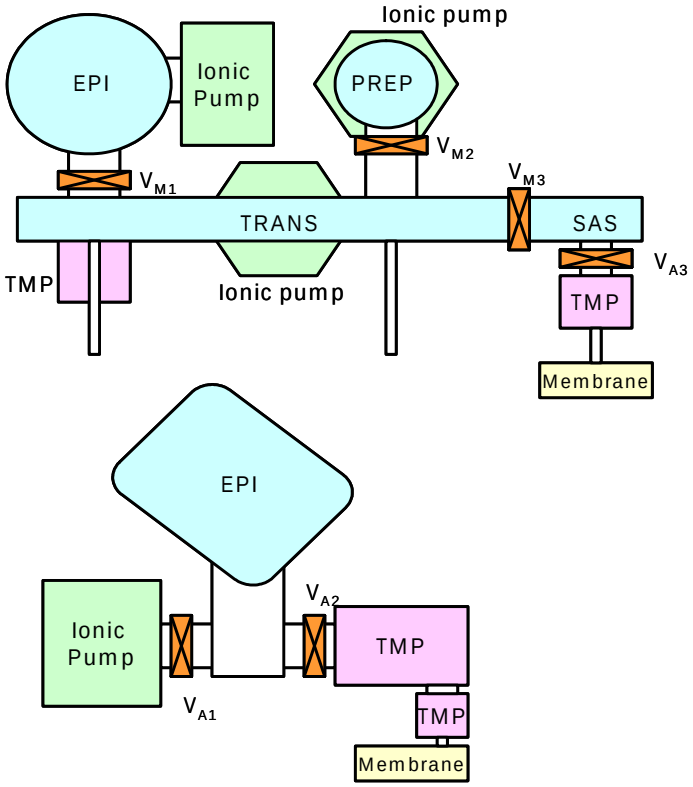

Figure 11.1: *Photo and schema of the build up and used MBE system. The epitaxy chamber (EPI) is visible in front on the left of the photo.*

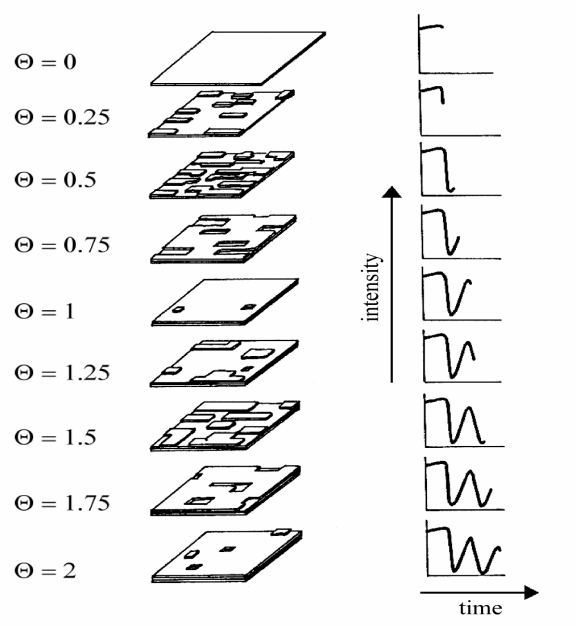

Figure 11.2: RHEED intensity oscillations for different surface coverages between 1 and 2 monolayers. From [Joy86].

Furthermore the growth chamber and the effusion cells are cooled with liquid nitrogen for additional cryogenic pumping.

The transfer of the samples between the different chambers was realized by manipulators working mechanically or with help of a magnetic system. The physics of MBE is described in more detail in [Ade02].

11.2 Growth with in-situ RHEED

Reflection high electron diffraction (RHEED) is a common method to control in-situ and in real time the growth condition during MBE growth. In RHEED a high energy electron beam (34 kV) is impinging the sample in grazing incidence (1° to 3°). The low angle between the incident beam and the sample corresponds to a penetration depth of about 1 nm which allows one to be sensitive to the surface. A change of the surface morphology can be observed in real time with a camera. The RHEED images give information about the lattice constant near the surface, but more important about the growth mode. The intensity changes of the reflected beam allow

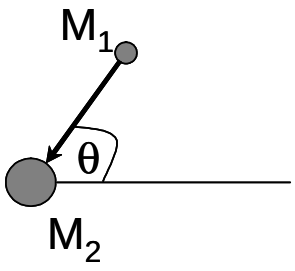

Figure 11.3: *Simple schema of ion scattering during RBS. M_1 is the mass of the scattered ion and M_2 the mass of the target atom.*

studying the growth rate and the chosen growth conditions by RHEED intensity oscillation. One example is shown in Figure 11.2 where it can be seen that the intensity of the specular reflected electron beam is depending on the step density of the sample surface. Further information about RHEED can be found in several textbooks. See for instance [Ade02, Lüt97].

11.3 Rutherford backscattering spectroscopy

In Rutherford backscattering spectrometry (RBS) an ion beam is backscattered after colliding with atoms in the near surface region of the sample at which the beam has been targeted. This backscattering process occurs after elastic collision with an atomic nucleus which is illustrated in Figure 11.3. Then depending on parameters of the collision (mass and energy of ions, mass of the target atom and the angle between the impinging and colliding particles) a specific energy is given up to the target atom. Then the backscattered ions can be detected as a function of its energy to determinate different elements in thin films and the elemental concentrations versus depth below the surface.

For ion acceleration a Van de Graaf ion accelerator has been used. The used setup has a typical uncertainty of ± 2% using 1.8 MV alpha particles and a depth resolution of about 5 nm for nitrides.

We will show now, how we can relate from the energy loss of the scattered particles to elemental composition of the material at a given depth. The ratio between the energy of the ion beam E and the backscattered energy E_1 can be written as:

$$E_1 / E = \left(\frac{\sqrt{M_2^2 - M_1^2 \sin^2 q} + M_1 \cos q}{M_1 + M_2} \right)^2 \text{(*)},$$

Here M_1 is the mass of ions, M_2 is the mass of the target atom and q the angle between the perpendicular axis to the substrate and the backscattered ion.

The total amount of detected particles n is: $n = s\,\Omega Q N t$ with Ω the solid detection angle, Q the total number of incident projectiles, N the number of target atoms per cm^3, t the target thickness in cm and s the scattering cross section (cm^2). For an elastic collision the scattering cross section can be calculated by formular:

$$s = \frac{Z_1 Z_2 e^2}{4E} \frac{4}{\sin^4 q} \frac{\left(\sqrt{1-(M_1/M_2 \cdot \sin q)^2} + \cos q\right)^2}{\sqrt{1-(M_1/M_2 \cdot \sin q)^2}} \qquad (**).$$

In this formula it is important to note that the number of backscattered ions is proportional to the square of the atomic masses (See formular **). This is the reason why RBS is much more sensitive to heavier atoms, whereas their mass/energy separation is more problematic than in case of lighter ones (*). In other words if heavy atoms with slightly different masses have to be well identified, the mass of the scattered ions has to be increased.

Most of the ions are not directly backscattered by the first layer of surface atoms but deeper inside the sample. During this way the ions in the sample are losing energy, from interaction with the electron shells of the sample atoms. This energy loss $\Delta E = e\,N \Delta x$ at a depth x can be calculated using the stopping power $e = \frac{1}{N}\left(\frac{dE}{dx}\right)$. A typical energy loss for 2 MeV $^4He^+$ ion beam is between 100 and 800 eV/nm, depending on the material. This law can be used to estimate thicknesses of layers. It has to be remarked that more detailed theoretical predictions of the stopping power are complicate and mostly inaccurate, so that in simulations usually empirical data are used [May77].

After passing through a target the beam will not only lose energy, it will get furthermore less monoenergetic. The effect increases with higher atom masses of the elements since it is affected by the number of electrons from the passing material. This effect limits depth and mass resolution.

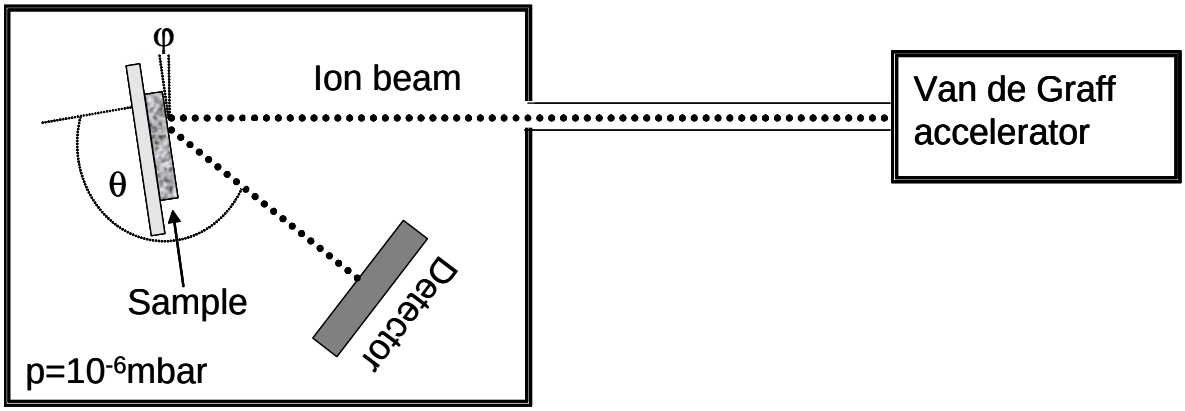

Figure 11.4: *Schema of an RBS experiment.*

In case of to many different elements in different depth other methods as SIMS have to be used for determination of structure and composition. SIMS is also the preferable method when the concentration of to detect element is low (<0.001%). As RBS is most sensitive to heavier atoms, SIMS is the method of choice for scanning lighter atoms.

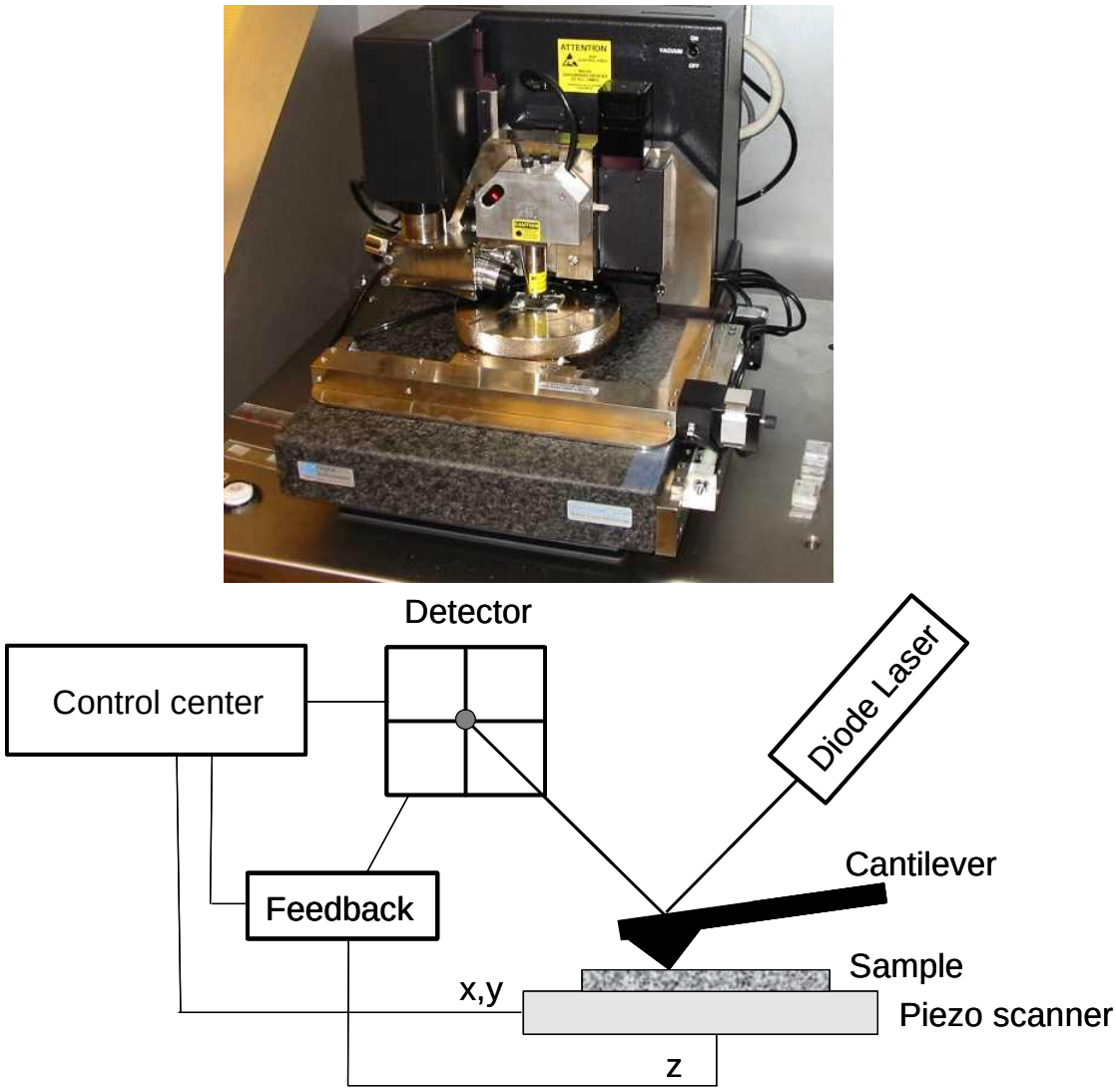

Figure 11.5: *Foto and schema of the used Dimension 3100 microscope.*

11.4 Atomic force microscopy

An atomic force microscope (AFM) uses the interaction between tip and surface for imaging the surface morphology [Bin86]. This interaction can be a direct contact between tip and surface (contact mode) or van der Waals forces, which depend on the distance between tip and surface (non contact mode). Practically, the tip is attached to a micro-cantilever arm. For detection of the small forces F between sample and tip, which can be in the order of 10^{-10} N a laser is adjusted onto the tip and detected by a three element detector. Then with a piezo the x- and y-position can be changed to scan the sample in a selected region. To obtain good AFM images the user cannot only change the working distance z between sample and tip but also the integral and proportional parts of a feedbackcontol.

The experimental setup used here was a Dimension 3100 microscope working at room temperature and in air. A photo and a schema of the setup is shown in Figure 11.5.

In this work a non contact (tapping mode) mode has been used. In this mode, the tip oscillates with its resonant frequency $w_0 = \sqrt{k/m}$, of the order of one hundred hertz. Then changes of the resonant frequency are detected, which are proportional to the gradient of the force between sample and tip.

$$w = w_0 \cdot \sqrt{1 - \frac{1}{k}\frac{\partial F}{\partial z}} \; .$$

The difference of the tapping mode to other non-contact modes is that the tip slightly taps the sample surface by contacting the surface at the bottom of its swing. The advantages of this mode are a high lateral resolution and lower used forces compares to the other non-contact mode. However the used scan speed is generally lower than in the case of the contact mode.

For higher resolution images lower temperature and vacuum conditions are preferable. Nevertheless our experiment had high enough resolution (down to 0.3 nm) to study the morphology of nitride surfaces and especially QDs.

An AFM image is the result of the interaction between sample surface and tip. For not plane surfaces the tip and the surface structure start to interact. To study this interaction, it is important to notice that real tips have a finite diameter, increasing with the distance from the last atom [Mon93]. Due to this property of the tip the image is a convolution of both geometries, namely the one of the tip and the one of the sample [Mar94, Mar95]. A typical artefact is the overestimation of the diameter of structures, as illustrated for clarity in Figure 11.6. Another problem can be an underestimation of the height of QDs, especially when the dot density is high.

From the theoretical side several algorithms exist to conclude on the exact structure of the surface [Mar94, Mar95, Kel93, Vil97], but it is necessary to know the exact shape of the tip or the sample geometry of a reference [Mil95]. During the data analysis here, 1 nm from the measured diameter has been typically substracted. In order to obtain a better estimation of the amount of material, a comparison with RBS data can be useful (Figure 3.15) [Tab97].

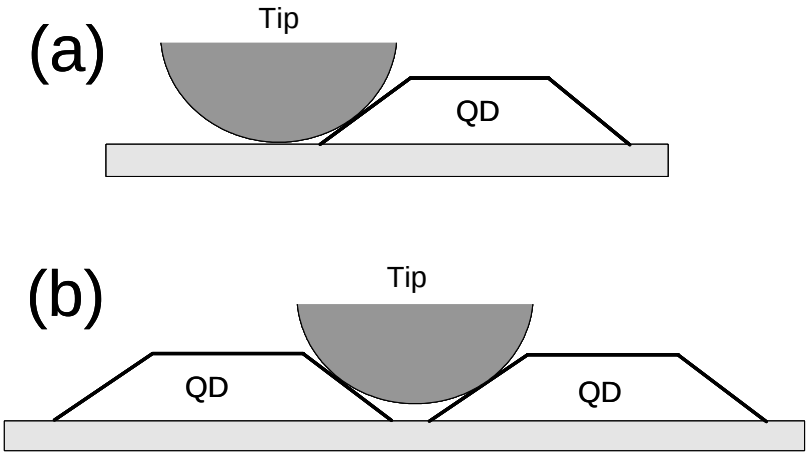

Figure 11.6: a) *Simple schema to show the increase of the lateral island size during AFM measurements with respect to the real island size due to the finite size of the tip.* **b)** *Schema to show problems during height measurements, for samples with high QD densities.*

11.5 Optical characterization methods

If electron and hole pairs are excited and recombine radiatively the phenomenon is called luminescence. The electrons and holes can be created for example by an impinging electron beam in Cathodoluminescence (CL), or by light in Photoluminescence (PL) or as in case of a p-n junction by carrier injection in electroluminescence (EL). All experiments are used to proof optical properties of semiconductors [Pan75, Hau90, Kil95].

11.5.1 Photoluminescence

In PL an electron from the valence band is raised up by a photon to the conduction band. Thus it leaves a hole with + charge in the valence band. If this electron hole pair recombines, the light emission is called PL.

Therefore the simplest PL setup consists of an excitation source and a detector for measuring the intensity of the luminescence.

Figure 11.7 shows a typical PL setup, which has been used also during this work. The light of the excitation source can be focused with a focal lens onto the sample to enhance its excitation density. Then the luminescence is collected by a collection lens and again focused into a monochromator.

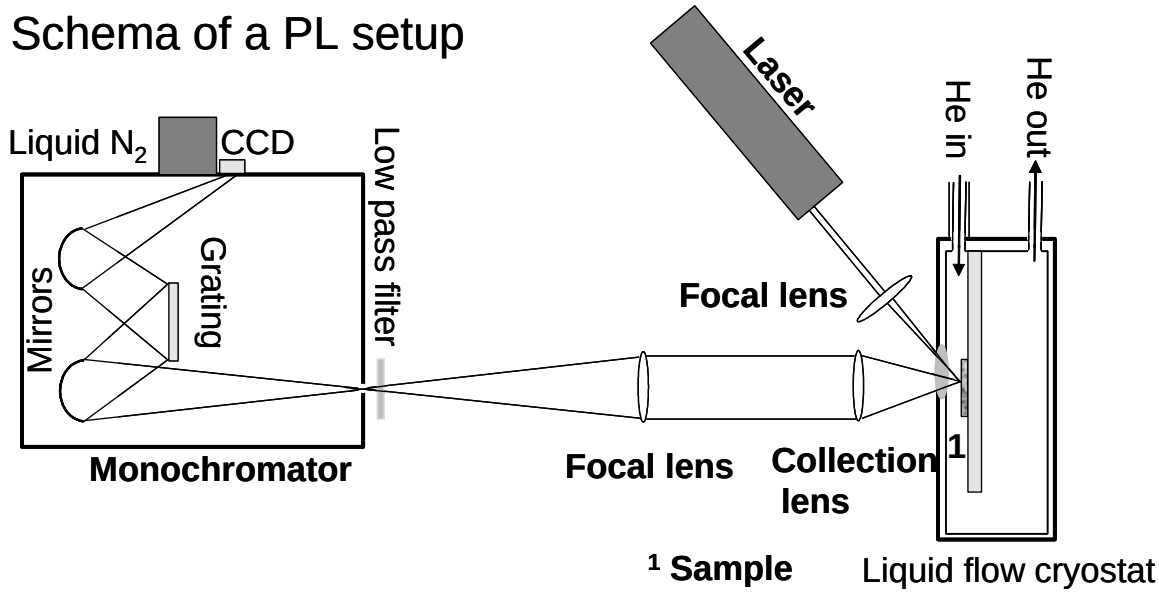

Figure 11.7: *Schema of a typical PL setup used during this work.*

This can be realized with one or better two lenses. For detection the luminescence passes the entrance slit of the monochromator containing a parabolic mirror, to reflect the light onto a grating for wavelength separation and another parabolic mirror to focus the light onto a detector. As the energetic resolution of the final spectrum is proportional to the square of the number of slits of the grating, in the present case 600, 1200 or 1800, it is important to enlight all the area of the grating.

Then, finally, detection was realized using either a CCD camera operating at liquid nitrogen temperature or a photomultiplier tube operating (PMT) in the photon counting mode. During this work a Jobin-Yvon grating monochromator had been used (Focal length 550 mm or 480 mm) with a typical spectral resolution down to 0.025 nm.

To protect the detection system from direct excitation light exposure a long-pass filter can be used in front of the entrance slit of the monochromator.

As III-nitrides are wide band-gap semiconductors, only UV excitation sources are suited for above band-gap excitation (at least 360 nm). The excitation has been done by an Ar^+ (305, 330 nm, etc.) [Int] and its frequency doubled line (488 nm) at 244 nm. Complementary measurements have been carried out with the fourth harmonic of a pulsed YAG:Nd laser emitting at 266 nm, with a pulse width of 0.5 ns, repetition rate of 8 kHz and average excitation power of 4.5 mW. The peak power of this laser, (1.17 kW) is very high.

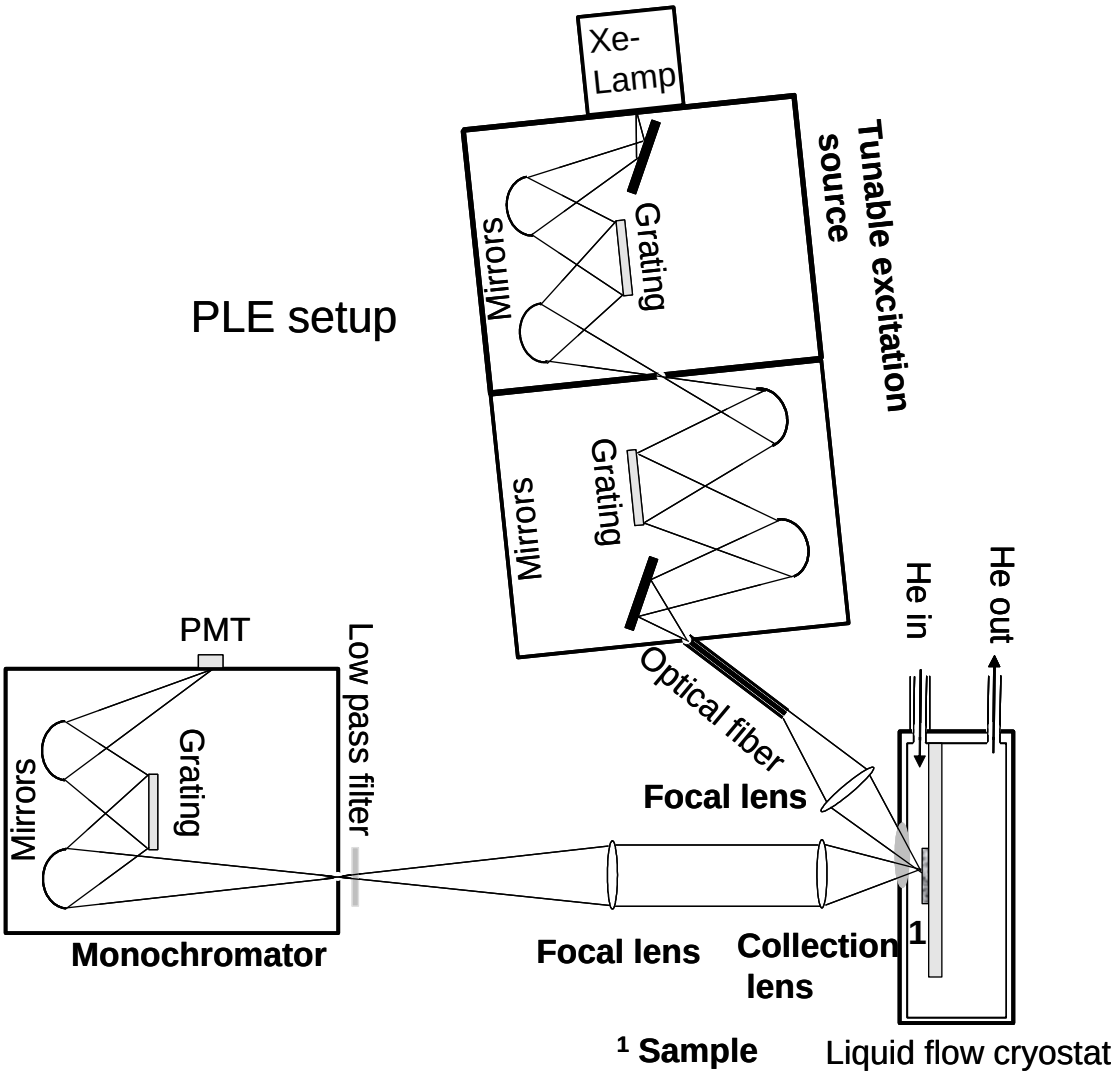

Figure 11.8: *Schema of a typical PLE setup.*

The excitation power of the lasers has been reduced using a filter, so that typically PL spectra have been measured with an average excitation power of about 1 mW. Also in the setup UV achromatic lenses have been used to avoid undesirable achromatic effects.

For temperature dependent measurements a cold finger of a liquid helium cryostat but also a liquid flow cryostat have been used, which allow to measure in temperature ranges between 5 K and 400 K.

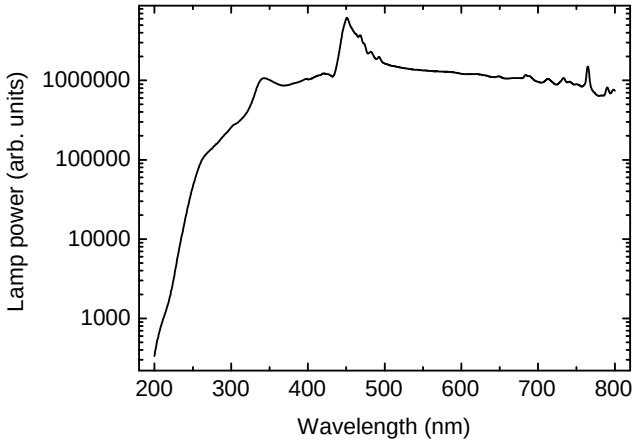

Figure 11.9: *Measured excitation power of the used Xe-lamp system in logarithmic scale.*

11.5.2 Photoluminescence excitation spectroscopy

Photoluminescence excitation spectroscopy (PLE) allows measuring the intensity changes of one chosen emission line as a function of the excitation wavelength. With this method it is possible to obtain information about the excitation mechanism of the monitored line. It is also possible to have an idea about the density of states of semiconductor material.

The basic PL setup shown in Figure 11.7 can be extended rather simply into a PLE experiment by using a tunable excitation source and a PMT for detection. A simplified schema of a PLE setup used in this work is shown in Figure 11.8.

The excitation has been carried out with a 500 W high-pressure Xe-lamp equipped with a Jobin-Yvon high-resolution double-grating monochromator (Gemini 180) for wavelength separation. The use of a double monochromator allowed sharper wavelength selection (below 1 nm).

It is important to use an achromatic UV focal lens in order to control the excitation density and the focal point.

Then the detection has been carried out with another Jobin-Yvon grating monochromator (Triax 550) equipped with a PMT operating in the photon counting mode.

The excitation power of the used Xe-lamp, about 200 $\mu W/cm^2$ at 350 nm, is rather low and strongly depending on the selected wavelengths, which is shown in Figure 11.9. Sharp lines form Xe atoms can be also found for wavelengths higher that 400 nm. For this reason all measured PLE spectra have been divided by the excitation power.

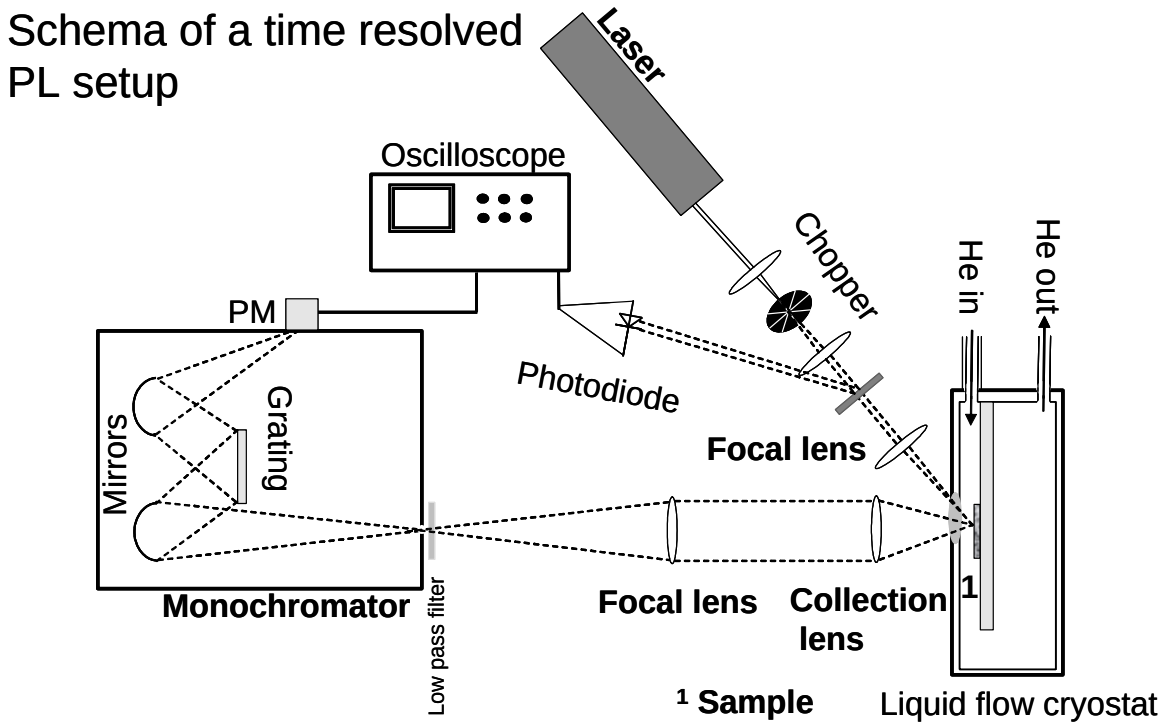

Figure 11.10: *Schema of a time resolved PL setup using a mechanical chopper.*

11.5.3 Time resolved photoluminescence

With time resolved PL it is possible to measure the decay (and rise) time of luminescence of semiconductor materials.

During this work luminescence decay times have been measured in a wide time range. The decay time from the (In)GaN host is in the ps regime. Tm^{3+} ions exhibit also quick decay times lower than 3 µs. For measuring this short decay times, time resolved measurements have been carried out using the tripled output of a pulsed titanium: sapphire laser emitting at 250 nm with an average power of 1 mW. The base repetition rate of this system was 54 MHz. It was furthermore possible to lower down the repetition rate with a Cavity dumper. Finally the detection of time resolved PL has been carried out with a Hamamatsu Streak camera in single sweep mode. This camera has the advantage to allow measurements of the decay time versus the wavelength of the PL in a chosen spectral range. A good introduction and a detailed experimental description for measuring these quick decay times are given in Ref. [Sim01].

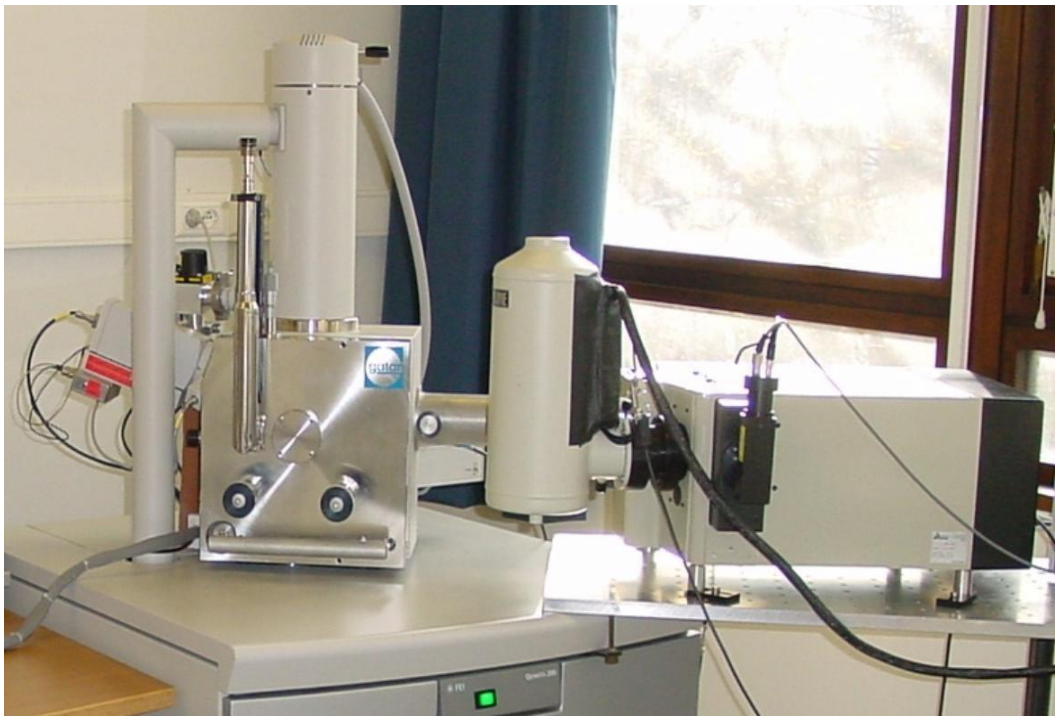

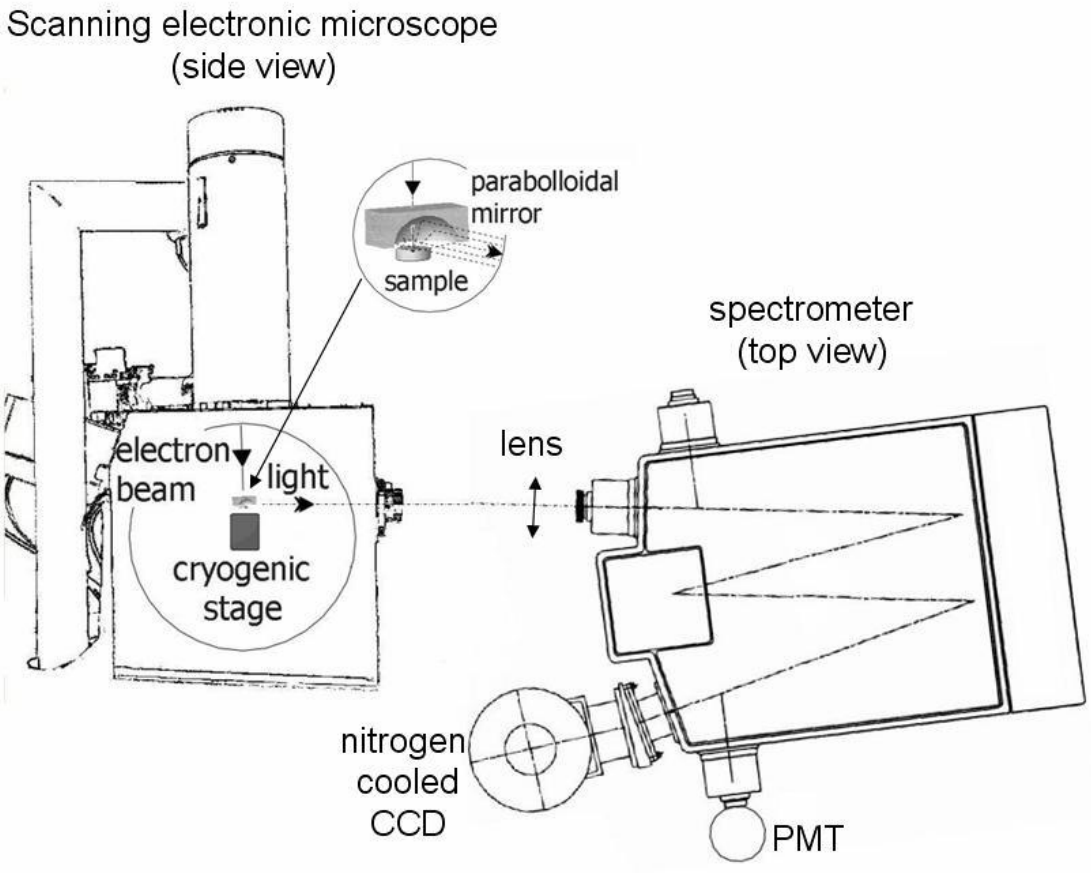

Figure 11.11: *Photo and schema of the FEI Quanta 200 SEM CL experiment.*

However RE^{3+} ions typically have longer decay times, in the order of the hundred of microseconds (Eu) up to milliseconds (Tb). To measure these long decay times the above described setup is limited, as high division rates of the Cavity dumper are necessary. A division rate of 11000 is for example needed for a measurement of a decay time in the order of 200 µs (Eu), so that the average excitation power would decrease down to about 9 nW, and very long accumulation times would be needed.

To overcome this problem, the time resolved PL setup shown in Figure 11.10 has been built up, using a mechanical chopper to chop the continuous beam of the frequency doubled Ar+ laser, which has an average excitation power up 100 mW. Then the PL can be detected with a time sensitive PM, while the signal from the PM is measured with an oscilloscope. In order to increase the signal to noise ratio and to allow an easier triggering of the signal, a part of the pulsed Laser beam is converted via a photodiode into an electrical trigger.

To enhance the resolution of the decay time measurement, the beam of the Laser has been focused onto the chopper. This is important since the time resolution is not only depending on the angular speed of the chopper, but also on the spot size.

11.5.4 Cathodoluminescence

Semiconductors can be also excited by a high energy electron beam. The transferred energy creates electron hole pairs, which can recombine radiatively. The number of electron-hole pairs created per impinging electron can be obtained using the empirical equation $N_{e-hPairs} = U_{acc} / 3E_g$ with ($E_{g,GaN} = 3.4eV$).

The setup used here was a FEI Quanta 200 SEM as shown in Figure 11.11. Electrons are created by thermal electron emission from a filament. Then the beam is accelerated by an electric field. For this a high vacuum environment is necessary. The luminescence is reflected through a parabolic mirror and a lens into a monochromator and finally analyzed by a PMT or a CCD. The mentioned parabolic mirror has a hole so that the electron beam can pass through it. The CL setup contains also an SEM, which allows to image the sample by detecting secondary electrons. Measurements in temperature ranges between liquid Helium and room temperature can be performed.

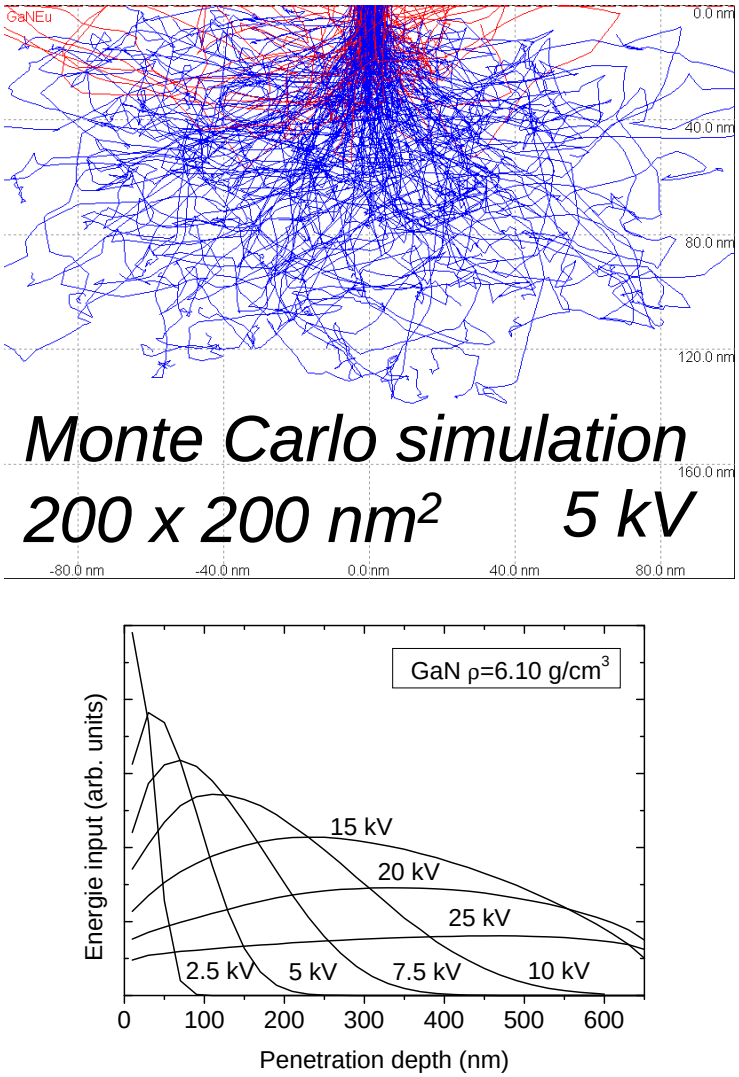

Figure 11.12:a) *Monte Carlo simulation of 200 injected electrons accelerated by a voltage of 5 kV. The precise penetration depth is depending on the parameters of simulation. For this simulation the software CASINO V2.42 has been used.* **b)** *Energy input as a function of the penetration depth for different acceleration voltages in GaN. From [Bar02].*

We want to point out some advantages of CL with respect to PL. The spot size of the electron beam which can be changed between 0.002 µm and 1 µm. With this small spot sizes it is possible to measure the luminescent at different positions of the sample. The combination with a SEM (secondary electrons), also allows luminescence mapping by measuring the intensity of only one line (fixed wavelength) with a PMT as a function of the lateral position.

One other advantage of CL is that one can change the accelerated voltage of the electron beam in the range between 0.3 kV and 30 kV. In doing this the luminescence can be measured as a function of the depth.

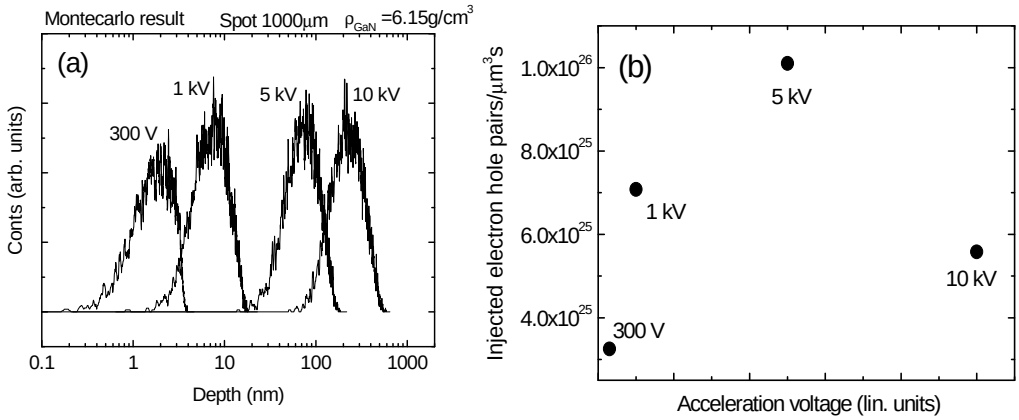

Figure 11.13: a) *Energy input as a function of the penetration depth for 4 acceleration voltages in GaN.* **b)** *Number of created electron hole pairs per second in GaN.*

The penetration depth can be simulated by Monte Carlo technique taking the density of the material into account (GaN=6.15 g/cm^3 and AlN=3.24 g/cm^3) and of course the acceleration voltage itself. The density is needed for simulations as the mean free path of an electron in solid material is drastically depending on the density of the material [Bar03]. One example for a Monte Carlo simulation is shown in Figure 11.12a. We can see that most electrons stay inside the sample, whereas some others leave the sample surface, those used for imaging the surface morphology (SEM). From these simulations one can plot the energy input versus the penetration depth, for various acceleration voltages. Figure 11.12a shows the result in the case of GaN. Lower penetration depths can be found for lower acceleration voltages in agreement with the above discussion. It is also visible that for higher acceleration voltages the distribution of the energy input is getting broader [Bar03].

It has to be remarked that the injected current was found to behave linearly as a function of acceleration voltage in the used setup (pA to nA region). Then taking into account the different excited volume one can estimate the number of created electron-hole pairs per second in a µm^3, which has been calculated in Figure 11.13. It is interesting to notice that only a slight change in the electron hole pair density can be found for the 4 measured examples, which is reasonable as the excited volume is getting much smaller for lower acceleration voltages, whereas this effect is counteracted by a lower number of total injected electrons. This means, in other words, that the “excitation power” of our used CL setup is for the 4 shown acceleration voltages not very different. However in case of III – nitrides layers the diffusion length of bound carriers vary from 30 nm up to 100 nm, depending on the

quality of the material [Evo99, Gon01, Ros97, Che96]. This effect can become important when probing a sample as a function of depth.

In addition to the possibility to probe the sample either laterally or vertically another advantage of CL is that the excitation energy is high enough to excite isolators like AlN or BN, which is rather hard in PL, as lasers emitting very short wavelengths (200 nm) are expensive and not easy to handle.

One disadvantage of CL is that the excitation with electrons is not as specific as with light, as they have high kinetic energies, which can finally yield to a slight broadening of the observed linewidths compared to PL. For that reason not to high acceleration voltages have to be chosen. The use of too high acceleration voltages can be also detrimental to the sample. This shows that in its detail CL results are much more difficult to understand than PL, so that a comparison of both types of data is often useful.

References

[Ade02] H. C. Adelmann, *Growth and Strain Relaxation Mechanisms of Group III Nitride Heterostructures*, PhD. thesis, Université Joseph Fourier, Grenoble (2001).

[Bar02] J. Barjon, *Etude d'un laser UV compact à semiconducteurs (Al, Ga)N pompé par micropointes*, PhD. thesis, Université Joseph Fourier, Grenoble (2001).

[Bar03] J. Barjon, J. Brault, B. Daudin, D. Jalabert, and B. Sieber, *Cathodoluminescence study of carrier diffusion in AlGaN*, J. of Appl. Phys. **94**, 2755 (2003).

[Bin86] G. Binnig, C. Quate, and C. Gerber, *Atomic force microscope*, Phys. Rev. Lett. **56**, 930 (1986).

[Che96] L. Chernyak, A. Osinsky, H. Temkin J. W. Yang, Q. Chen, and M. A. Khan, *Electron beam induced current measurements of minority carrier diffusion length in gallium nitride*, Appl. Phys. Lett. **69**, 2531 (1996).

[Evo99] S. Evoy, H. G. Craighead, S. Keller, U. K. Mishra, and S. P. DenBaars, *Scanning tunneling microscope-induced luminescence of GaN at threading dislocations*, J. Vac. Sci. Technol. B **17**, 29 (1999).

[Gon01] J. C. Gonzalez, K. L. Bunker and P. E. Russell, *Minority-carrier diffusion length in a GaN-based light - emitting diode*, Appl. Phys. Lett. **79**, 1567 (2001).

[Hau90] H. Haug and S. W. Koch, *Quantun Theory of the Optical and Electronic Properties of Semiconductors* (World Scientific, Singapore, 1990).

[Int05] Found in the jear 2005 in the internet under: http://www.flowcyt.salk.edu/laserlines.html.

[Joy86] B. A. Joyce, P. J. Dobson, J. H. Neave, K. Woodbridge, Jing Zhang, P. K. Larsen, and B. Bôlger, *RHEED studies of heterojunction and quantum well formation during MBE growth - from multiple scattering to band offsets*, Surf. Sci. **168**, 423 (1986).

[Kil95] C. F. Klingshirn, *Semiconductor Optics* (Springer, Berlin, 1995).

[Lüt97] H. Lüth, *Surfaces and Interfaces of Solid Materials* (Springer, Berlin, 1997), 3rd edn.

[Mar94] Markiewicz and M. C. Goh, *Simulation of atomic force microscope tip-sample/sample-tip reconstruction*, J. Vac. Sci. Technol. B **13**, 1115 (1995).

[Mar95] Markiewicz and M. C. Goh, *Atomic force microscope tip deconvolution using calibration arrays*, Rev. Sci. Instrum. **66**, 3186 (1995).

[May77] J. W. Mayer and E. Rimini, *Ion Handbook for Material Analysis*. (Academic Press, New York, 1977).

[Mil95] R. Miller, J. Vesenka, M. Henderson, *Tip reconstruction for the atomic force microscope*, J. Appl. Math **55**, 1362 (1995).

[Mon93] L. Montelius and J. O. Tegenfeldt, *Direct observation of the tip shape in scanning probe microscopy*, Appl. Phys. Lett. **62**, 2628 (1993).

[Kel93] D. Keller and F. Franke, *Tip Deconvolution and Image Restoration*, Surf. Sci. **294**, 409 (1993).

[Pan75] J. I. Pankove, *Optical processes in semiconductors* (Dover Publications, New York, 1975).

[Ros97] S. J. Rosner, E. C. Carr, M. J. Ludowise, G. Girolami, and H. I. Erikson, *Correlation of cathodoluminescence inhomogeneity with microstructural defects in epitaxial GaN grown by metalorganic chemical-vapor deposition*, Appl. Phys. Lett. **70**, 420 (1997).

[Sim01] J. Simon, *Etude des propriétés optiques de nanostructures quantiques à base de nitrures d'éléments III*, PhD. thesis, Université Joseph Fourier, Grenoble (2001).

[Tab97] M. F. Tabet and F. K. Urban III, *Deconvolution of tip affected atomic force microscope images and comparison to Rutherford backscattering spectrometry*, J. Vac. Sci. Technol. B **15**(4) 800 (1997).

[Vil97] J. S. Villarrubia, A*lgorithmus for Scanned Probe Microscope Image Simulation, Surface Reconstruction, and Tip Estimation*, J. Res. Natl. Inst. Stand. Technol. **102**(4), 425 (1997).

12. Appendix B

Classic 'Dieke Diagram' for Rare Earth Ions

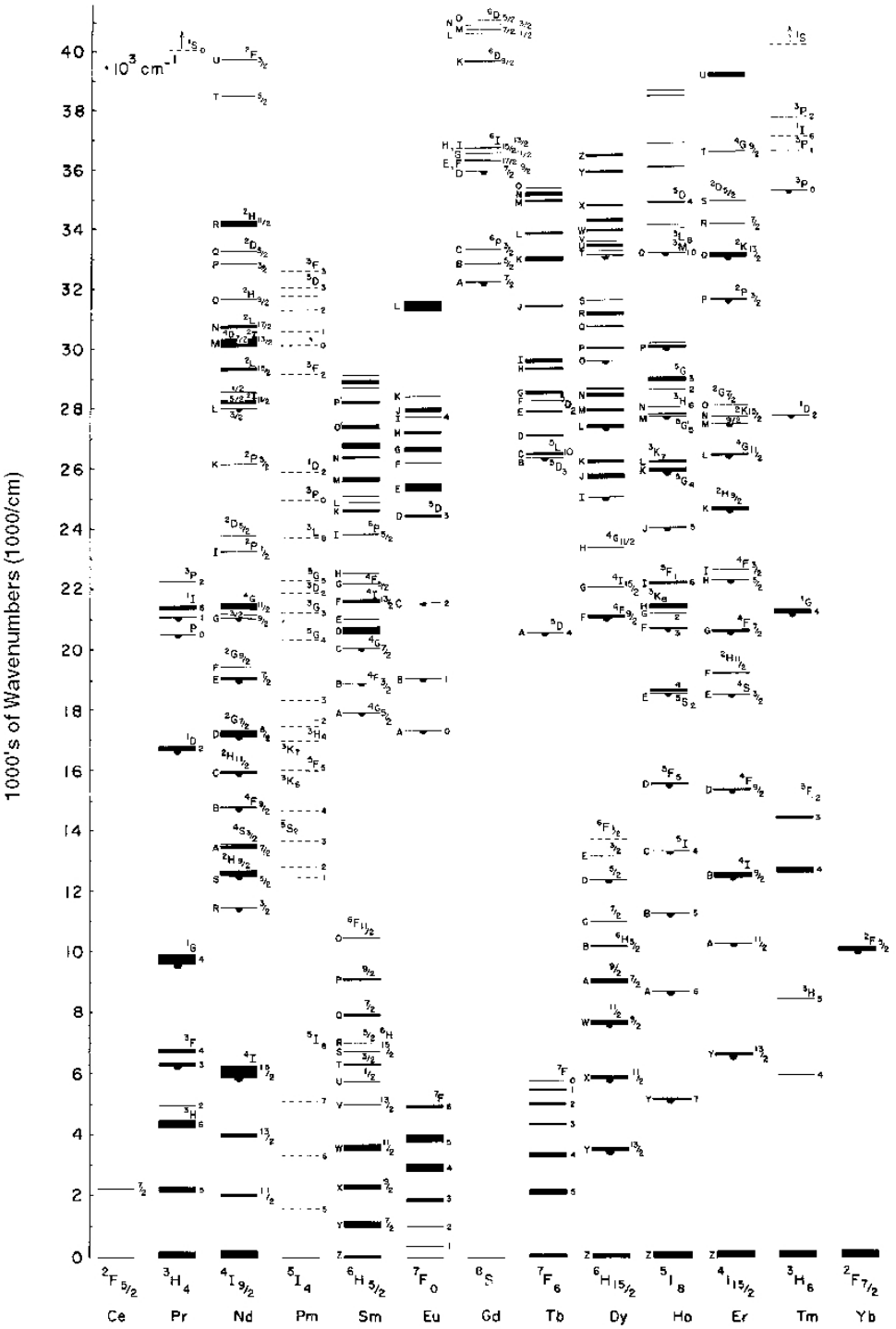

G. H. Dieke. Spectra and energy levels of rare earth ions in crystals (Interscience Publishers. New York. 1968)

Glossary

AFM --- Atomic Microscopy

BEP --- Beam equivalent pressure

CL --- Cathodoluminescence

EL --- Electroluminescence

EXAFS --- Extended X-ray adsorption fine structure

FWHM --- full-width-at-half-maximum

IR --- infrared

LED --- Light emitting diode

MBE --- molecular beam epitaxy

MEIS --- Medium ions scattering

MOCVD --- metal organic vapour deposition

MOVPE --- metalorganic vapor phase epitaxy

n.i.d --- Non-intentionally doped

PAMBE --- plasma assisted molecular beam epitaxy

PL --- Photoluminescence

PM --- Photo multiplier

PMT --- Photo multiplier tube

PLE --- Photoluminescence excitation spectroscopy

QD --- quantum dot

QW --- quantum well

RBS --- Rutherford backscattering spectroscopy

RE --- Rare earth

RHEED --- Reflection high electron diffraction

SEM --- Scanning electron microscope

SK --- Stranski Krastanow

UV --- ultraviolet

UHV --- ultra high vacuum

XRD --- X-ray diffraction

YAG --- Yttrium Aluminium Granat

Publications

1. E. Monroy, **T. Andreev**, P. Hollinger, E. B. Amalric, T. Shibata, M. Tanaka, and B. Daudin, *"Modification of GaN(0001) growth kinetics by Mg doping"*, Appl. Phys. Lett. **84**, 2554 (2004).
2. E. Monroy, M. Hermann, E. Sarigiannidou, **T. Andreev**, P. Hollinger, S. Monnoye, H. Mank, B. Daudin, and M. Eickhoff, *"Polytype transition of N-face GaN:Mg from wurzite to zinc-blende"*, J. of Appl. Phys. **96**, 3709 (2004).
3. Y. Hori, D. Jalabert, **T. Andreev**, E. Monroy, M. Tanaka, Oda, and B. Daudin, *"Morphological properties of Eu doped QDs"*, Appl. Phys. Lett. **84**, 2247 (2004).
4. **T. Andreev**, Y. Hori, X. Biquard, E. Monroy, D. Jalabert, A. Farchi, M. Tanaka, O. Oda, Le Si Dang, and B. Daudin, *"Optical and morphological properties of GaN quantum dots doped with Tm"*, Phys. Rev. B **71**, 115310 (2005). **Selected for:** Virtual Journal of Nanoscale Science &Technology
5. **Thomas Andreev**, Eva Monroy, Bruno Gayral, Bruno Daudin, Nguyen Quang Liem, Yuji Hori, Mitsuhiro Tanaka, Osamu Oda, and Daniel Le Si Dang *"Eu locations in Eu-doped InGaN/GaN quantum dots"*, Appl. Phys. Lett. **87**, 21906 (2005). **Selected for:** Virtual Journal of Nanoscale Science &Technology
6. Y. Hori, **T. Andreev**, D. Jalabert, E. Monroy, Le Si Dang, M. Tanaka, O. Oda, and B. Daudin "GaN quantum dots doped with Tb", Appl. Phys. Lett. 88, 53102 (2006). **Selected for:** Virtual Journal of Nanoscale Science &Technology
7. **Thomas Andreev**, Nguyen Quang Liem, Yuji Hori, Mitsuhiro Tanaka, Osamu Oda, Daniel Le Si Dang und Bruno Daudin, "*Optical transitions of Eu^{3+} ion in GaN:Eu grown by molecular beam epitaxy"*, submitted to Phys. Rev. B
8. **Thomas Andreev**, Nguyen Quang Liem, Yuji Hori, Mitsuhiro Tanaka, Osamu Oda, Daniel Le Si Dang, Bruno Daudin, and Bruno Gayral, "*Optical study of excitation and de-excitation of Tm in GaN quantum dots"*, in preparation (Physical Review B).
9. **Thomas Andreev**, Ingo Barke, and Heinz Hövel "Adsorbed rare-gas layers on Au(111): Shift of the Shockley surface state studied with ultraviolet photoelectron spectroscopy and scanning tunneling spectroscopy" Physical Review B **70**, 205426 (2004).

Proceedings

1. **T. Andreev**, Y. Hori, X. Biquard, E. Monroy, D. Jalabert, A. Farchi, M. Tanaka, O. Oda, Le Si Dang and B. Daudin, *"Optical and structural properties of rare earth doped GaN quantum dots",* Superlattices and Microstructures **36***,* 707 (2004).
2. Y. Hori, **T. Andreev**, D. Jalabert, X. Biquard, E. Monroy, M. Tanaka, O. Oda, Le Si Dang, and B. Daudin, *"Structural and optical properties of rare-earth doped quantum dots grown by plasma-assisted MBE"*, Phys. Stat. sol. (b), **241**, 2787 (2004).
3. S. Founta, F. Rol, **T. Andreev**, B. Gayral, E. Bellet-Amalric, H. Mariette, and B. Daudin, *"GaN quantum dots grown on non-polar a-plane SiC by plasma-assisted molecular beam epitaxy"*, Phys. Stat. sol. (c), **241**, 2787 (2004).

4. E. Sarigiannidou, E. Monroy, M. Hermann, **T. Andreev**, P. Holliger, S. Monnoye, H. Mank, B. Daudin, M. Eickhoff, *"Phase transition by Mg doping of N-face polarity GaN"*, Phys. stat. sol. (c), **2**, 2216 (2005).
5. B. Daudin, N. Gogneau, C. Adelmann, E. Sarigiannidou, **T. Andreev**, E. Monroy, F. Fossard, J.-L. Rouvière, Y. Hori, X. Biquard, D. Jalabert, Le Si Dang, M. Tanaka, O. Oda, *"Structural and optical properties of GaN quantum dots"*, Mat. Res. Soc. Symp. Proc. 798, Y4.7 pp. 1-6 (2004).
6. Y. Hori, **T. Andreev**, X. Biquard, E. Monroy, D. Jalabert, Le Si Dang, M. Tanaka, O. Oda, and B. Daudin, *"Rare earth doped GaN and InGaN quantum dots grown by plasma-assisted MBE"*, Phys. Stat. sol. (c), **2**, 2373 (2005).
7. **T. Andreev**, N. Q. Liem, Y. Hori, M. Tanaka, O. Oda, B. Daudin, and Le Si Dang, *"Comparative optical study of Eu^{3+} ions doping in InGaN/GaN quantum dots and GaN layer grown by molecular beam epitaxy"* Journal of Optical Materials.
8. **Thomas Andreev**, Nguyen Quang Liem, Yuji Hori, Mitsuhiro Tanaka, Osamu Oda, Daniel Le Si Dang, und Bruno Daudin, "*Eu^{3+} location in Eu doped GaN thin films and quantum dots*", submitted to Phys. stat. sol.
9. Yuji Hori, **Thomas Andreev**, Thomas Florian, Edith Bellet - Amalric, Daniel Le Si Dang, Mitsuhiro Tanaka, Osamu Oda, und Bruno Daudin "*Undoped and rare earth doped GaN quantum dots grown on AlGaN*", submitted to Phys. stat. sol.
10. Yuji Hori, **Thomas Andreev**, Denis Jalabert, Mitsuhiro Tanaka, Osamu Oda, Daniel Le Si Dang, und Bruno Daudin "*Tb doped GaN quantum dots grown by plasma assisted molecular beam epitaxy*", submitted to Phys. stat. sol.

Publications in other journals

1. In CEA technologies: "Boîtes quantiques et terres rares, une nouvelle voie pour les LED?"